University of New Mexico
UNM Digital Repository

Spring 5-1-2018

DESIGNING SYNTHETIC ENVIRONMENTS TO CONTROL VALVULAR INTERSTITAL CELLS IN VITRO

Kent E. Coombs

Kent E. Coombs
_____
Candidate

Biomedical Sciences Graduate Program
_____
Department

This *dissertation* is approved, and it is acceptable in quality and form for publication:

Approved by the Dissertation Committee:

Elizabeth Hedberg-Dirk, PhD., Chairperson
_____

Nancy L. Kanagy, PhD.
_____

Jennifer M. Gillette, PhD.
_____

Thomas Howdieshell, M.D.
_____

_____

_____

_____

_____

_____

**DESIGNING SYNTHETIC ENVIRONMENTS
TO CONTROL VALVULAR INTERSTITAL CELLS
IN VITRO**

By

KENT COOMBS

Degrees:
B.A. Biology 2010,
Hendrix College, Conway, Arkansas

DISSERTATION

Submitted in Partial Fulfillment of the
Requirements for the Degree of

Doctor of Philosophy in Biomedical Science

The University of New Mexico
Albuquerque, New Mexico

May 2018

Printed in the United States of America

University of New Mexico

1 University of New Mexico,

Center for Biomedical Engineering

Albuquerque, NM 87131

Acknowledgments

I first would like to thank my mentor Elizabeth for the many words of support and scientific discussions that culminated as this work. Thank you for sharing your knowledge and giving me the opportunity to work on something we both love. Also, I would like to give a special thanks to my fellow graduate student Matthew Rush. Without him I would have never been able to finish my PhD. Thanks to the lab members past and present that I have had the opportunity to work with over the years. You always helped me have some fun in lab and I greatly appreciate that.

Thank you to my family for your support and encouragement throughout this experience. You have always been there to support me and help me keep my sanity even in my most stressed moments. Thank you!

Finally, I want to thank my wife Caitlin. Your unwavering support, patience, and sacrifice over the past years has allowed me to obtain this degree. I hope that now I can return the favor and we can continue our life journey together.

Designing Synthetic Environments to Control

Valvular Interstitial Cells *In Vitro*

By: Kent E Coombs

Abstract

Aortic valve disease (AVD) is a large contributor to health costs in the United States affecting 2.8% of the population greater than 75 years old. With a growing elderly population due to medical advances, AVD will continue to rise in prevalence over time. Current treatments for AVD are insufficient due to a lack of preventative therapies and the bioprosthetic valves used for surgical replacement have major limitations. Tissue engineered heart valves (TEHVs) present an ideal solution to current AVD needs because of their biocompatibility, capability to integrate with the host's tissue, and ability to utilize the natural repair mechanisms of the body. To achieve this goal, we designed synthetic environments with specific cell phenotypes and scaffold properties in order to direct cellular behavior and tissue growth *in vitro*. In this work cell subpopulations, mechanical stiffness of the substrate, and material surface charge were all studied to understand how the primary cells of the aortic valve, valvular interstitial cells (VICs), were affected by specific environmental cues. These studies were then translated from monolayer culture into a three-dimensional hydrogel system for the study of VICs in a more physically relevant cell culture system.

Table of Contents

Contents

Chapter 1

Introduction

Cardiovascular Disease and the Heart Structure

Cardiovascular disease (CVD) is the number one killer in industrialized countries, responsible for 1 of every 3 deaths in the United States [1]. Disproportionately affecting individuals greater than 65 years of age, CVD presents a significant burden on the healthcare system. A common type of CVD is heart valve disease, which can cause heart failure due to increased overall burden on the heart. Of the patients with severe aortic valve stenosis, fifty percent are referred for cardiothoracic surgery which typically costs between $80,000 - $200,000 dollars [1].

During normal function, the heart is responsible for unidirectional flow of blood throughout the cardiovascular system. It is composed of four main chambers and four valves. Deoxygenated blood enters the right atrium from the veins before being forced, by contraction of the right atrium, through the tricuspid valve into the right ventricle. The expansion of the right ventricle causes blood to fill the cavity and force the tricuspid valve closed. Next, the right ventricle contracts to push deoxygenated blood through the pulmonary valve and pulmonary artery to the lungs. Oxygenated blood returns from the lungs through the pulmonary veins into the left atrium before passing through the mitral/bicuspid valve into the left

ventricle. Contraction of the left ventricle ejects blood through the aortic valve and out into the body.

All four valves have one of two general structures, semilunar and atrioventricular. The atrioventricular valves (pulmonary and mitral) have chordae tendineae extending from the valve leaflets to the corresponding atria wall, which force these valves to open and close with the expansion and contraction of the corresponding ventricles. The semilunar valves on the other hand have a tricuspid structure and are opened and closed purely by the changing pressure gradients created by pumping heart chambers. As the ventricle contracts, the atrioventricular valve closes, and the pressure increases to force open the semilunar valve. As the ventricle relaxes the pressure decreases and is overcome by the pressure on the arterial side of the valve causing the atrioventricular valves to open.

The aortic valve (AV) is the most commonly diseased valve of the heart [2]. This due to the higher-pressure gradients the AV must endure in normal day to day functions [3]. The AV is a tricuspid valve with three leaflets that are less than 1 mm thick [4, 5]. Despite the thinness of the valve, there are three identifiable layers with specific functions and microstructures; the ventricularis, spongiosa, and fibrosa [4, 6-9]. The fibrosa lies on the atrial side of the aortic valve and is composed of organized collagen 1 bundles (Figure 1). Lining the leaflets circumferentially, these collagen bundles provide physical durability against the compressive forces exerted on the valve in the closed position [10]. However, the

collagen fibers crimp as the AV opens to allow the leaflet to bend easily. The spongiosa layer is comprised of mainly sulfated glycoaminoglycans (GAGs) like chondroitin sulfate, dermatan sulfate, hyaluronan, as well as other proteoglycans [2]. This layer acts as a lubricating layer between the fibrosa and the ventricularis. The ventricularis lies on the ventricle side of the AV and is composed of elastin bundles. Aligned radially, these elastin fibers help the AV stretch and retract properly with the cycling heart [2, 4, 11]. The specific extracellular matrix (ECM) proteins and specialized structure of the aortic valve are designed to deal with the dynamic environment in the heart. However, due to the high-pressure gradients, flow profiles, and varying mechanical stresses, the AV is the most common valve to become diseased. As a result, it is the most the frequently studied valve and is targeted for developing tissue engineered AV replacements.

Aortic Valve Disease (AVD)

Age and factors such as family history, diet, and weight increase the risk of developing AVD. AVD impairs the proper opening and closing of the valve due to increased thickness and decreased flexibility (Figure 2) [12]. Thickening and stiffening of the AV disrupts the ability of the leaflet edges to coapt, allowing blood to leak back through the valve from the arterial side into the ventricle, a process known as regurgitation. Simultaneously the decreases in the ability for the valve to open and close, known as stenosis, disrupts the efficient movement

of blood out of the heart creating eddies and reducing pressures [11]. This is particularly important because the coronary arteries which feed the heart oxygenated blood are on the arterial side of the AV. Improper blood flow and pressure gradients caused by AVD disrupt the distribution of blood to the heart muscles through the coronary arteries to induce further stress. These conditions force the heart to work harder to pump blood out to the rest of the body with an inferior blood supply. This increases the burden on the heart, and without treatment will eventually result in heart failure.

Despite its prevalence, the exact mechanism of development for AVD remains unclear. This is in part due to the difficulty in diagnosing AVD at early stages, as well as a lack of laboratory models to study pathological AVD progression in relevant controlled systems. The most commonly accepted theory of AVD development is long term wear and tear with altered mechanical loading both acute and chronic due to hypertension, high blood pressure, or inflammation increases stress on the valve [13, 14]. These stresses lead to inflammation and breakdown of ECM. Valvular interstitial cells (VICs) activate to repair the damage but persistent inflammation, repeated repairs, and in increases in collagen 4 over time form scar tissue. Failure to properly replace tissue is accompanied by increases in disorganized ECM resulting in thickening of the valve [14]. This process of thickening known as fibrosis alters the valve microenvironment which affects neighboring VIC and causes ECM changes to cascade out in the surrounding valve leading to AVD [13].

Without a better understanding of the mechanisms that cause AVD, better markers to diagnose AVD in early stages of development, and better preventative treatments, AVD prevalence will continue to rise and generate a large burden on the healthcare system. If better *in vitro* models that closely mimic the AV could be developed then these models could be studied to develop new drug treatments and a better understanding of AVD at the cellular signaling level. Furthermore, creating better valve replacements for diseased valves will decrease the cost of AVD care and increase patients' quality of life.

Treatment of AVD

Currently the gold standard of treatment for AVD is to completely replace the diseased AV using either a biological or synthetic valve (Figure 3). Biological valves are derived from xenograft tissue, normally porcine or bovine, and are treated to mimic the structural and mechanical properties of the aortic valve. This treatment includes cutting and molding the tissue into the correct shape before undergoing decellularization and crosslinking. This process removes all the donor animal's cells and DNA from the tissue graft preventing host immune response [15].

One of the major drawbacks of biological xenograft valves are that they degrade over the timespan of 5-20 years dependent on the level of patient's physical activity [2, 16]. This happens because the crosslinking process destroys the functional properties of the proteins that make up the implanted valve, so the

valve no longer supports proper cellular attachment, growth, or repair. These biological valves are also prone to calcification and degradation over time. Although 10-15 years is fine in older less active patients, this presents a problem in active younger adults and in pediatric patients with longer lifespans. Many of these younger patients will require additional surgeries as the biological valve wears out and pediatric patients will need the valve replaced periodically as they grow to match the valve size to the growing aorta.

Synthetic valves, which have different mechanical properties compared to biological valves do not wear out and are generally made of metals or plastics [16]. Their long lifetime makes them more suitable for younger patients who will need a functional valve for a longer period of time. However, because they are made of synthetic materials they have thrombogenic surfaces, which can cause blood clotting and increase the risk of stroke [16]. To counteract clot formation, patients must use anticoagulation therapies, decreasing quality of life due to increased risk of bleeding, drug side effects, and the time and money required to maintain lifelong therapy. Also, like biological replacement valves, synthetic heart valves do not grow with the body so again pediatric patients would require multiple replacement surgeries as they grow.

The final type of valve less commonly available are human allograft valves harvested from cadavers, organ donors, or heart transplant recipients [17, 18]. This type of replacement has the best functional properties with excellent hemodynamic function, low thrombogenicity, and resistance to infections, but still

commonly fail between 10-20 years after implantation [17-19]. In addition, since their natural source is humans, the supply is severely limited.

Despite the effectiveness of current valve replacements to treat AVD they all exhibit major limitations. When combined with the fact that current valve replacements can't grow or integrate into the host there is significant room for improvement.

Tissue engineered heart valve (TEHV) replacements that could integrate into the native tissue, utilize the body's self-repair mechanisms to maintain themselves, and grow would overcome all the issues mentioned above. However, to develop these TEHVs a better understanding the aortic valve cell biology during health and disease needs to be established.

Cells of the Aortic Valve

Within each leaflet of the AV there are two main cell types. The first cell type, valvular endothelial cells (VECs), are found lining the outside surface and are important in presenting a non-thrombogenic exterior to prevent blood clotting. VECs help to maintain valve homeostasis through their ability to detect mechanical stresses as well as through the secretion of signaling factors to control VIC behavior [20-22]. An example of the importance of VEC maintenance of homeostasis can be seen in bicuspid aortic valves (BAV). These valves are inherited congenitally and have a two-leaflet structure instead of the tri-leaflets normally seen in this area. The BAV structures creates an environment of

increased mechanical stress which makes them prone to endothelial dysfunction and denudation. Loss of the endothelial layers result in the BAV leaflets quickly becoming diseased and is therefore commonly replaced early in life. A study of bicuspid aortic valves (BAV) correlates the increase in endothelial dysfunction and inflammation to decreases in endothelial nitric oxide synthase (eNOS) expression within the valve. Without eNOS expression in VECs the VICs of the aortic valve became diseased [23]. This interaction is dictated through the molecule nitric oxide (NO) which is produced by eNOS in VECs. Loss of this critical homeostasis molecule allow VICs to enter a diseased state and modify the valves causing AVD.

Confirmation of the role of NO was confirmed *in vitro* using VIC cultures where NO donors or NOS inhibitors were added to inhibit or promote differentiation of VICs to a diseased osteoblastic VIC (OB VIC) phenotype, respectively. Using both single cultures of VICs and co-cultures of VIC/VECs, addition of NO helped to prevent VIC activation and switching to an OB VIC phenotype. Inhibition of NO did the opposite allowing VICs to remain inappropriately activated, which is hypothesized to eventually lead to AVD *in vivo* [21, 22, 24]. The notch 1 signaling pathway was identified as one mechanism by which NO prevented aVIC calcification, but many other pathways still need to be explored [25-27]. In summary the presence of VECs *in vitro* and *in vivo* can alter the behavior of VICs and should be considered for tissue engineering applications.

The second more commonly studied cell type VICs are found dispersed throughout the three layers of the AV. They are responsible for synthesizing new tissue to repair the valve and play important roles in the fibrosis and calcification of the valve during AVD. The wide-ranging roles of VICs are possibly due to subpopulations in each layer of the AV, as well as the natural plasticity of VICs which allows them to switch phenotypes in response to the environmental factors around them.

The VIC phenotypes identified to date include quiescent VICs (qVICs), activated or myofibroblastic VICs (aVICs), osteoblastic VICs (OB VICs), and progenitor VICs (pVICs) (Figure 4). The main cell phenotype that dominates the adult valve is quiescent VICs (qVICs). During normal valve activity qVICs maintain valvular structure and stability with low ECM turnover and little to no proliferation. qVICs respond to inflammatory factors and cytokines released by damaged valve tissue and switch to an activated VIC (aVIC) phenotype. aVICs repair the heart valve when it becomes damaged or diseased and then undergo apoptosis or switch back to a qVIC phenotype when the tissue is repaired and inflammation decreases. aVICs are also the most commonly seen phenotype in the laboratory proliferating rapidly, laying down extracellular matrix, migrating, and expressing alpha smooth muscle actin. If aVICs remain inappropriately *in vivo*, remodeling and disorganization of the heart valve ECM leads to valve thickening and stiffening referred to as fibrosis [14]. Disorganization of the heart valve ECM due to fibrosis is hypothesized to lead aVICs to differentiate to osteoblastic VICs (OB VICs) expressing osteoblastic markers like osteocalcin,

runX2, CBFa, and osteopontin. OB VICs exacerbate valvular disease by calcifying surrounding matrix and forming calcific nodules. The local stiffening of tissue due to calcification and fibrosis is thought to promote nearby VICs to switch to an OB phenotype to propagate disease throughout the valve.

In vitro, OB VICs form calcified nodules via two separate mechanisms. The first mechanism, osteogenic calcification, is caused by the differentiation of VICs in osteoblastic induction media. When exposed to certain factors like TGF-β1, dexamethasone, and ascorbic acid, aVIC in culture switch to an OB VIC phenotype, clump up, and surround themselves in a calcific matrix. This process is similar to that of ectopic bone formation with a calcified matrix surrounding living cells and is seen in later stages of AVD. The second mechanism, dystrophic calcification is also seen during valve disease and occurs when VICs contract into a large clump of cells to form an amorphous calcium crystal with an apoptotic core [28]. This type of nodule is commonly seen *in vitro* when VICs grow to super confluence with edges of cells pulling back from the substrate to form large aggregates. Once detached, the VICs in the center begin to apoptosis and form a calcified nodule. Both osteogenic and dystrophic nodules are seen during disease development *in vivo* but these mechanisms are not usually differentiated in *in vitro* cultures. Therefore, designing better model systems to help identify signaling molecules unique to each process is very important for future research for growth of healthy TEHVs.

pVICs are one of the less studied phenotypes. They are assumed to be stem cell derived VICs that either circulate in the blood before entering the valve or reside in small amounts within the AV. Their role is thought to be in valve repair where they support repair through unknown processes [29]. Until these cells can be definitively isolated using defined progenitor markers their exact role in AVD and valve repair will remain unclear.

An interesting aspect of VICs that remains less explored is that they are a heterogeneous population of cells. These cells reside throughout the three distinct layers of the aortic valves with very different ECM environments, therefore it is likely these cells have different functions within each valve layer. Yet most studies isolate the entire populations of VICs from the valve to use for experimentation without further separation. Recent work has shown that from the entire population of VICs a very small subpopulation of progenitor cells can be isolated by flow cytometry using the progenitor marker $ABCG2^+$ or a colony formation assay [30, 31]. In both cases VICs characterized as progenitor cells were more sensitive to osteoblastic (OB) differentiation when exposed to osteogenic induction media than unseparated VICs. Separation of VICs in these studies either yielded a very small amount of cells or required isolation of single cells to grow into colonies for characterization, so developing a robust and efficient method to separate distinct subpopulations from the valve needs to be developed. In addition, it has been shown that fibrotic and calcific lesions first appear on the fibrosa layer while disease of the spongiosa side of the leaflet is seen later. This suggests that within the valve there may be specific VIC

subpopulations in each leaflet that might be disease resistant or disease prone. Separating these subpopulations is a huge challenge as there are no surface markers currently identified in VIC literature for the different VIC phenotypes and our current isolation method collects all VICs from the valve and combines them for culture. If 1) VICs could be separated into subpopulations with distinct differences in phenotype and 2) unique surface markers could be identified for each subpopulation, then VICs could be more easily sorted into subpopulations immediately after extraction and used more appropriately in TEHV endeavors.

With most research currently using the entire VIC population extracted from valves, small differences between different VICs subpopulations is largely ignored. If healthy TEHVs are going to be made, cell subpopulations need to be fully understood to avoid unintended side effects. The problem of unique surface markers is addressed in chapter two, which looks at separating different VIC subpopulations based on adhesion characteristics and then characterizing the subpopulations for phenotypic differences and unique surface markers.

Biological Tissue Engineered Heart Valves

Due to the complications of allogenic, biological, and synthetic valves, tissue engineers are developing TEHV as better replacements. Ideally, TEHVs should be composed of biologically compatible tissue and material which would have the ability to integrate into the host and become tissue in the body. Properly designed TEHVs could provide an ideal solution to current valve limitations of

thrombogenicity, poor hemodynamic profiles, and lack of longevity. Additionally,

TEHVs that truly integrate into the host would revolutionize pediatric care by

eliminating the need for additional surgeries. While no TEHV currently exists in

the medical market there are several strategies currently being used for their

development.

One common approach is to design biological TEHVs with or without cells

that have the mechanical stability to act as a replacement valve immediately after

surgery. However, these TEHV also exploit the body's natural regenerative

capacity to induce cellular repair and tissue formation [32]. In this system, the

TEHV could be made of natural and/or synthetic biomaterials with or without

seeded cells. After implantation, these TEHVs would immediately act as a

functioning valve, but over time would promote cellular infiltration, migration, and

growth onto the scaffold to induce tissue formation. The scaffold would then

either reside permanently in the tissue creating a hybrid cell/biomaterial valve or

slowly degrade away as it is replaced by naturally created tissue. To be

successful, the slow maturation of this type of valve inside the body would need

to be fine-tuned and have carefully controlled cellular growth. Furthermore, the

mechanical properties of this material or material/cell hybrid would need to

remain stable at all stages of tissue formation so that the valve always works

properly.

One of the most successful examples using the strategy above is using a

natural biomaterial to create a tube within a tube heart valve (Figure 5). By

collapsing one of two decellularized ECM tubes inside the other, a tricuspid valve

structure is created [33, 34]. The ECM tubes are 16mm long and grown *in vitro*

on a circular scaffold in a bioreactor using a fibrin ECM coated with ovine

endothelial cells over two weeks. The resulting cell ECM tube is decellularized

and one tube is placed inside the other. The inner tube is attached to the outer

tube in a specific pattern using degradable sutures before being collapsed to

make a structure very similar to that of the pulmonary valve (Figure 5). These

tube-within-tube valves have been implanted into sheep and shown to function

up to 8 weeks, at which point the study was ended. Analysis of the valves shows

there is still room for improvement due to declining valve function caused by a

loss of tensile strength, as well as large differences in valve thickness at 4-6

weeks *in vivo*.

Synthetic Tissue Engineered Heart Valves

A second TEHVs development strategy is to grow mature, functional valve

tissue in the laboratory using synthetic materials. These synthetic materials could

be engineered to promote specific cellular behaviors to guide cell growth to

produce mature tissue in a bioreactor. As a fully functional tissue grown in the

lab, it would directly replace diseased tissue much like current replacement

valves. However after healing, the body's natural repair mechanisms would

maintain the valve. The advantage of this type of TEHV would be that all the

biomaterials and non-biological factors could be removed or degraded before

implantation leaving only biological material. Also, because the tissue should already be fully mature, this strategy does not rely on *in vivo* maturation and tailoring of material degradation with tissue deposition.

Examples in the literature implementing this strategy in TEHV development can been found in the biomaterials field of hydrogels. Hydrogels are made from natural or synthetic polymers that produce very soft scaffolds and are currently being investigated as platforms to create model AV systems and grow viable soft tissue. The soft nature (2-12 kPa) of hydrogels and tunability of their physical and chemical properties make them a useful platform to try to control cellular growth and differentiation using bioactive molecules [35-38].

In the realm of synthetic hydrogels, modified polyethylene glycol (PEG) is the most commonly used synthetic material. As a hydrophilic molecule that absorbs water, PEG forms hydrogels that allow for efficient nutrient diffusion and waste removal while providing a self-supporting three-dimensional structure. However, the very hydrophilic backbone of unmodified PEG does not allow proteins to stick to its surface preventing cellular attachment. This creates an environment where PEG based hydrogels provide a unique non-fouling surface that can be modified with bioactive molecules that cells interact with. Ideally, the proper bioactive molecules incorporated into PEG-based hydrogel will not only induce cellular attachment, but also promote advantageous cellular behaviors through the activation of certain cellular signaling pathways.

Bioactive molecules are commonly attached to PEG by attaching reactive molecules like acylate or N-hydroxysuccinimide to PEG's hydroxyl end groups. These reactive end groups can in turn be used for a number of different chemistries attaching various bioactive molecules. For example, a modified PEG gel in VIC literature is PEG-PQ/PEG-RGDS hydrogel [35, 38, 39]. In this hydrogel, the PQ peptide (GGGPQGYIWGQGK) is an MMP-2 degradable amino acid sequence while peptide RGDS promotes VIC attachment to the hydrogel [38, 39]. To encapsulate VICs, the modified PEGs are mixed together and then crosslinked using light-initiated free radical polymerization. In these hydrogels, VICs survived long term culture up to 42 days and mimicked the normal cellular morphology of valve tissue with deposition of relevant ECM molecules; collagen, elastin, and glycosaminoglycans.

While the results are very promising, the main disadvantage of system is that once the cells are encapsulated in the hydrogel, the formation ECM was random and unlike the controlled structures seen *in vivo* [22, 39]. A lack of knowledge about what signaling pathways are activated, which biological peptide combinations are ideal for controlling VIC behavior, and how the deposition of ECM is guided during development means the structures currently being made do not have the physical characteristics of native valve tissue. Also, in the PEG-PQ/PEG-RGDS hydrogels, a peptide sequence originally found on fibronectin known as the RGD motif was used to promote cellular attachment. Fibronectin coated surfaces have been shown to help protect VIC from osteoblastic differentiation, but it is not one of the main ECM proteins found in the AV [40-43].

The main components of AV ECM are collagen 1, elastin, and sulfated (GAGs) glycosaminoglycans, all of which do not have available RGD sequences for binding in their native conformations [43]. Interestingly, RGDs are present on the bone forming protein osteopontin, and upregulation of osteopontin gene expression in diseased valves is considered a marker of VIC osteoblastic differentiation [37]. While RGD allows VICs to adhere to the gel, the signaling pathways activated in VICs by these adhesion molecules are unknown. Research in the downstream signaling of VICs in RGD based gels need to be further studied. To make matters more complex, the AV has multiple ECM proteins with different binding motifs for VICs. Recapitulating this complex environment *in vitro* using multiple peptides distributed in a hydrogel in a specific orientation and concentration could be a useful tool to control VIC behavior and growth.

Degradation rate of the hydrogels scaffold are also crucial to future studies. PEG by itself is not degradable, however by attaching specific peptides or molecules the degradation rate of the hydrogel can be tailored to support certain cellular functions. For example, to proliferate in hydrogels cells need to have space created by removing/degrading the surrounding material. The rate of degradation of the hydrogel must be fast enough to allow cells to proliferate without compromising the three-dimensional (3D) structure and mechanical properties of the scaffold. In recent studies, degradation rates have been shown to effect VIC behavior in PEG-RGD/PEG-PQ hydrogels [35, 39]. VICs grown in softer gels with fewer crosslinks were compared to cells in stiffer hydrogels with

17

more crosslinks [38]. The cells showed a maximal spreading at 7 days in the softer gels compared to the cells in stiffer gels which took 14 days to fully spread. These gels took advantage of VIC's ability to degrade the hydrogel by producing proteases. The space created by protease degradation of the molecule PQ allowed for VIC spreading and proliferation.

Another interesting approach to increase the biological relevance of hydrogels is to culture two cell types in a co-culture system. VICs were encapsulated in hydrogels by partially crosslinking them inside a PEG-PQ/PEG-RGDS hydrogel. Next an RKR peptide, which promotes VEC attachment, in buffer was used to cover the surface of the gel and this gel was exposed to light a second time. The second light exposure finished crosslinking the hydrogel internally while also attaching RKR peptides to the surface. After washing away excess RKR peptide, VECs were seeded on the surface of the hydrogel. This unique cell culture platform with VICs on the inside and VECs lining the surface mimics the native valve structure [22, 35, 39]. Long term analysis of these studies show increased VIC viability and secretion of ECM normally found in the AV, but the system still lacks the complexity and protein structures seen *in vivo*.

One of the limitations of PEG hydrogel chemistry is the reliance on end group functionalization, meaning that each PEG molecule is limited to the ends being modified. This limits each PEG molecule to having a bioactive molecule added to one side since while the other is needed for crosslinking. Therefore, developing a material that can be modified at multiple sites that can be used

interchangeably as crosslinking sites or attachment site for biomolecules would be superior in making complex hydrogels. With such a molecule, more than one bioactive molecule could be attached to a hydrogel to investigate how combinations affect cellular behavior. A current example of a multi-functionalizable PEG molecule from the lab of Kristi Anseth is an eight-armed poly(ethylene glycol)-norborene (PEG-N). This PEG molecule exists in a star formation with eight end groups available for functionalization. Utilizing a thiol-ene reaction, cysteine specific peptides and a protease degradable linker peptide were added to PEG-N [38]. This PEG-N hybrid molecule was used to form hydrogels with one of three cysteine functionalized adhesive peptides, fibronectin (RGD), elastin (VGVAPG), or collagen-1 (P15), with either the degradable linker peptide KCGGPQG↓IWGQGCK or KCGGPQG↓IAGQGCK from collagen [38]. Results showed that VICs had an elongated morphology in RGD hydrogels as well as significantly more global MMP production at 14 days in RGD and P15 hydrogels. Despite the elegance of this system, it stills lacks a degree of tunability because of the massive size of an eight-star PEG molecule. These molecules are made of 8 PEG molecules with MW of 40,000. Because of this the hydrogel formed from this molecule creates extremely soft hydrogels and cannot be tailored easily to alter stiffness.

A different strategy to making hydrogels uses natural methacrylated polymers like hyaluronic acid, collagen, and gelatin [37, 44]. Using mixtures of methacrylated gelatin and methacrylated hyaluronic acid (HA), one study encapsulated VICs in natural polymer hydrogels of various stiffness [37]. With the

gel's compressive moduli ranging from 4-12 kPa, the changes seen in VIC behavior were attributed to differences in gel stiffness. However, as the ratios of gelatin to hyaluronic acid are changed to achieve different stiffness's, the number of cell-adhesive sites and the local chemistries in the gel also changed. VICs have been shown to be sensitive to these types of changes and are likely affected [39, 45-47]. While natural polymers are advantageous in that they have multiple adhesion sites for VIC attachment, support VIC survival, and cellular remodeling they also have inherent biological variations that are difficult to control. Therefore, replication of environments to test cellular responses in natural polymers is difficult [48]. Additionally, natural polymers are less tunable than synthetic polymers so functionalizing or changing specific aspects of a natural polymer is problematic.

The main issue with current TEHV strategies comes from the lack of knowledge of cellular signaling and growth of healthy heart valve tissue in the laboratory. For example, understanding how mechanical cues from the scaffold control cell function and growth remains largely unstudied. For TEHVs to become a reality, detailed knowledge of how cells react to scaffold macro and microenvironments *in vitro* is required. Without well designed and highly controllable cell culture environments to mimic the heart valve as well as methods to control cellular growth and differentiation, creating functional TEHVs will continue to fall short.

Microenvironmental Cues

Understanding how changes in the scaffold microenvironment effect VIC behavior is crucial in the design and synthesis of future biomaterials. In current studies, VICs are expanded to relevant numbers in plastic culture flasks made from treated tissue culture polystyrene (TCPS). TCPS is used as a cell culture platform because cells attach well and proliferate rapidly, and VICs are no exception. However, after reaching confluence on TCPS, VICs contract and form dystrophic OB nodules. This diseased behavior cannot be tolerated in lab grown healthy heart valve tissue.

We hypothesize that there are a two microenvironmental cues that are commonly overlooked on TCPS that may affect VIC behavior. First, TCPS is a stiff plastic with a compressive modules around 30.6 ± 10.9 GPa, which is high compared to tissues of the body [49]. For comparison, the aortic valve measured using different procedures has been shown to have a modulus ranging from 0.3 to 25 kPA [50-52]. Literature also reports that stiffness of the underlying substrate affects the behavior of many different cell types i.e., fibroblasts, neuronal cells, cardiovascular endothelial cells, and pre-osteoblastic cell lines [36]. This evidence, combined with the observation that the valve environment stiffens with age and AVD progression, suggests that mechanical cues like stiffening of the substrate may induce VICs toward a disease state [52, 53]. To investigate this possibility we designed unique co-polymers with compressive moduli ranging from 25 to 4700 kPa, that did not have changing surface chemistries. This co-polymer system was one of the first to examine cell behavior over a large range

of moduli independent of surface chemistry, to isolate reactions to changes in substrate stiffness alone. The results of this project are presented in chapter 2 of this dissertation.

The second micro-environmental cue that has been overlooked on TCPS is surface chemistry. TCPS is treated with an oxygen plasma to insert oxygen functionalities at the ring site of polystyrene [54]. This process imparts a net negative charge to the surface of TCPS which increases cell attachment and viability [54]. A negative charge is important to consider because it is also seen during aortic valve development on hyaluronic acid, a molecule seen at high concentrations in the endocardial cushion [55]. This developmental environment is supportive of cellular proliferation and migration. We hypothesized that if the material culturing VICs had a negative charge, VICs would attach easily and proliferate rapidly.

In chapter three we use a model system in which the surface chemistry of the underlying substrate can be easily modified by creating an ordered monolayer of self-assembled alkanethiols with specific chemistries. Using this technology, we tested how negatively charge, positively charge, hydrophobic, and hydrophilic surfaces affect VIC behavior.

To further improve biomaterials for TEHV development, our studies of stiffness and surface chemistry need to be transitioned into a 3D cell culture system. Therefore, we synthesized a PEG based hydrogel oligo ((polyethylene) glycol fumarate) (OPF). This molecule has a number of advantages over other

PEG hydrogels because it is degradable though ester hydrolysis, easily tailored to alter stiffness, and has multiple sites per molecule which can be functionalized to alter the molecular structure. This molecule has not been used extensively due to a lack of availability in the market and it's difficultly to synthesize. In chapter four we address these issue with a new synthesis method that takes less time, generates less waste, requires less post-processing, and decreases the overall difficultly of synthesizing OPF.

Using this newly generated OPF polymer we engineered a model system to test how VICs react to charge in 3D hydrogels. In chapter 5 we show that OPF can be functionalized with different alkanethiols to create OPF molecules with specific charged alkanethiols from previous work. We then used the modified OPF-alkanethiol molecules to create hydrogels to encapsulated VICs and study their behavior in charge environments. Additionally, these gels were engineered so that they would have low stiffness levels to better mimic native aortic valve tissue. The results from this study are described in chapter five.

In summary, understanding the microenvironmental cues at the cell-material interface of a scaffold how they are interpreted by VICs is important to advance the synthesis of TEHVs. Selecting a relevant VIC subpopulation and defining an efficient way of isolating them is an important first step in this process. Using engineered materials to isolate the specific mechanical cues that affect cellular growth and behavior will expand understanding of how to include mechanical cues in 3D hydrogel systems. These tailored hydrogels with advantageous

properties will grow the best TEHV for further study. Eventually, reiterations of this process will advance biomaterials enough that cell signaling and behavior can be completely controlled, and the TEHV created in a lab can be used a functional replacements for AVD.

Figures

Fibrosa
Spongiosa
Ventricularis

Suture Ring
Leaflets
Hinges

α-Smooth Muscle Actin (**αSMA**)

Osteocalcin (**OCN**)
• Transformaing Growth Fac...
Beta-1 (**TGF-β1**)
• α-Smooth Muscle Actin
(**αSMA**)

50μm

50μm
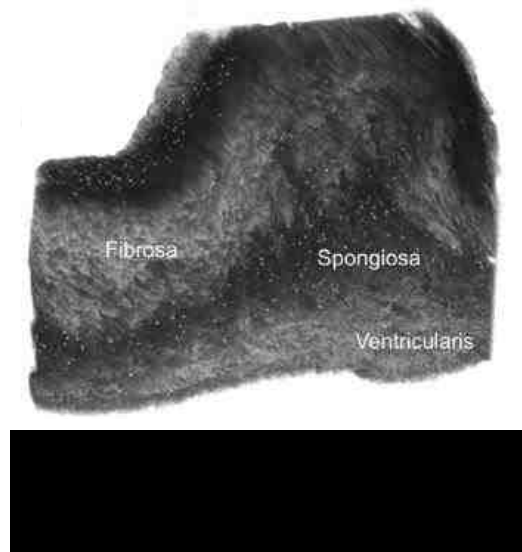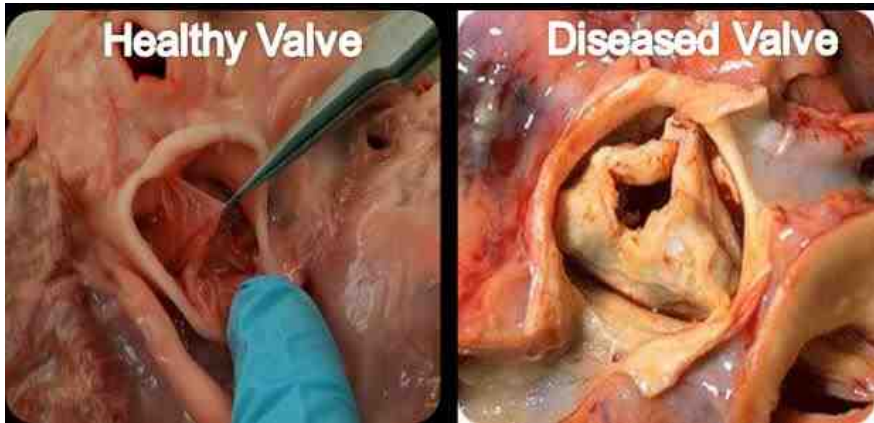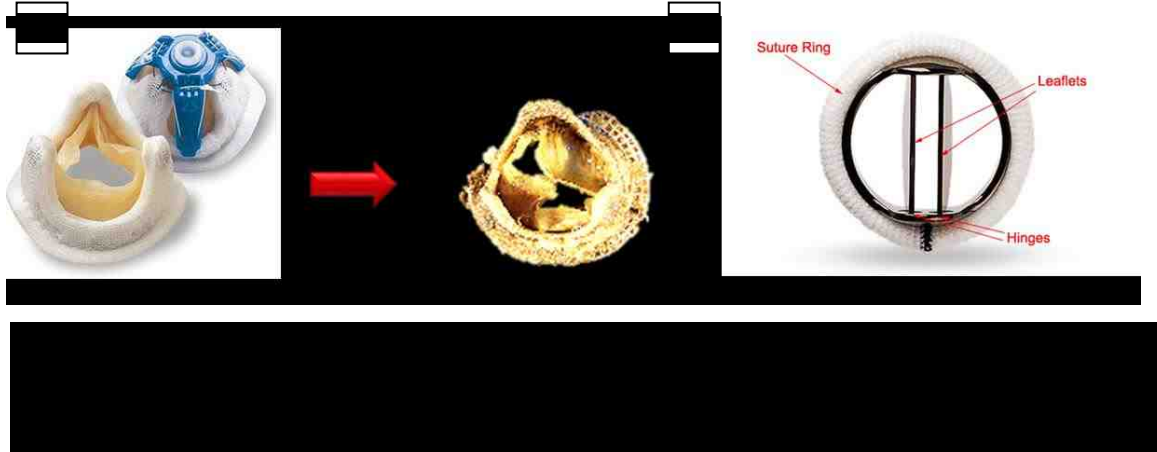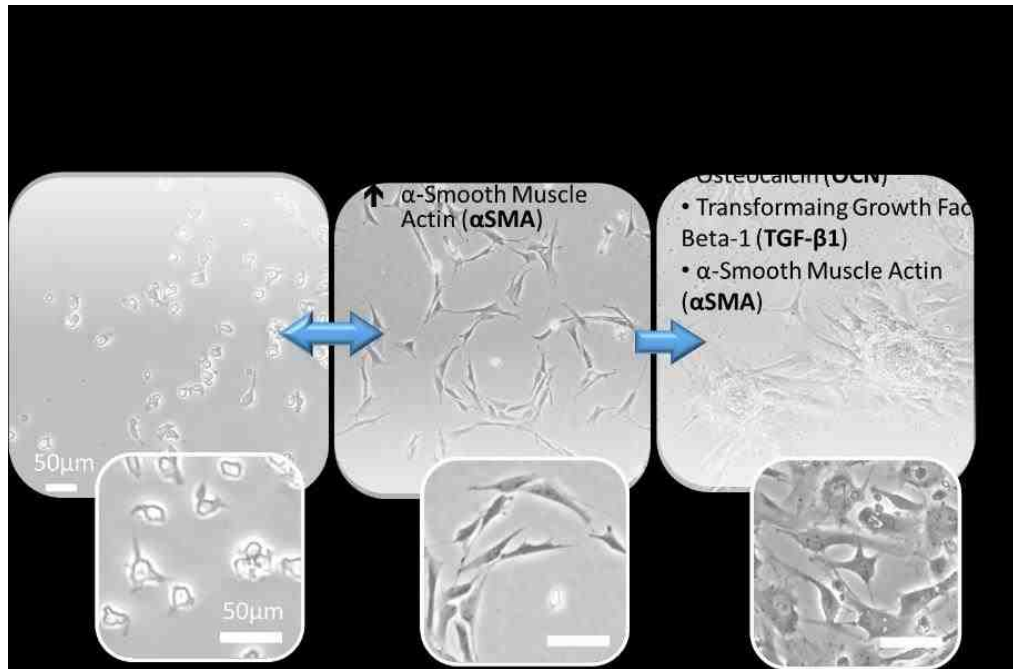
References

1.   Go, A.S., et al., *Heart disease and stroke statistics--2014 update: a report from the American Heart Association.* Circulation, 2014. **129**(3): p. e28-e292.

2.   Schoen, F.J. and R.J. Levy, *Tissue heart valves: Current challenges and future research perspectives.* Journal of Biomedical Materials Research, 1999. **47**(4): p. 439-465.

3.   Cuniberti, L.A., et al., *Development of mild aortic valve stenosis in a rabbit model of hypertension.* Journal of the American College of Cardiology, 2006. **47**(11): p. 2303-2309.

4.   Mendelson, K. and F.J. Schoen, *Heart Valve Tissue Engineering: Concepts, Approaches, Progress, and Challenges.* Annals of Biomedical Engineering, 2006. **34**(12): p. 1799-1819.

5.   Dweck, M.R., N.A. Boon, and D.E. Newby, *Calcific Aortic Stenosis A Disease of the Valve and the Myocardium.* Journal of the American College of Cardiology, 2012. **60**(19): p. 1854-1863.

6.   Freeman, R.V. and C.M. Otto, *Spectrum of calcific aortic valve disease - Pathogenesis, disease progression, and treatment strategies.* Circulation, 2005. **111**(24): p. 3316-3326.

7.   Kershaw, J.D.B., et al., *Specific regional and directional contractile responses of aortic cusp tissue.* Journal of Heart Valve Disease, 2004. **13**(5): p. 798-803.

8.   Hinton, R.B. and K.E. Yutzey, *Heart Valve Structure and Function in Development and Disease*, in *Annual Review of Physiology, Vol 73*, D. Julius and D.E. Clapham, Editors. 2011, Annual Reviews: Palo Alto. p. 29-46.

9.   Buchanan, R.M. and M.S. Sacks, *Interlayer micromechanics of the aortic heart valve leaflet.* Biomechanics and Modeling in Mechanobiology, 2014. **13**(4): p. 813-826.

10.   Doehring, T.C., M. Kahelin, and I. Vesely, *Mesostructures of the aortic valve.* Journal of Heart Valve Disease, 2005. **14**(5): p. 679-686.

11.   Merryman, W.D. and F.J. Schoen, *Mechanisms of Calcification in Aortic Valve Disease: Role of Mechanokinetics and Mechanodynamics.* Current cardiology reports, 2013. **15**(5): p. 355-355.

12.   Mozaffarian, D., et al., *Heart Disease and Stroke Statistics—2016 Update. A Report From the American Heart Association*, 2016. **133**(4): p. e38-e360.

13.   Tomasek, J.J., et al., *Myofibroblasts and Mechano: Regulation of Connective Tissue Remodelling.* Nature Reviews Molecular Cell Biology, 2002. **3**(5): p. 349-363.

14.   Schroer, A.K. and W.D. Merryman, *Mechanobiology of myofibroblast adhesion in fibrotic cardiac disease.* J Cell Sci, 2015. **128**(10): p. 1865-1875.

15.   Legg, M., E. Mathews, and R. Pelzer, *The design and development of a stented tissue mitral and aortic heart valve replacement for human implantation.* Cardiovascular Journal of Africa, 2012. **23**(3): p. 126-130.

16.   Schmidt, C.E. and J.M. Baier, *Acellular vascular tissues: natural biomaterials for tissue repair and tissue engineering.* Biomaterials, 2000. **21**(22): p. 2215-2231.

17.   Yap, C.-H. and M. Yii, *Allograft Aortic Valve Replacement in the Adult: A Review.* Heart, Lung and Circulation, 2004. **13**(1): p. 41-51.

18.   Palka, P., et al., *Primary Aortic Valve Replacement With Cryopreserved Aortic Allograft.* Circulation, 2002. **105**(1): p. 61.

19.   O'Brien, M.F., et al., *Allograft aortic valve replacement: Long-term follow-up.* The Annals of Thoracic Surgery, 1995. **60**(SUPPL. 2): p. S65-S70.

20.   Balaoing, L.R., et al., *Age-Related Changes in Aortic Valve Hemostatic Protein Regulation.* Arteriosclerosis Thrombosis and Vascular Biology, 2014. **34**(1): p. 72-+.

21.   Richards, J., et al., *Side-Specific Endothelial-Dependent Regulation of Aortic Valve Calcification Interplay of Hemodynamics and Nitric Oxide Signaling.* American Journal of Pathology, 2013. **182**(5): p. 1922-1931.

22.   Gould, S.T., et al., *The role of valvular endothelial cell paracrine signaling and matrix elasticity on valvular interstitial.* Biomaterials, 2014. **35**(11): p. 3596-3606.

23.   Ali, O.A., et al., *Interactions between inflammatory activation and endothelial dysfunction selectively modulate valve disease progression in patients with bicuspid aortic valve.* Heart, 2014. **100**(10): p. 800-805.

24.   Kennedy, J.A., et al., *Inhibition of calcifying nodule formation in cultured porcine aortic valve cells by nitric oxide donors.* European Journal of Pharmacology, 2009. **602**(1): p. 28-35.

25.   Bosse, K., et al., *Endothelial nitric oxide signaling regulates Notch1 in aortic valve disease.* Journal of Molecular and Cellular Cardiology, 2013. **60**: p. 27-35.

26.   Zeng, Q.C., et al., *Notch1 Promotes the Pro-Osteogenic Response of Human Aortic Valve Interstitial Cells via Modulation of ERK1/2 and Nuclear Factor-kappa B Activation.* Arteriosclerosis Thrombosis and Vascular Biology, 2013. **33**(7): p. 1580-1590.

27.   Chen, J., et al., *Notch1 mutation leads to valvular calcification through enhanced myofibroblast mechanotransduction.* Arterioscler Thromb Vasc Biol, 2015. **35**(7): p. 1597-1605.

28.   Chen, J., et al., *Biophysical analysis of dystrophic and osteogenic models of valvular calcification.* J Biomech Eng-T ASME, 2015. **137**(2): p. 6.

29.   Liu, A.C., V.R. Joag, and A.I. Gotlieb, *The emerging role of valve interstitial cell phenotypes in regulating heart valve pathobiology.* Am J Pathol, 2007. **171**(5): p. 1407-1418.

30. Wang, H., et al., *Characterization of cell subpopulations expressing progenitor cell markers in porcine cardiac valves.* Plos One, 2013. **8**(7): p. 11.

31. Chen, J.H., et al., *Identification and characterization of aortic valve mesenchymal progenitor cells with robust osteogenic calcification potential.* Am J Pathol, 2009. **174**(3): p. 1109-1119.

32. Kheradvar, A., et al., *Emerging Trends in Heart Valve Engineering: Part I. Solutions for Future.* Annals of Biomedical Engineering, 2015. **43**(4): p. 833-843.

33. Reimer, J., et al., *Implantation of a Tissue-Engineered Tubular Heart Valve in Growing Lambs.* Annals of Biomedical Engineering, 2017. **45**(2): p. 439-451.

34. Reimer, J.M., et al., *Pediatric tubular pulmonary heart valve from decellularized engineered tissue tubes.* Biomaterials, 2015. **62**: p. 88-94.

35. Puperi, D.S., et al., *3-dimensional spatially organized PEG-based hydrogels for an aortic valve co-culture model.* Biomaterials, 2015. **67**: p. 354-364.

36. Nemir, S. and J.L. West, *Synthetic Materials in the Study of Cell Response to Substrate Rigidity.* Annals of Biomedical Engineering, 2010. **38**(1): p. 2-20.

37. Duan, B., et al., *Three-dimensional printed trileaflet valve conduits using biological hydrogels and human valve interstitial cells.* Acta Biomaterialia, 2014. **10**(5): p. 1836-1846.

38. Gould, S.T. and K.S. Anseth, *Role of cell–matrix interactions on VIC phenotype and tissue deposition in 3D PEG hydrogels.* Journal of Tissue Engineering and Regenerative Medicine, 2016. **10**(10): p. E443-E453.

39. Benton, J.A., B.D. Fairbanks, and K.S. Anseth, *Characterization of Valvular Interstitial Cell Function in Three Dimensional Matrix Metalloproteinase Degradable PEG Hydrogels.* Biomaterials, 2009. **30**(34): p. 6593-6603.

40. Dsouza, S.E., M.H. Ginsberg, and E.F. Plow, *Arginyl-Glycyl-Aspartic acid (RGD) -a cell- adhesion motif.* Trends in Biochemical Sciences, 1991. **16**(7): p. 246-250.

41. Rodriguez, K.J. and K.S. Masters, *Regulation of valvular interstitial cell calcification by components of the extracellular matrix.* Journal of Biomedical Materials Research Part A, 2009. **90A**(4): p. 1043-1053.

42. Ruoslahti, E. and M.D. Pierschbacher, *New perspectives in cell -adhesion-RGD and integrins.* Science, 1987. **238**(4826): p. 491-497.

43. Taubenberger, A.V., et al., *The effect of unlocking RGD-motifs in collagen I on pre-osteoblast adhesion and differentiation.* Biomaterials, 2010. **31**(10): p. 2827-2835.

44. Rodriguez, K.J., L.M. Piechura, and K.S. Masters, *Regulation of valvular interstitial cell phenotype and function by hyaluronic acid in 2-D and 3-D culture environments.* Matrix Biol, 2011. **30**(1): p. 70-82.

45.   Gu, X.X. and K.S. Masters, *Regulation of valvular interstitial cell calcification by adhesive peptide sequences.* J Biomed Mater Res A, 2010. **93A**(4): p. 1620-1630.

46.   Gould, S.T., N.J. Darling, and K.S. Anseth, *Small peptide functionalized thiol-ene hydrogels as culture substrates for understanding valvular interstitial cell activation and de novo tissue deposition.* Acta Biomaterialia, 2012. **8**(9): p. 3201-3209.

47.   Rush, M.N., K.E. Coombs, and E.L. Hedberg-Dirk, *Surface chemistry regulates valvular interstitial cell differentiation in vitro.* Acta Biomater, 2015. **28**: p. 76-85.

48.   Baker, B.M. and C.S. Chen, *Deconstructing the third dimension – how 3D culture microenvironments alter cellular cues.* Journal of Cell Science, 2012. **125**(13): p. 3015.

49.   Leonard, A.T., *Fabrication and Characterization of Synthetic Substrates for Use in Rigididty Cell Culture Studies of Valvular Interstital Cells for Aortic Valve Tissue Engineering.* 2011.

50.   Merryman, W.D., et al., *Correlation between heart valve interstitial cell stiffness and transvalvular pressure: implications for collagen biosynthesis.* American Journal of Physiology-Heart and Circulatory Physiology, 2006. **290**(1): p. H224-H231.

51.   Maleki, H., et al., *A metric for the stiffness of calcified aortic valves using a combined computational and experimental approach.* Medical & Biological Engineering & Computing, 2014. **52**(1): p. 1-8.

52.   van Geemen, D., et al., *Age-dependent changes in geometry, tissue composition and mechanical properties of fetal to adult cryopreserved human heart valves.* Plos One, 2016. **11**(2): p. 20.

53.   Martin, C. and W. Sun, *Biomechanical characterization of aortic valve tissue in humans and common animal models.* Journal of Biomedical Materials Research Part A, 2012. **100A**(6): p. 1591-1599.

54.   France, R.M. and R.D. Short, *Plasma treatment of polymers: The effects of energy transfer from an argon plasma on the surface chemistry of polystyrene, and polypropylene. A high-energy resolution X-ray photoelectron spectroscopy study.* Langmuir, 1998. **14**(17): p. 4827-4835.

55.   Schroeder, J.A., et al., *Form and function of developing heart valves: coordination by extracellular matrix and growth factor signaling.* Journal of Molecular Medicine, 2003. **81**(7): p. 392-403.

Chapter 2

Specific Aims

Overall Objective

As the world population becomes more aged, the burden on medical care systems continues to increase. With a disproportionate effect on the elderly, valvular heart disease in the US is estimated to affect 2.8% of the population. The current replacement valves for diseased heart valves have major limitations in their limited lifespan or requirement of lifelong anticoagulation therapies. Therefore, the <u>objective of this body of work</u> was to identify and develop synthetic environments to grow healthy tissue engineered aortic valve tissue *in vitro*.

In the course of this work the following specific aims were investigated:

Specific Aim 1: Identify relevant VIC subpopulations for tissue engineering.

To identify possible subpopulations within valvular interstitial cells for use in synthetic culture systems, subpopulations of VICs were isolated and characterized based on differences in adhesion during culture.

Specific Aim 2: Define environmental factors that create the ideal substrate to grow valvular interstitial cells models of health or disease.

To define how specific environmental factors such as surface charge and substrate stiffness affect valvular interstitial cell behavior *in vitro* and identify scaffolds for the control of valvular interstitial cell behavior.

Specific Aim 3: Develop a modifiable 3D hydrogel system to elucidate the effects of microenvironmental cues on VIC behavior in 3D.

To develop a tunable, three-dimensional scaffold to study the effects of charged environments and material stiffness on the growth and behavior of valvular interstitial cells in a relevant tissue engineering model.

By characterizing valvular interstitial cell subpopulations and environmental cues of synthetic scaffolds that support valvular interstitial cell growth while dictating tissue formation, we have advanced the knowledge of aortic valve tissue engineering. In addition, this work has also provided new cell culture systems that are more accurate models of the aortic valve for the development of better AVD therapeutics.

Chapter 3

Isolation and Characterization of Valvular Interstitial Cell Subpopulations

Kent E. Coombs[1,2], Matthew N. Rush[2,3], David Santistevan[2], Elizabeth L. Hedberg-Dirk[2,4]

[1]*Biomedical Science Graduate Program,* [2]*Center for Biomedical Engineering,* [3]*Nanoscience and Microsystems Engineering Graduate Program,* [4]*Department of Chemical and Biological Engineering, University of New Mexico, Albuquerque, NM.*

Abstract

Valvular interstitial cells are a heterogeneous population that are normally isolated as a single population from the aortic heart valve. Separating VICs into different subpopulations has been difficult *in vitro* due to a lack of unique markers. This study uses a simple adhesion based detachment technique to isolate subpopulations of VICs which we call more adherent and less adherent. Characterization of these subpopulations shows that the more adherent VIC subpopulation is an osteoblastic-like (OB) phenotype expressing increased alpha smooth muscle actin (αSMA), osteocalcin (OCN), and transforming growth factor beta 1 (TGF-β1). Three different integrins were investigated as possible surface markers of VIC differentiation; alpha-V beta-3 (αVβ3), alpha-V beta-5 (αVβ5), and alpha-2 beta-1 (α2β1) in more adherent, less adherent, and unsorted VICs, respectively. αVβ3 was significantly upregulated in more adherent VICs and, when correlated with the increase in osteoblastic markers, αVβ3 should be an interesting marker for sorting VIC subpopulations directly from the aortic valve in future work. Additionally, the more adherent subpopulation proliferates more slowly and has a rhomboidal morphology similar to that of osteoblastic media induced VICs. Less adherent VICs on the other hand, proliferate significantly faster, don't express OB markers, and don't express αVβ3. These data suggest less adherent VICs are a healthier active subpopulation that would be useful for heart valve tissue engineering research. Overall, differential detachment methods were used to isolate a more adherent subpopulation with an osteoblastic phenotype and an active "healthy", less adherent VIC subpopulation from the

heterogeneous VIC population exists in the valve. These results highlight the

heterogeneity of recently excised VICs and show that relevant subpopulations

exist in the valve to study both valve health and disease.

Background

  Aortic valve disease (AVD) elevates mortality and cardiovascular complications due to increased burden on the heart caused by obstructed blood flow due to calcification and stenosis of the valve (1, 2). Disease progression is attributed to a native valve cell population, valvular interstitial cells (VICs). *In vivo* these cells are dispersed throughout the three layers of the aortic valve the fibrosa, spongiosa, and ventricularis. VICs are responsible for the build-up of matrix and the formation of calcific nodules that result in thickening and loss of flexibility of the valve leaflets leading to AVD (3). Interestingly, calcified nodules first appear in the fibrosa layer of the valve (4). This suggests that the unique environment of the fibrosa make VICs in that area more likely to undergo osteoblastic differentiation and create nodules. Despite this observation, when VICs are taken from the valve, little work has been done to try and separate this more osteoblastic-prone subpopulation of cells.

  Instead, VICs have been removed from the entire valve and treated as a homogenous group characterized as having a highly plastic phenotype with the ability to differentiate *in vitro* into activated/myofribroblastic, osteoblastic-like, progenitor, and quiescent phenotypes (5-9). In the laboratory the two most commonly observed phenotypes are activated/myofibroblastic (aVICs) and osteoblastic (OB VICs), identified by markers outlined in Table 1. aVIC are characterized as VICs that proliferate rapidly and secrete ECM, whereas OB VIC represent the disease phenotype that form calcific nodules *in vitro* with the expression of bone specific genes like osteocalcin, osteopontin, and alkaline

43

phosphatase (Table 1). It is unclear from this work if the multiple phenotypes *in vitro* are a result of the *in vivo* VIC population changing phenotype or if culture conditions allow a specific subpopulation of VICs to become dominate and take over the culture. To answer this question, the first step is to identify specific subpopulations of VICs.

In prior studies, a small but distinct VIC morphologic and phenotypic subpopulations have been isolated and shown to be more reactive to osteoblastic (OB) differentiation in OB induction media (10-12). For example, a mesenchymal progenitor cell population isolated from VICs using a colony forming unit assay, can differentiate into osteogenic, adipogenic, chondrogenic, or myofibrogenic lineages using different induction medias (10).

Another progenitor cell subpopulation was isolated using the cell surface marker ABCG2$^+$ and fluorescent activated cell sorting. This small (~5%) ABCG2$^+$ VIC subpopulation showed increased secretion of calcified extracellular matrix in osteoblastic induction media over ABCG2$^-$ populations (11). These studies demonstrate the existence of VIC subpopulations which are responsive to specific environmental cues.

Currently, osteogenic media induction is commonly used *in vitro* to make VIC's exhibit osteoblastic-like (OB) properties (10, 11, 13-15). However, the use of osteogenic induction media does not recapitulate disease development conditions *in vivo* (16, 17). Presumably, chronic buildup of extracellular matrix (ECM) causing valve thickening and stiffening is due to a small population of OB VICs (16, 18). It seems more likely, therefore, that a small OB-like or OB-prone

44

subpopulation of VICs exists natively within the valve that can cause disease later in life. Despite these observations, little work has been done to isolate, separate, or identify an OB prone VIC subpopulation within the valve. Therefore, we designed studies to identify a method to directly isolate various VIC subpopulations that can be used to better study VIC disease progression and to identify a healthy subpopulation for heart valve tissue engineering.

Some VICs take longer to detach from TCPS during passaging than others and in 2006 Belvins *et al* used a differential adhesion method to separate VICs grown on tissue culture polystyrene (12). They concluded that increased adhesion strength corresponded with a myofibroblastic phenotype using αSMA as the primary marker. However, recent work has shown that both the aVIC and OB VIC phenotypes show increased levels of αSMA *in vitro* (9, 19-21). We hypothesized that the more adherent VIC subpopulation is actually an osteoblastic phenotype that would have a faster doubling time and increased expression of OB genetic markers. The rationale behind this hypothesis was that the more adherent VIC subpopulation display an irregular cuboidal morphology similar to OB VICs. As such, additional markers to test for OB VICs were evaluated. The best marker of VIC OB differentiation is the bone specific protein osteocalcin (OCN) which is only seen in OB VICs. Additionally, transforming growth factor beta 1 (TGF-β1) which is upregulated in AVD and used to force VIC to an OB phenotype was also measured as a marker of VIC OB differentiation (16, 19, 22, 23).

To reliably separate these subpopulations directly from the valve, surface markers that can be used for fluorescent activated cell sorting need to be identified. Given recent studies correlating integrin expression levels to changes in the phenotype of other cell types, differences in integrin expression of VIC cell subpopulations were examined (3, 24-26). α2β1, a collagen 1 binding integrin, was investigated because during AVD collagen 1 expression and fragmentation greatly increases (16, 27). Therefore, increased presence of α2β1 in VICs is reflective of VICs during AVD. Additionally, the integrins αVβ3 and αVβ5 were measured. In the valve αVβ3 is minimally expressed, but becomes significantly upregulated in aVICs *in vitro.* αVβ5 increases when pre-osteoblastic cell lines are induced to and osteoblastic phenotype (16, 25, 26, 28-30). These markers were investigated as potential markers id aVIC and OB VIC subpopulations. The overall aim of this work was to characterize the VIC subpopulations isolated from the heterogeneous population of VICs and to identify cell surface markers.

Material and Methods

Cell Culture

VICs were extracted from porcine aortic heart valves using a previously published method (31). Briefly, hearts were shipped overnight on ice (Hormel). Aortic valve leaflets were excised from hearts and treated with collagenase II (Worthington) (15 min, 37°C) and scraped to remove the unwanted valvar endothelial cells (VECs) located on the surface of the leaflet. Tissue was then incubated in fresh collagenase to release the valvular interstitial cells. After a 60

to 70 min incubation, the remaining tissue was removed and the collagenase/cell

solution collected and spun down. The cell pellet was resuspended in growth

media [199 EBSS Hyclone media supplemented with 10% fetal bovine serum

(FBS) (Hyclone), 1% penicillin/streptavidin (Hyclone), and 1% fungizone

(Hyclone)]. The cell suspension was treated with Dynabeads CD31+ Endothelial

Cell (ThermoFisher Scientific) to remove any residual valvular endothelial cells.

The resulting VICs were plated onto TCPS and cultured under normal conditions

at 37ºC with 5% CO_2 in growth media. These cells were considered to be

passage 0. At ~80% confluence, these cells, underwent the differential

attachment protocol.

Osteoblastic media [199 EBSS Hyclone media supplemented with 10%

FBS, 10^{-8} M dexamethasone, 10 mM ß-glycerolphosphate, 2mM ascorbic acid]

was added 12 hours after seeding to induced VICs to OB phenotype. A small

portion of VICs from P0 did not undergo differential attachment and were frozen

to be used as unsorted heterogeneous VICs.

Differential Detachment Protocol and Kinetic Study

P0 VICs were grown to 80% confluence, media removed and cells were washed

in Dulbecco's Phosphate Buffer Saline (DPBS) without calcium or magnesium

and treated with 2 mL of dilute trypsin EDTA (0.025% DPBS). After two minutes

of incubation at 37˚C, the solution and lifted cells were collected. New dilute

trypsin solution was added to the flask and incubated for 2 additional minutes at

37 °C and again the solution and released cells were collected. Additional dilute

trypsin treatment steps with incubation and collection were repeated until all cells were detached from the flask as determined by optical microscopy. The cell number of each collection was counted using a Z2 Beckman Coulter Counter to determine the total number of cells. The first 25% of cells to detach (less adherent), and the last 25% of cells to detach (more adherent) were kept. Less adherent and more adherent VICs were reseeded separately under normal conditions, becoming passage 1 cells (P1), and grown to 80% confluence. The dilute trypsin method described above was repeated except that from less adherent cell population only the 1st 25% of VICs to detach and from more adherent only the last 25% of VICs to detach were reseeded and used in subsequent passages. After the third dilute trypsin treatment, the cell number of each fraction of the less and more adherent cell populations was plotted before reseeding. The next passage was done using a normal trypsinization and freeze down of P3 cells. A small proportion of the P0 VICs did not undergo the differential attachment protocol and were passaged 3 times normally before being frozen to generate the heterogeneous and OB VIC cell populations.

Growth Curve

The doubling times of the less adherent, more adherent, heterogeneous VICs and OB VICs populations were determined. Briefly, all cell types were seeded at 25,000 cells/cm^2 in a 6-well TCPS plates with growth media. OB VIC induction media was added to OB VICs 12 hours after seeding. Media was changed every 2 days. At each time point 3-5 wells of growing VICs were

trypsinized, and counted on a Z2 Beckman Coulter Counter. Doubling times were

calculated as the slope of the best fit line to the area of exponential growth of

each curve.

Gene Expression

 Less adherent, more adherent, and heterogeneous VIC gene expression was

examined at day 3. VIC mRNA was extracted using RNeasy plus Micro kits

(Qiagen) and concentration determined using a NanoDrop 2000C. Next, 100 ng

of mRNA were converted to cDNA as per manufacture's instructions using two-

step RT PCR GoScript Reverse Transcription Kit (Promega). The cDNA was

then interrogated by the ΔΔCT method using qPCR on a Step-One RT PCR

System (Applied Biosystems). Taq-Man probes for alpha smooth muscle actin

(αSMA) (Ss04245588_m1), osteocalcin (OCN) (Ss03373655_s1), transforming

growth factor beta 1 (TGF-β1) (Ss03382325_u1), Collagen 1 (Ss03375690_u1),

elastin (AJLJIR9), and the endogenous control glyceraldehyde 3-phosphate

dehydrogenase (GAPDH) (Ss03374854_g1) were used.

Integrin Expression

 Heterogeneous, more adherent, and less adherent VICs were grown for 3 days

and treated with 5mM EDTA in DPBS to facilitate detachment followed by gentle

scraping. Collected cells were pelleted and resuspended at ~500,000 cell/ml in

ice cold phosphate-buffered saline (PBS), 1% BSA, and 0.02% sodium azide.

Cells were then labeled with 3uL/ml of the following antibodies (ab), αvβ5-Alexa

647 MS (Novus, FAB2528R), αvβ3-FITC mouse (Sigma-Aldrich, MAB1976F),

α2β1 mouse (Sigma-Aldrich, MAB1998Z), mouse IgG1 κ -FITC (Biolegend,

400110), mouse IgG1, κ- Alexa 647 (Biolegend, 400130), and mouse IgG1 κ

(Biolegend, 401402) for 30 min at 4°C. The secondary ab Alexa 488 goat anti-

mouse (Life Technologies A11017) 1.5 uL/mL was added to samples stained

with primary α2β1 Ms, mouse (BALB/c) IgG1, or IgG1 κ primary ab's and

incubated for another 20 min on ice. All samples were kept on ice until read on

the Attune NXT Flow cytometer.

Statistics

All results were analyzed using one-way ANOVA and two-tailed t-tests to

determine significance at a 95% confidence interval ($p < 0.05$). All analyses were

done using GraphPad Prism 7 software.

Results

VIC Subpopulation Isolation and Growth

Two subpopulations of VICs (more adherent and less adherent) were

isolated (Fig 1). Less adherent VICs detached more rapidly than more adherent

VICs with 90% of each subpopulation detaching in 8 and 14 minutes,

respectively (Fig 2). Distinct morphologies were also observed at day 3 with less

adherent having an elongated morphology compared to more adherent which

have a more irregular cuboidal morphology (Fig 3). Heterogeneous VICs

displayed a combination of both morphologies. Growth curves determined that

50

the doubling times of less adherent VICs and OB VICs were significantly faster than those of more adherent and heterogeneous VICs (Fig 4) ($p \leq 0.05$ n=3).

VIC Phenotype

To test for differences in VIC phenotype between the VIC subpopulations at day 3, mRNA expression of αSMA, OCN, TGF-β1, collagen 1, and elastin were measured. αSMA and OCN expression were significantly higher in more adherent VICs compared to all other groups (Fig 5). TGF-β1 expression was higher in more adherent VICs compared to less adherent VICs. Collagen expression was similar between all cell subpopulations, while elastin expression was significantly higher in more adherent cells when compared to heterogeneous but not less adherent VICs (Fig 5). The upregulation of αSMA, OCN, and TGF-β1 in more adherent VICs suggests this subpopulation is an osteoblastic phenotype.

Subpopulation Surface Markers

To identify surface markers for the different subpopulations of VICs, integrin expression was determined. Levels of integrins αVβ5, αVβ3, and α2β1 were investigated using flow cytometry (Fig 6). αVβ5 was not statistically different in more adherent and less adherent VICs but was significantly higher in the heterogeneous subpopulation. αVβ3 was significantly higher between more adherent VICs compared to heterogeneous VICs and was not detected in the less adherent subpopulation. α2β1 was significantly lower in less adherent VICs compared to other VIC subpopulations. Therefore, αVβ3 and α2β1 are good

markers to distinguish the less adherent from the more adherent VIC subpopulations.

Discussion

VICs are a heterogeneous population of cells within the spongiosa, ventricularis, and fibrosa layers of the aortic valve. Each layer has a distinct ECM environment as well as different mechanical properties (32). Therefore, VICs residing in different layers are expected to have a slightly different phenotype. This idea is also supported by the observation that VICs cultured *in vitro* display multiple morphologies (12). However, separating VICs to study the behaviors of subpopulations has been difficult due to a lack of methods and unique markers to distinguish and separate subpopulations. Using a differential detachment method, two distinct subpopulations of VICs with differing levels of adhesion to TCPS were isolated. Less adherent and more adherent VIC subpopulations were tested for differences in morphology, proliferation rate, gene expression, ALP activity, and integrin expression. In previous studies, VICs induced to an OB phenotype using OB media had an increased rate of proliferation compared to untreated VICs (20, 21, 23). We therefore hypothesized that the more adherent VIC population would be an osteoblastic phenotype with a faster doubling time and increased expression of OB genetic markers (19, 23). A difference in proliferation rates was found, but the more adherent VICs grew significantly slower than OB and less adherent VICs (Fig 4).

The cytoskeletal protein αSMA was originally used to identify activated/myofibroblastic VICs. More recently it has been shown to be upregulated in osteoblastic VICs both *in vitro* and *in vivo* with a correlation to increased αSMA stress-fiber formation (16, 19, 21, 23). In this study αSMA expression was significantly higher in more adherent VICs and, as seen previously, associated with a more cuboidal VIC morphology (12). The late stage marker for osteoblastic differentiation in VICs, osteocalcin, was also upregulated in more adherent VICs, corresponding to recent findings suggesting an osteoblastic phenotype (19, 21). Furthermore, TGF-β1 expression was upregulated in the more adherent subpopulation (33). While TGF-β1 expression is not an established marker of OB differentiation *in vitro*, it has been shown to be upregulated in stenotic and calcified valves and is commonly added to VIC media to induce an OB phenotype (16, 33, 34). In conclusion, osteoblastic media induced unsorted VICs to proliferate but, it is the slower growing, more adherent VIC subpopulation which exhibits OB markers and morphology. If this subpopulation's behaviors exists *in vivo,* it would suggest that the faster proliferation rate of less adherent VICs may dominate heart valve repair over the slow growing OB-like more adherent VICs. However, the long term behaviors of osteoblastic more adherent but slow growing VICs could eventually lead to valve fibrosis and calcification.

Another difference observed between less and more adherent VICs is the differential expression of ECM proteins. In the heart valve, collagen and elastin are the most common ECM proteins (8, 27, 35-37). During AVD and with aging

collagen content increases. *Ex vivo* studies of the AV cells show VICs undergo OB differentiation when the collagen in the valve is degraded (16, 27, 38). Although in this study no significant differences in collagen I expression were detected between populations, the differences in the ECM proteins should be further investigated as potential causes of differential growth and phenotype.

Elastin has an intricate role in the control of heart valve health. Proper formation of elastin with fibrillin microfibrils regulates TGFβ activity (39, 40). TGFβ is normally sequestered in the ECM on the elastin/fibrillin microfibrils to inhibit biological activity. As elastin becomes dysregulated during AVD, sequestration of TGFβ is disrupted resulting in increased availability of TGFβ and therefore increased signaling (39, 40). Increased elastin expression has been correlated with VIC OB differentiation caused by surface stiffness and surface chemistry, independent of OB differentiation media (19, 21). In this study, the highest levels of elastin were seen in the more adherent VIC subpopulation, with an OB-like phenotype. We hypothesize that early elastin expression and possibly loss of proper structural control *in vitro* leads to loss of fibrillin microfibrils to sequester TGF-β1. As a result, increased TGF-β1 expression could then help to force VIC toward the OB VIC phenotype. To test this hypothesis, expression of other ECM proteins such as fibronectin should be measured and secreted proteins levels examined along with elastin fiber formation.

During AVD collagen 1 expression increases and existing fibers fragment (16, 27). Because the primary integrin binding partner for collagen 1 is α2β1,

increased binding and activation of α2β1 may be related to AV disease progression. Interestingly in this study, the less adherent subpopulation expresses less α2β1 than either more adherent or heterogeneous VICs. As this population seems to be the most resistant to OB differentiation *in vitro,* α2β1 expression may be a marker of an osteoblastic VIC subpopulation.

VICs with αvβ3 in previous VIC literature have been considered an activated phenotype that express αSMA and have increased spreading in hydrogels (26). One of αvβ3's binding partners in the ECM is fibronectin which increases in expression during AVD (16, 28). We observed that αvβ3 is highest in more adherent VICs so that high levels of αvβ3 correlated with an osteoblastic VIC phenotype rather than an activated phenotype as previously suggested (3, 26). However, unlike previous studies, increases in osteoblastic markers OCN and TGF-β1 were also seen in more adherent VICs. These data suggest that the more adherent VICs have transitioned from the activated VIC phenotype to an osteoblastic phenotype. αvβ3 has also been shown to bind to the bone protein OPN which is also upregulated during AVD. It would be interesting to measure OPN in the current subpopulations. Upregulation of OPN in less adherent VICs would further support that they are an osteoblastic subpopulation (41, 42). In conclusion, αvβ3 may be an integrin surface marker that identifies the osteoblastic prone VIC subpopulation within the AV. Future work could use this integrin as a surface marker to sort healthy and OB prone VICs directly from the valve.

Another interesting aspect of this work is that the heterogeneous VIC population did not always fall directly between more adherent and less adherent VICs. This is likely due to the influence of the different VIC subpopulations have on each other within heterogeneous VIC cultures. Additionally, there is a strong likelihood that there are subpopulations of VICs that we didn't isolate with the adhesion based separation technique and these unidentified populations influence the overall behavior of the larger group.

In summary, this study examined osteoblastic disease markers of different VIC subpopulations through simple differential detachment methods, without using OB induction media. The more adherent VIC subpopulation isolated had increased mRNA expression of αSMA, OCN, TGF-β1, as well as increased ALP protein activity, suggesting that strongly adhered VICs are an osteoblastic VIC phenotype. Furthermore, doubling times show that the more adherent subpopulation of VICs proliferate at a slower rate than less adherent cells, contradicting the current hypothesis that OB VICs proliferate more quickly than activated VICs (23). Integrins αvβ3 and α2β1 were also found to be upregulated in the more adherent subpopulation and therefore may be surface markers to separate VIC subpopulations using fluorescence activated cell sorting. Overall, these results demonstrate the heterogeneity of VICs and identify a simple method to isolate a proliferative healthy subpopulation from an osteoblastic prone subpopulation within porcine aortic valves.

Figures and Tables

Table 1. VIC Phenotype Marker Summary			
Marker	VIC Phenotype	First Found	Citations
Alpha smooth muscle actin*	Activated[1,2,3]	Extracted from Valves[1,2,3]	1. Mulholland GL 1996
	Osteoblastic?[4,6]	*In vitro* systems[4,5]	2. Rabkin E. 2001 3. Lui 2007 4. Rush 2016 5. Coombs 2017
Osteocalcin	Osteoblastic	Human calcified valves[7] and vascular smooth muscle cells[8]	6. Srivatsa SS. 1997 7. Giachelli C.M. 2003
Osteopontin	Osteoblastic	Human and canine calcified valves[9,10] and vascular smooth muscle cells[3]	8. Srivatsa SS. 1997 9. Mohler, 1999 10. Giachelli C.M. 2003
Alkaline Phosphatase	Osteoblastic	Human calcified aortic valves[12] and *in vitro* culture[13]	11. Rajamannan, N.M. 2003 12. Monzack M.S. 2011
TGF-β1	Osteoblastic	Human calcified aortic valve cusps[14,15]	13. Jian B. 2003 14. Walker, G.A. 2004 15. Coombs 2016

*Originally a marker for activated/myofibroblastic VICs it has now be detected in high levels in osteoblastic VICs. List is not exhaustive.
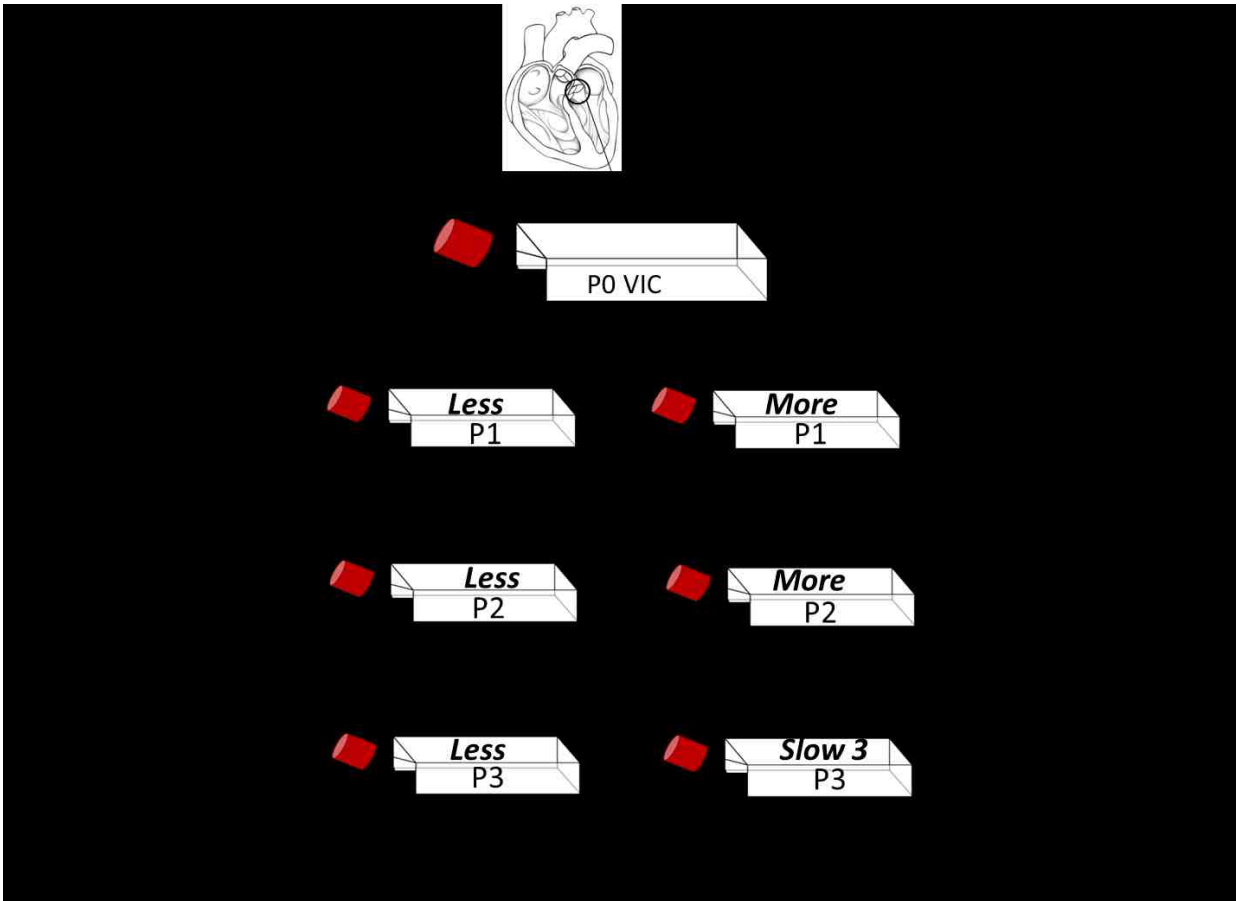
Figure 1. Schematics of pop-off procedure.
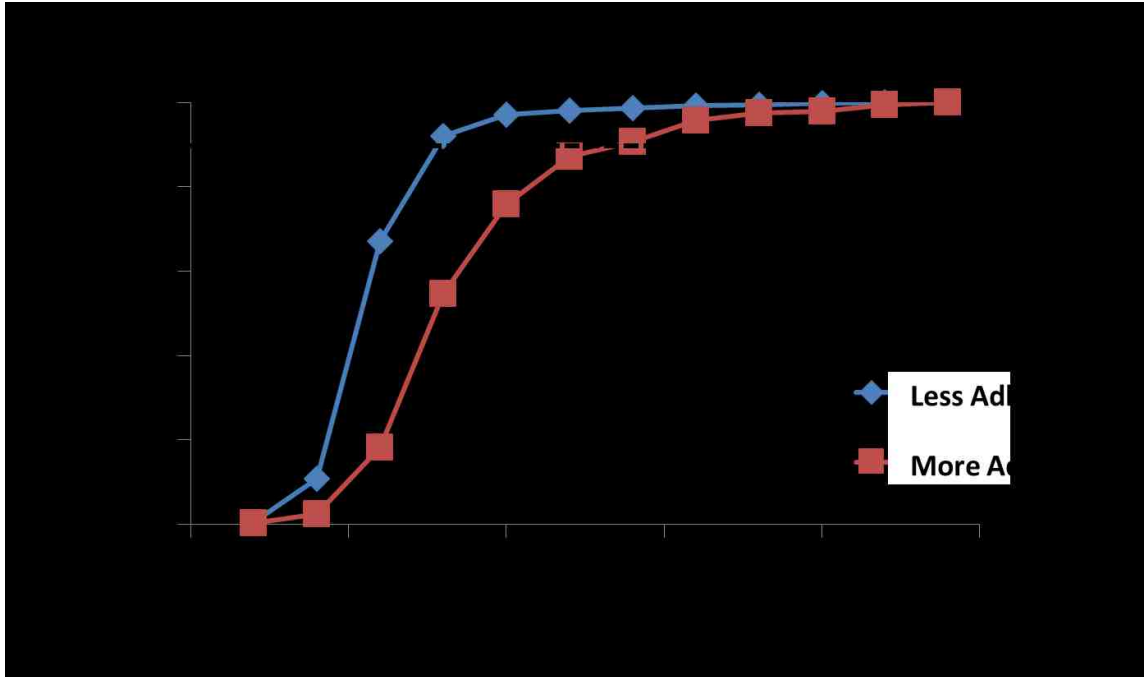
Figure 2. Detachment profile of more adherent and less adherent VIC subpopulations isolated through sequential addition of dilute (0.025%) trypsin. 90% of less adherent VICs are removed from the flask after 8 min (4 dilute trypsin treatments) while for more adherent VICs it take 14 minutes (7 trypsin treatments).
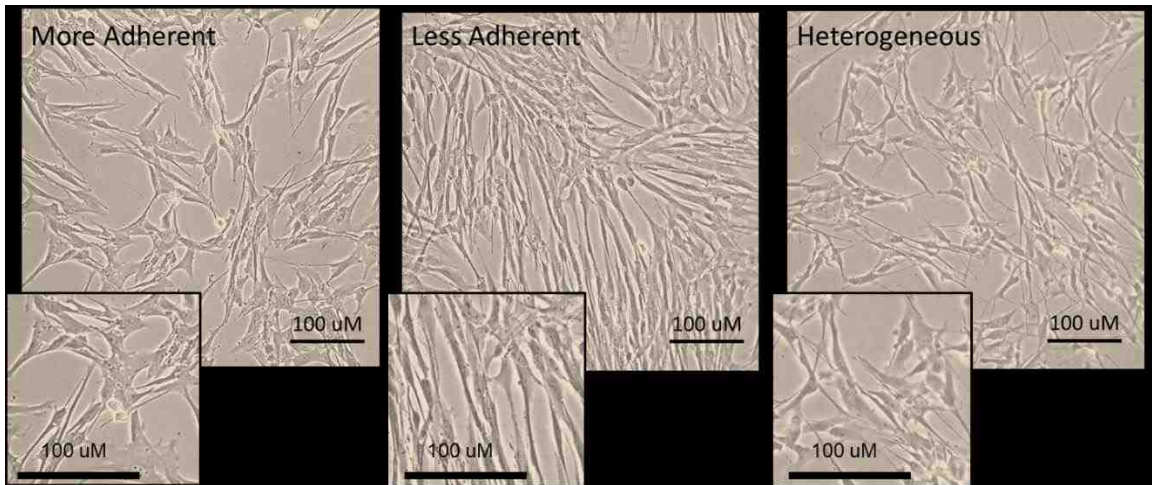
Figure 3. Optical microscopy after 3 days of growth shows the representative morphologies of different VIC subpopulations, with a rhomboidal morphology of more adherent VICs in comparison to less adherent VICs which have an elongated spindle like morphology.
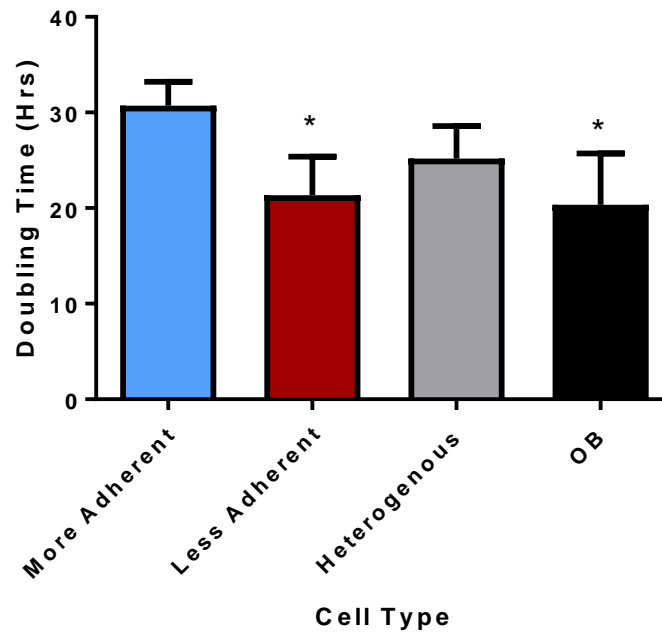
Figure 4. Doubling times in hours of heterogeneous, osteoblastic media induced, less adherent and more adherent VICs. OB and less adherent VICs grew significantly faster than more adherent VICs (p≤ 0.05*).
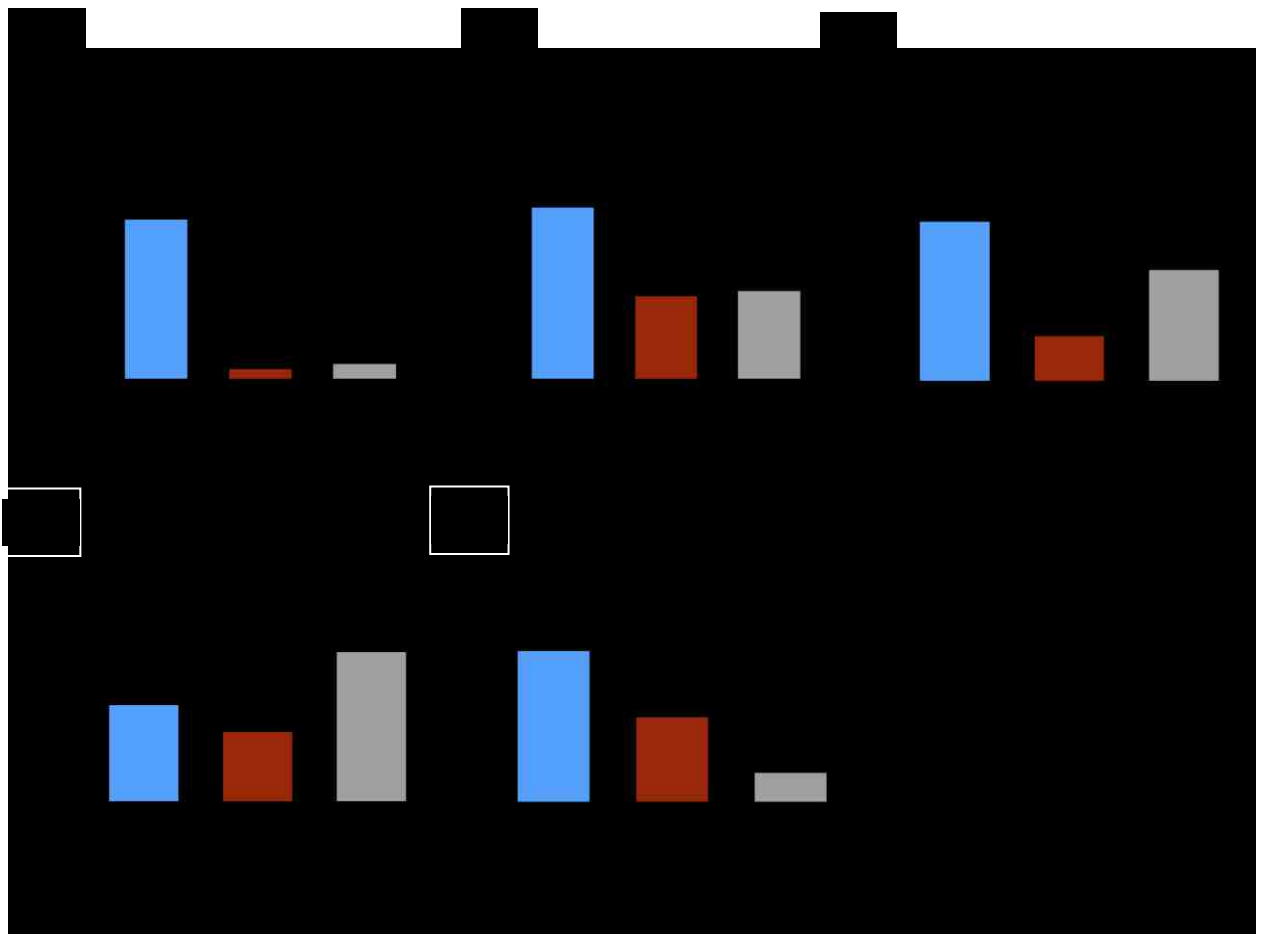
Figure 5. Genetic expression of αSMA, OCN, TGF-β1, collagen 1, and elastin normalized to the heterogeneous control population. A) More adherent VICs have significantly higher αSMA than all other subpopulations. B) OCN is upregulated in more adherent VICs. C) TGF-B1 is significantly higher in more adherent compared to less adherent VICs. D) No difference is seen in collagen expression. E) Heterogeneous VICs have significantly less elastin than other subpopulations (p≤ 0.05*).

Figure 6. Flow cytometry results of A) αVβ3 integrin b) αVβ5 and c) α2β1 expression in the three VICs subpopulations at day 3. A) Heterogeneous VICs have significantly less αVβ5 than more and less adherent VICs (*p = 0.05). B) More adherent VICs have significantly higher levels of αVβ3 than other VIC subpopulations. C) α2β1 is significantly lower in less adherent VICs.

References

1. Roberts, W.C., and Ko, J.M. Frequency by decades of unicuspid, bicuspid, and tricuspid aortic valves in adults having isolated aortic valve replacement for aortic stenosis, with or without associated aortic regurgitation. Circulation 2005;920-925.

2. Otto, C.M., Kuusisto, J., Reichenbach, D.D., Gown, A.M., and Obrien, K.D. Characterizationof the early lesion of degenerative valvular aortic-stenosis-histilogical and immunohistochemical studies. Circulation 1994;844-853.

3. Schroer, A.K., and Merryman, W.D. Mechanobiology of myofibroblast adhesion in fibrotic cardiac disease. Journal of Cell Science 2015;1865-1875.

4. Merryman, W.D., and Schoen, F.J. Mechanisms of Calcification in Aortic Valve Disease: Role of Mechanokinetics and Mechanodynamics. Current cardiology reports 2013;355-355.

5. Liu, A.C., Joag, V.R., and Gotlieb, A.I. The emerging role of valve interstitial cell phenotypes in regulating heart valve pathobiology. American Journal of Pathology 2007;1407-1418.

6. Furukawa, K.I. Recent advances in research on human aortic valve calcification. J Pharmacol Sci 2014;129-137.

7. Liu, A.C., Joag, V.R., and Gotlieb, A.I. The emerging role of valve interstitial cell phenotypes in regulating heart valve pathobiology. Am J Pathol 2007;1407-1418.

8. Spadaccio, C., Mozetic, P., Nappi, F., Nenna, A., Sutherland, F., Trombetta, M., Chello, M., and Rainer, A. Cells and extracellular matrix interplay in cardiac valve disease: because age matters. Basic Res Cardiol 2016;16.

9. Chen, J., Ryzhova, L.M., Sewell-Loftin, M.K., Brown, C.B., Huppert, S.S., Baldwin, H.S., and Merryman, W.D. Notch1 mutation leads to valvular calcification through enhanced myofibroblast mechanotransduction. Arterioscler Thromb Vasc Biol 2015;1597-1605.

10. Chen, J.H., Yip, C.Y.Y., Sone, E.D., and Simmons, C.A. Identification and characterization of aortic valve mesenchymal progenitor cells with robust osteogenic calcification potential. Am J Pathol 2009;1109-1119.

11. Wang, H., Sridhar, B., Leinwand, L.A., and Anseth, K.S. Characterization of cell subpopulations expressing progenitor cell markers in porcine cardiac valves. Plos One 2013;11.

12. Blevins, T.L., Carroll, J.L., Raza, A.M., and Grande-Allen, K.J. Phenotypic characterization of isolated valvular interstitial cell subpopulations. J Heart Valve Dis 2006;815-822.

13. Walker, G.A., Masters, K.S., Shah, D.N., Anseth, K.S., and Leinwand, L.A. Valvular myofibroblast activation by transforming growth factor-beta - Implications for pathological extracellular matrix remodeling in heart valve disease. Circ Res 2004;253-260.

14. Hjortnaes, J., Shapero, K., Goettsch, C., Hutcheson, J.D., Keegan, J., Kluin, J., Mayer, J.E., Bischoff, J., and Aikawa, E. Valvular interstitial cells suppress calcification of valvular endothelial cells. Atherosclerosis 2015;251-260.

15. Onishi, M., Fujita, Y., Yoshikawa, H., and Yamashita, T. Inhibition of Rac1 promotes BMP-2-induced osteoblastic differentiation. Cell Death Dis 2013;7.

16. Schroer, A.K., and Merryman, W.D. Mechanobiology of myofibroblast adhesion in fibrotic cardiac disease. J Cell Sci 2015;1865-1875.

17. Chen, J., Peacock, J.R., Branch, J., and Merryman, W.D. Biophysical analysis of dystrophic and osteogenic models of valvular calcification. J Biomech Eng-T ASME 2015;6.

18. van Geemen, D., Soares, A.L.F., Oomen, P.J.A., Driessen-Mol, A., den Broek, M., van den Bogaerdt, A.J., Bogers, A., Goumans, M., Baaijens, F.P.T., and Bouten, C.V.C. Age-dependent changes in geometry, tissue composition and mechanical properties of fetal to adult cryopreserved human heart valves. Plos One 2016;20.

19. Rush, M.N., Coombs, K.E., and Hedberg-Dirk, E.L. Surface chemistry regulates valvular interstitial cell differentiation in vitro. Acta biomaterialia 2015;76-85.

20. Rush, M.N., Coombs, K.E., and Hedberg-Dirk, E.L. Surface chemistry regulates valvular interstitial cell differentiation in vitro. Acta Biomater 2015;76-85.

21. Coombs, K.E., Leonard, A.T., Rush, M.N., Santistevan, D.A., and Hedberg-Dirk, E.L. Isolated effect of material stiffness on valvular interstitial cell differentiation. Journal of Biomedical Materials Research Part A 2017;51-61.

22. Monzack, E.L., and Masters, K.S. A time course investigation of the statin paradox among valvular interstitial cell phenotypes. Am J Physiol Heart Circul Physiol 2012;H903-H909.

23. Monzack, E.L., and Masters, K.S. Can valvular interstitial cells become true osteoblasts? A side-by-side comparison. J Heart Valve Dis 2011;449-461.

24. Rodriguez, K.J., and Masters, K.S. Regulation of valvular interstitial cell calcification by components of the extracellular matrix. Journal of Biomedical Materials Research Part A 2009;1043-1053.

25. Rodriguez, K.J., Piechura, L.M., and Masters, K.S. Regulation of valvular interstitial cell phenotype and function by hyaluronic acid in 2-D and 3-D culture environments. Matrix Biol 2011;70-82.

26. Benton, J.A., Fairbanks, B.D., and Anseth, K.S. Characterization of valvular interstitial cell function in three dimensional matrix metalloproteinase degradable PEG hydrogels. Biomaterials 2009;6593-6603.

27. Rodriguez, K.J., Piechura, L.M., Porras, A.M., and Masters, K.S. Manipulation of valve composition to elucidate the role of collagen in aortic valve calcification. BMC Cardiovasc Disord 2014;10.

28. Gu, X.X., and Masters, K.S. Regulation of valvular interstitial cell calcification by adhesive peptide sequences. J Biomed Mater Res A 2010;1620-1630.

29. Stephens, E.H., Durst, C.A., Swanson, J.C., Grande-Allen, K.J., Ingels, N.B., and Miller, D.C. Functional Coupling of Valvular Interstitial Cells and Collagen Via alpha(2)beta(1) Integrins in the Mitral Leaflet. Cell Mol Bioeng 2010;428-437.

30. Keselowsky, B.G., Collard, D.M., and Garcia, A.J. Surface chemistry modulates focal adhesion composition and signaling through changes in integrin binding. Biomaterials 2004;5947-5954.

31. Johnson, C.M., Hanson, M.N., and Helgeson, S.C. Porcine cardiac valvular subendothelial cells in culture: Cell isolation and growth characteristics. J Mol Cell Cardiol 1987;1185-1193.

32. Buchanan, R.M., and Sacks, M.S. Interlayer micromechanics of the aortic heart valve leaflet. Biomechanics and Modeling in Mechanobiology 2014;813-826.

33. Jian, B., Narula, N., Li, Q.-y., Mohler Iii, E.R., and Levy, R.J. Progression of aortic valve stenosis: TFG-B1 is present in calcified aortic valve cusps and promotes aortic valve interstitial cell calcification via apoptosis. Ann Thorac Surg 2003;- 465.

34. Hjortnaes, J., Camci-Unal, G., Hutcheson, J.D., Jung, S.M., Schoen, F.J., Kluin, J., Aikawa, E., and Khademhosseini, A. Directing Valvular Interstitial Cell Myofibroblast-Like Differentiation in a Hybrid Hydrogel Platform. Adv Healthc Mater 2015;10.

35. Janson, I.A., and Putnam, A.J. Extracellular matrix elasticity and topography: Material-based cues that affect cell function via conserved mechanisms. J Biomed Mater Res A 2015;1246-1258.

36. Gu, X.X., and Masters, K.S. Role of the Rho pathway in regulating valvular interstitial cell phenotype and nodule formation. Am J Physiol Heart Circ Physiol 2011;H448-H458.

37. Latif, N., Sarathchandra, P., Taylor, P.M., Antoniw, J., and Yacoub, M.H. Localization and pattern of expression of extracellular matrix components in human heart valves. J Heart Valve Dis 2005;218-227.

38. Bashey, R.I., Torii, S., and Angrist, A. Age-related collagen and elastin content of human heart valves. J Gerontol 1967;203-&.

39. Halper, J., and Kjaer, M. - Basic components of connective tissues and extracellular matrix: Elastin, fibrillin, fibulins, fibrinogen, fibronectin, laminin, tenascins and thrombospondins. 2014;- 47.

40. Ramirez, F., Sakai, L.Y., Dietz, H.C., and Rifkin, D.B. Fibrillin microfibrils: multipurpose extracellular networks in organismal physiology. Physiological Genomics 2004;151.

41. Yokosaki, Y., Tanaka, K., Higashikawa, F., Yamashita, K., and Eboshida, A. Distinct structural requirements for binding of the integrins αvβ6, αvβ3, αvβ5, α5β1 and α9β1 to osteopontin. Matrix Biol 2005;418-427.

42. Passmore, M., Nataatmadja, M., Fung, Y.L., Pearse, B., Gabriel, S., Tesar, P., and Fraser, J.F. Osteopontin alters endothelial and valvular interstitial cell behaviour in calcific aortic valve stenosis through HMGB1 regulation. European Journal of Cardio-thoracic Surgery 2015;e20-e29.

Chapter 4

Isolated Effect of Stiffness on Valvular Interstitial Cell Differentiation

Kent E. Coombs[1,2], Alex T. Leonard[1,3], Matthew N. Rush[1,4], David A. Santistevan[1], Elizabeth L. Hedberg-Dirk[1,3,4]

[1]Center for Biomedical Engineering, University of New Mexico, Albuquerque, NM, USA
[2]Biomedical Sciences Graduate Program, University of New Mexico, Albuquerque, NM, USA
[3]Department of Chemical and Biological Engineering, University of New Mexico, Albuquerque, NM, USA
[4]Nanoscience and Microsystems Engineering, University of New Mexico, Albuquerque, NM, USA

Corresponding Author: Elizabeth L. Hedberg-Dirk
Address: Center for Biomedical Engineering
      MSC01 1141
      1 University of New Mexico
      Albuquerque, NM 87131
Email: edirk@unm.edu
Fax: 505-277-6209
Phone: 505-277-5906

Alternate Author Email:
Kent E. Coombs, kcoombs@salud.unm.edu
Matthew N. Rush, mrush@unm.edu

Abstract

Previous methods for investigating material stiffness on cell behavior have focused on the use of substrates with limited ranges of stiffness and/or fluctuating surface chemistries. Using the co-polymer system of n-octyl methacrylate crosslinked with diethylene glycol dimethacrylate (DEGDMA/nOM), we developed a new cell culture platform to analyze the isolated effects of stiffness independent from changes in surface chemistry. Materials ranging from 25 kPa to 4,700 kPa were fabricated. Surface analysis including goiniometry and X-ray photoelectron spectroscopy (XPS) confirmed consistent surface chemistry across all formulations examined. The mechanosensitive cell type valvular interstitial cell (VIC) was cultured DEGDMA/nOM substrates of differing stiffness. Results indicate that order of magnitude changes in stiffness do not increase gene expression of VIC alpha-smooth muscle actin (αSMA). However, structural organization of αSMA is altered on stiffer substrates, corresponding with the appearance of the osteoblastic marker osteocalcin and nodule formation. This research presents the co-polymer DEGDMA/nOM as ideal substrate to investigate the influence of stiffness on VIC differentiation without the confounding effects of changing material surface chemistry.

Keywords: Valvular interstitial cell, stiffness, mechanosensing, extracellular matrix, microenvironment

71

Introduction

Cellular functions such as adhesion, spreading, proliferation and gene expression are affected by the chemical and physical factors of the extracellular environment [1-9]. Cells respond to these extracellular cues through mechanosensing proteins, which activate cell signaling cascades [2, 10, 11]. Given the importance of substrate stiffness in controlling mechanosensing behavior, investigations into the effects of matrix mechanics on cell signaling have become more prevalent. However, *in vitro* studies examining substrate's mechanical properties effects on cells have been limited due to a lack of material platforms capable of isolating stiffness over a significant range without changing the material's surface chemistry [1-6].

During aortic valve disease, changes in protein deposition and overall stiffness of the valve are known to increase over time [12, 13]. The primary cells of the aortic valve, valvular interstitial cells (VICs), are a heterogeneous and dynamic population that are particularly sensitive to the substrate on which they are grown [5, 14-16]. *In vitro*, VICs expanded on tissue culture polystyrene (TCPS) exhibit myofibroblastic characteristics with an elongated spindle shaped morphology, rapid proliferation, and expression of alpha smooth muscle actin (αSMA) [16-20]. Over time, VICs on TCPS adopt an osteoblastic-like (OB) phenotype attributed to cell confluence [5, 14, 15, 21, 22]. It has also been suggested that stiffening of the aortic valve's extra cellular matrix (ECM) may be able to signal VICs to differentiate to a disease inducing OB phenotype [12, 13,

16, 23-25]. These observations have led to investigation of the influence of substrate stiffness on VIC differentiation *in vitro*.

Classically, αSMA has been used as a marker for myofibroblastic activation of VICs. More recently, however, αSMA expression has also been shown to increase in OB VICs [5, 26]. While studies have begun to look at the role of αSMA as a marker of osteoblastic potential, at this point seminal studies of stiffness have not included OB markers such as osteocalcin [3, 24, 27-29].

Given the low compressive moduli present in healthy valve tissue, past studies have focused on relatively small changes in stiffness in the range of soft tissues. Poly(ethylene glycol) (PEG), photodegradable-PEG/PEG monoacrylate hybrids, and collagen materials have been used to create substrates of varying stiffness for investigating VIC behavior. On lower range moduli materials (2-10 kPa) VICs have exhibited a dormant fibroblastic phenotype with minimal αSMA expression and a low rate of proliferation. Slightly stiffer materials (10-15 kPa) induced upregulation of αSMA and the VICs were classified as activated/myofibroblastic phenotype [3, 18, 24, 29]. Quinlan and Biller used collagen coated polyacrylamide gels to investigate a larger range of stiffness (150 Pa – 153kPa) [3]. From this range it was shown increasing stiffness results in greater αSMA expression and stress fiber formation. However, the stiffness ranges examined in all these previous studies are still too narrow as they failed to include high compressive moduli materials akin to calcified valve tissue [2, 12]. Although PDMS scaffolds have been studied to cover larger ranges, PDMS requires surface modification to allow cell adhesion [1, 2]. Further complicating

the systematic investigation of stiffness effects on VIC behavior, is the use of materials with varying surface chemistry. Surface chemistry of the underlying substrate has been shown to have a dramatic effect on VIC behavior [5]. Therefore, a consistent surface chemistry needs to be maintained in order to reduce the convolution of surface chemistry effects on VICs, leading us to develop a new material platform.

In this report we describe the development of a unique cross-linked polymer system. Using this co-polymer system composed of diethylene glycol dimethacrylate (DEGDMA) and n-octyl methacrylate (n-OM) monomers, a material with a wide range of stiffness and a consistent surface chemistry can be achieved. To our knowledge no systematic study isolating the effect of stiffness greater than 153 kPa has been reported while looking at VIC osteoblastic differentiation. This system allows us to investigate the isolated effects of stiffness on VIC behavior over a wider range of moduli than previously reported [3, 14, 15, 21, 23, 24, 29]. Comparing soft (25 kPa) and hard (4,700 kPa) substrates it was hypothesized that increasing stiffness with consistent surface chemistry would cause VICs to undergo osteoblastic differentiation. As such, this research marks the best attempt thus far at decoupling underlying stiffness from changing surface chemistry and isolating stiffness effects on VIC behavior over a wider range of stiffness.

Materials and Methods

Substrate Fabrication

Substrates were fabricated using free radical polymerization through solutions of the monomers n-octyl methacrylate (nOM) and diethyleneglycol dimethacrylate (DEGDMA) (Scientific Polymer Products) with 1-[4-(2-hydroxyethoxy)phenyl]-2-hydroxy-2-methylpropan-1-one (IRGACURE 2959) as a free radical initiator. Three substrate formulations were fabricated with 3, 19, or 33 wt% DEGDMA, 0.025 wt% IRGACURE 2959, and the remaining wt% of nOM.

Liquid monomers and initiator were mixed for 1 hr at room temperature, poured into quartz glass molds (3 x 5 x 0.1 cm) and polymerized under UV 365 nm light in a CL-1000 UV light box (UVP LLC) for 300 minutes. DEGDMA/nOM sheets were cut into 6, 15, and 22 mm diameter circular samples used for contact angle, surface chemistry, and VIC culture experiments. Before testing, all samples were submerged in 200 proof ethanol for 48 hours, degassed overnight under vacuum, and submerged in 18 MΩ water (Millipore) for at least 24 hrs.

Compressive Modulus

Cylindrical samples for testing of compressive modulus were fabricated in glass vials with an inner diameter of 6 mm and cut to a 2:1 height to diameter with a wet saw TechCut 5™ (Allied High Tech Products Inc.). Compressive modulus of the bulk material was determined for all three formulations (n=5) using an Instron 5500R following ASTM 695 – 02a. The experiment was performed using MTS ReNew software. Stress – strain curves were analyzed in

the linear elastic regime (5 – 20% strain) to determine sample compressive
modulus.

Contact Angle Goniometry

Samples were dried under vacuum overnight. Contact angles were
determined using the sessile drop technique on a goniometer (Model 100-00-
115, ramé-hart). The contact angle between the water droplet and the sample
surface was determined using the DROPimage Standard (ramé-hart).

X-Ray Photoelectron Spectroscopy (XPS)

X-Ray Photoelectron Spectroscopy survey and high resolution spectra
were obtained using Kratos Axis Ultra spectrometer with a monochromatic Al
K(α) (1486.6 eV) source at 225W. Survey spectra were obtained at pass energy
80 eV and high-resolution spectra at pass energy 20 eV. Base pressure was less
than 5×10^{-9} Torr. Charge compensation was accomplished using low energy
electrons. Linear background was used for elemental quantification of C1s and
O1s spectra. Quantification utilized sensitivity factors provided by the
manufacturer. All the spectra were charge referenced to the aliphatic carbon at
285 eV. Curve fitting was carried out using individual peaks of constrained width,
position and 70% Gaussian/30% Lorentzian line shape.

Valvular Interstitial Cell Isolation and Culture

Valvular interstitial cells were isolated using collagenase digestion from porcine hearts received within 24 hrs of slaughter (Hormel) as previously described [5, 30]. After harvesting, residual valvular endothelial cells were removed from the extracted cell population using CD31+ magnetic dynabeads [5]. VICs were cultured under normal conditions (37ºC, 85% RH, 5% CO_2) in classical medium 199 (Hyclone) supplemented with 10% fetal bovine serum (Hyclone), 1% penicillin/streptavidin (Hyclone), and 1% fungizone (Thermo Fisher Scientific). VICs were frozen after passage one. Low passage (2-4) VICs were used in all experiments for consistency. For all cell experiments, VICs were cultured under normal conditions on treatment surfaces 3, 19, 33% DEGDMA/nOM or on TCPS surfaces with or without osteogenic induction media [199 media, 10% FBS, 10 mM β-glycerophosphate, 2mM ascorbic acid, and 10^{-8} M dexamethasone] added 12 hours after seeding. TCPS was used as the control surface.

Apoptosis

Apoptosis was measured using Dead Cell Apoptosis Kit with Annexin V Alexa Fluor 488 & propidium iodide (PI) (Thermo Fisher Scientitific). Annexin V is an apoptosis marker that becomes available for antibody binding as the cell loses the ability to regulate the position of inner and outer leaflet membrane proteins, while PI binds to the DNA of cells that have lost membrane integrity. When both markers are present, the cell is apoptotic. Briefly, VICs were seeded onto

DEGDMA/nOM substrates or TCPS and analyzed at seven days. Apoptosis

controls were exposed to 1uM staurosporin for 4 hrs before analysis. All cells

were trypsinized and stained as per manufactures instructions before measuring

fluorescence on the Accuri C6 Flow Cytometer.

Growth Curve

Valvular interstitial cells were seeded at 35,000 cells/cm^2. At each time

point, cells were trypsinized and counted on a Beckman Coulter Counter Z2.

Media was changed every two days. Doubling times were calculated based on

the slope of the best-fit line during the exponential phase of growth.

Quantitative Polymerase Chain Reaction

Valvular interstitial cells grown on DEGDMA/nOM substrates were

harvested for mRNA using RNeasy Micro Kits with gDNA removal (Qiagen).

mRNA quality and content was assessed on a NanoDrop 2000C UV/Vis

(ThermoFisher Scientific) and 100 ng converted to cDNA using GoScript Reverse

Transcription Kit (Promega). Gene expression of αSMA/ACTA

(Ss04245588_m1), collagen-1/COL1A1 (Ss03375690_u1), osteocalcin/bone

gamma-carboxyglutamate protein/ BGLAP (Ss03373655_s1) and elastin/EMILIN

(AJLJIR9) were analyzed with TaqMan primers using the ΔΔCT method, on a

StepOne Real Time-PCR System (Applied Bio.). All samples were compared to

GAPDH (Ss03374854_g1) TaqMan primer as the endogenous control and

normalized to TCPS.

Optical Microscopy and Immunocytochemical Staining (ICC)

Cells were imaged using a phase contrast Nikon Microscope over 7 days of growth to identify nodule formation. After three days of culture, VICs were fixed with 10% formalin for one hour and rinsed in DPBS. Cells were permeabilized with 0.01% (v/v) Tween20 in DPBS (PSBT). Reactive ion removal was conducted using 10% (m/v) sodium azide and 10µM H_2O_2 in PBST then rinsed in PBST. Primary antibody αSMA (ab7817, Abcam) at a 1:1000 dilution was incubated with sample after blocking with 3% Bovine Serum Albumin (BSA). After washing with PBST secondary antibody goat anti-mouse AlexaFluor 488 (A11001, Invitrogen) was diluted to 1:400 and incubated with samples for 60 minutes. Samples were rinsed with PBST and excess moisture removed before being mounted with Prolong Diamond Antifade with DAPI P36966 (Thermo Fisher Scientific). Samples were imaged on a Zeiss LSM 510 META microscope.

Statistics

All results were analyzed using a one-way ANOVA followed by a student's T-tests to determine significance at a 95% confidence interval ($p \leq 0.05$). All analyses were done using GraphPad Prism 6 software.

Results

Substrate Fabrication

Monomers of dietheyleneglycol dimethacrylate (DEGDMA) and n-octyl methacrylate (nOM) were mixed together with the photo initiator IRGACURE 2959. Exposure to UV light (365nm) results in the generation of two free radicals per molecule. IRGRACURE radicals then attack the acrylic groups of either monomer allowing for random co-polymerization (Figure 1). By varying ratios of DEGDMA:nOM cross-linked substrates with a range of material stiffness from 25 kPa to 4700 kPa were made.

Compressive Modulus

The compressive modulus (n=5) was determined for all three formulations with 3%, 19%, and 33% DEGDMA having a compressive moduli of 25 ± 2 kPa, 920 ± 60 kPa, and 4,700 ± 300 kPa, respectively (Figure 2). Differences in compressive modulus were correlate with DEGDMA content and published Tg values [31].

Sessile Drop Goniometry

Contact angles were used to determine the wettability of surfaces using 18 MΩ water. For 3, 19, and 33 wt% DEGDMA/nOM the contact angles were found to be 90.1 ± 2.2, 88.0 ± 3.2, and 87.3 ± 3.3, respectively with no statistical difference between groups indicating similar hydrophobicity.

X-Ray Photoelectron Spectroscopy (XPS)

The elemental composition and functional groups of the lowest and highest modulus DEGDMA/nOM material surfaces were analyzed using XPS. A broad spectrum scan determined the elemental and peak intensity in order to determine surface elemental composition (Figure 3A). High resolution spectra scans for carbon and oxygen were obtained to measure chemical species bonded to these elements. As shown in table 1, the formulations of 3 and 33% DEGDMA/nOM show nearly identical elemental composition. High resolution spectra of O1s show similar curves between 3 and 33% DEGDMA/nOM with peak assignments as follows; O=C, 532.3 eV; C-O-C, 533.9 eV; O-(C=O), 534.4 eV; O-H, 536 eV (Figure 3B, C) [32, 33]. High resolution of C1s peak show similar curves between 3 and 33% DEGDMA/nOM with the following peak assignments; aliphatic carbon, 285 eV; C-(C=O)-O, 285.7 eV; C-O, 286.8 eV, C=O, 288.8 eV (Figure 3D, E) [32, 33]. The observed peak for hydroxyl (O-H, 536 eV) is most likely due to oxidization at the surface from incomplete conversion of free radicals from polymerization. In both the Cs1 and Os1 spectra, peak fits for the, α-carbon (C-(C=O)-O, 285.7 eV) and the aliphatic carbons (C-C, 285 eV), α-oxygen (O-(C=O)) and ether (C-O-C), respectively, vary by less than 1 eV at the peak maxima. This variation in eV falls below the detection limit of our instrument and necessitates the combination of, α-carbon (C-(C=O)-O) and the aliphatic carbons (C-C) for Cs1, α-oxygen (O-(C=O)) and the ether (C-O-C) for Os1 peaks. The adjusted peaks were used to calculate (C-C/C-O) /(C-C/C=O) and (O-(C=O)/(C-O-C) ratios.

VIC Attachment, Growth, Cytocompatibility

VICs were seeded at 35,000 cells/cm^2 and counted at 24 hours to determine cellular attachment. Cell attachment was lower than controls but did not differ significantly between DEGDMA/nOM substrates (Figure 4A). Cell numbers were measured over nine days to calculate doubling times. Osteoblastic media (OB) VICs proliferated significantly faster than all other substrates. TCPS, 19% and 33% DEGDMA/nOM VICs showed no difference between groups. Finally, VICs on 3% DEGDMA/nOM grew significantly slower than all other substrates (Figure 4B). To confirm DEGDMA/nOM substrates were not inducing chronic toxicity, VIC apoptosis was measured after seven days of culture. No significant differences were found in VICs grown on TCPS, live controls, and DEGDMA/nOM substrates (Figure 4C).

Gene Expression and Immunocytochemical Staining (ICC) of VICs

Results from qPCR show a significant increase in αSMA gene expression of VICs grown in osteoblastic media at all time points (Figure 5A). However, there is no significant increase of VIC αSMA expression between different stiffness formulations of DEGDMA/nOM. ICC visualization of αSMA protein structure at day 3 shows stress fiber formation is more pronounced on OB VICs and 33% DEGDMA/nOM VICs compared to softer substrates 3% and 19% DEGDMA/nOM VICs (Figure 6).

At day 3 cells on, 3% and 19% DEGDMA/nOM have significantly lower osteocalcin expression than OB VICs (Figure 5B). By day 5 cells on, 33% DEGDMA/nOM have significantly higher OCN expression than 3% and 19%, and are at levels comparable to those expressed in OB VICs at the same time point. Trends remain at day 7 for 33% and OB VICs, however 19% DEGDMA/nOM VICs now have similar levels of OCN expression to 33% DEGDMA/nOM and OB VICs. Only 3% DEGDMA/nOM OCN expression levels remains low throughout the experiment.

Elastin mRNA is lower in VICs grown on DEGDMA/nOM surfaces compared to OB VICs on day 3. An increasing trend of elastin expression is seen in VICs on DEGDMA/nOM correlating to stiffness on day 5. Only VIC elastin expression on 3% DEGDMA/nOM are significantly lower than OB VICs on day 5 (Figure 5C). Col1α2 (collagen) mRNA expression in VICs on 3%, 19% and 33% DEGDMA/nOM surfaces are significantly increased compared to OB VICs on days 3 and 5 (Figure 5D). On all surfaces however, VICs show no difference in collagen or elastin expression on day 7 (Figure 5C, D).

Late Stage VIC morphology and Nodule Formation

At day 7 only OB VICs and VICs on 33% DEGDMA/nOM exhibit formation of nodules. TCPS and 3% DEGDMA/nOM VICs maintain an elongated morphology. 19% DEGDMA/nOM VICs shows both elongated and rhomboidal morphology indicative of a partial transition to the OB phenotype, however no nodules were visible (Figure 7).

83

Discussion

Controlling valvular interstitial cell (VIC) phenotype using synthetic materials is a promising technique with great potential for aortic valve tissue engineering. Before this can be realized a better understanding of cellular responses to biomaterial microenvironments, such as substrate stiffness, need to be established. Current attempts to measure the influence of stiffness on cell behavior using hydrogel, polyacrylamide, and polydimethylsiloxane surfaces have been inconsistent and confounded by a number of issues including limited ranges of stiffness, changes in surface chemistry presented to the cells, and/or material alteration and/or degradation [1-3, 14, 15, 21, 23, 24, 29].

The co-polymer network of diethelyene glycol dimethacrylate and n-octyl methacrylate (DEGDMA/nOM) was chosen to address the limitations of the available materials based on its biocompatibility as demonstrated by its use as a dental restorative material [34]. This copolymer can cover a large range of stiffness while maintaining a consistent surface chemistry, it does not require surface modification for cellular attachment, and it does not degrade under culture conditions. In this study, DEGMDA/nOM copolymers were made in three monomer ratios of DEGDMA to nOM: 3:97 (3%); 19:81 (19%); and, 33:67 (33%) by weight. The compressive modulus changes exhibited between these formulations represent a three order of magnitude range (Figure 2). The lower limit of 3% DEGDMA/nOM was selected to obtain the softest stable freestanding substrate. 19% DEGDMA/nOM, bounds a critical point for the copolymer where

84

additional DEGDMA content has a significant impact as a crosslinking agent. As a result the copolymer mechanical properties greatly increase with small additions of DEGDMA beyond this point [34, 35]. For the 3% and 19% DEGDMA/nOM formulations, the mechanics are primarily controlled by the concentration of crosslinked chains which is known as the 'crosslinking effect.' The 33% DEGDMA/nOM is below its glass transition temperature at 37°C and is a crystalline solid [34]. For the 33% DEGMA/nOM formulation, mechanical properties are controlled purely based on the monomer ratios present which is known as the 'co-polymerization effect' [31, 34]. As seen in figure 2, the compressive modulus of the 3% and 19% DEGDMA/nOM substrates increase from 25 ± 2 to 920 ± 60 kPa. Further increase of DEGDMA content to 33% results in an increase of ~3,600 kPa above that of the 19% formulation to achieve this study's highest compressive modulus of 4,700 ± 300 kPa. These data demonstrate the flexibility and wide range of the achievable compressive moduli available with this co-polymer system. This large range of stiffness is important for study of cells of the heart valve, because healthy tissue to very severe aortic stenosis stiffness ranges from .001 to 7.38 MPa [12].

Sessile drop goniometry and x-ray photoelectron spectroscopy (XPS) were conducted to examine the surface properties of the co-polymer network films. In order to truly isolate stiffness, it is imperative that all other surface characteristics are preserved between the different formulations. All formulations exhibit consistent contact angles of ~88.5° indicating that all surfaces exhibit the same wettability, a property that greatly influences protein adsorption. While

goniometry is an indirect method that allows us to infer that the surface chemistry among the formulations remains consistent, XPS was conducted to directly measure the elemental and chemical binding environment of the material surface. The maximum and minimum content DEGDMA formulations were evaluated to ensure that the formulations with the greatest difference in monomer ratio still maintained a consistent surface chemistry. XPS survey spectra showed that the elemental composition was the same in each formulation, while the high-resolution spectra showing that the surfaces also displayed consistent presentation of functional groups between treatment groups (Figure 3). These data indicate that the DEGDMA/nOM copolymer networks present consistent chemical surfaces regardless of copolymer ratio and stiffness (Table 1).

Utility as a substrate for *in vitro* cell culture of primary valvular interstitial cells was assessed by initial VIC attachment and apoptosis after 7 days in culture (Figure 4). Compared to TCPS, all DEGDMA/nOM substrates had reduced initial attachment, most likely due to the slightly increased hydrophobicity. This is shown by goniometry with a contact angle of ~88.5°of the DEGDMA/nOM compared to the 64.3° ± 1.5 of TCPS [36]. As the attachment results gave information on the initial response of the cells to the materials, apoptosis was assessed after 7 days to determine whether long-term exposure resulted in increased cell death. No increase in apoptosis was detected, signifying DEGDMA/nOM substrates were cytocompatibility and viable as a cell culture platform for VICs (Figure 4).

In previous studies, VICs grown on very soft stiffness moduli (<10 kPa) substrates exhibited quiescent fibroblastic qualities. While those grown on ~15–55 kPa substrates, similar to 3% DEGDMA/nOM (25 kPA), preferentially differentiate to myofibroblasts exhibiting high levels of αSMA [3, 17, 18, 29, 37]. Among all DEGDMA/nOM formulations, αSMA expression did not significantly differ throughout the experiments. In addition, VICs grown on the DEGDMA/nOM substrates had significantly lower αSMA expression on all formulations than VICs on TCPS and OB VICs at all time points (Figure 5A). Generally, αSMA expression has been considered a hallmark of myofibroblastic VIC differentiation [17, 23, 26, 29, 38, 39]. Despite consistent levels of αSMA gene expression on DEGMDA/nOM substrates, there are noticeable differences in αSMA stress fiber formation corresponding to increases in substrate compressive modulus (Figure 6). Increased actin fiber formation resulting from growth on stiff substrates has been linked to osteoblastic differentiation in the pre-osteoblastic cell line MC3T3's [40], suggesting that the increasing αSMA stress fiber assembly of VICs may be an important step in VIC OB differentiation [17]. At day 7, nodules were detected via brightfield microscopy on 33% (4.7 MPa), but not 3% (25 kPa) or 19% (920 kPa) DEGDMA/nOM supporting the theory that increased αSMA stress fiber formation may be related to VIC OB differentiation and nodule formation (Figure 7) [41, 42]. Investigation into the signaling pathways resulting in αSMA stress fiber formation in VICs without increasing gene expression has not yet been identified and warrants further study.

The hypothesis that substrate compressive modulus alone influences VIC OB differentiation is further supported by changes in VIC expression of the late stage osteoblastic marker osteocalcin (Figure 5B) [17]. On the softest substrate, 3% DEGDMA/nOM (25 kPa), osteocalcin expression was significantly lower than for the VICs cultured on the stiffest substrates, 33% DEGDMA/nOM (4.7 MPa) as well as OB VICs at days 5 and 7. When grown on 33% DEGDMA/nOM (4.7 MPa), VICs expressed OCN near the same levels of OB VICs, suggesting the higher moduli substrates induce expression of OCN (Figure 5B). We believe that seeding cells on DEGMA/nOM substrates with compressive moduli in the megapascal range upregulates osteoblastic gene expression through mechanical signaling, transmitted through mechanotransduction and integrin activation [2, 5, 16, 43, 44]. However, with lower αSMA gene expression on 33% DEGDMA/nOM (4.7 MPa) than TCPS and OB VIC controls, we hypothesize that the negatively charged surface chemistry of TCPS significantly contributes to the activation of signaling pathways leading to increased αSMA expression, much like that seen on charged SAMs surfaces described in Rush *et al.* [5, 7]. For DEGDMA/nOM substrates, αSMA expression is not changing with compressive modulus, but stress fiber formation is. Therefore, VIC differentiation to an OB phenotype may be tied more closely to αSMA fiber formation rather than expression.

Valvular interstitial cell extracellular matrix proteins (ECM) gene expression was also assessed. The underlying ECM has been shown to induce changes in VIC phenotype *in vitro* [5, 14-16, 21, 25]. A large upregulation of collagen is seen on all DEGDMA/nOM surfaces at day 3, with a significant down

regulation of collagen expression by day 5 and 7 (Figure 5D). Since collagen does not differ between DEGDMA/nOM formulations, we believe early collagen expression does not correlate with VIC OB differentiation. Rather, the VICs produce collagen to favorably modify the surface of the slightly hydrophobic DEGDMA/nOM to allow for better VIC attachment, spreading, and proliferation [15]. Our results also show that elastin gene expression is elevated at day 3 in OB VICs and VICs cultured on TCPS compared to those grown on DEGDMA/nOM surfaces (Figure 5C). By day 5, an increasing trend in elastin corresponding with increasing substrate compressive modulus can be seen, suggesting that increases in elastin expression may correlate with VIC differentiation on substrates that differ in compressive modulus.

It has been well established that physical cues from the extracellular environment influence the phenotypic behavior of cells [2, 5, 45]. However, studies focusing on the effects of a substrate's stiffness have been limited due to a lack of material platforms capable of isolating substrate compressive modulus without changing the material's surface chemistry [1-4]. The design of a tunable material with consistent surface chemistry is therefore very important to the fields of tissue engineering and biomedical sciences. With the aim of generating better tissue models of health and disease, use of mechanically relevant materials will allow for more precise control of growth environments and cellular behavior. As such, the material DEGDMA/nOM allows for the isolated testing of stiffness effects on cell behavior over a wide range of stiffness while maintaining consistent surface chemistry. Our results show that stiffness on the scale of

89

megapascals affects VIC behavior. Our 4,700 kPa substrates induce OB VIC behaviors that include upregulation of OB gene marker osteocalcin, creation of nodules, and changes in elastin production, all of which are correlated with VIC OB differentiation. Although αSMA expression did not vary between different substrate's compressive modulus, the increase in fiber formation on stiffer substrates suggests an alternative pathway is being activated to cause VIC OB differentiation that has not been previously reported. Further studies should examine the intracellular pathways involved in fiber rearrangement and mechanosensing of VICs caused by material stiffness.

Acknowledgements

References

1.   Brown, X.Q., K. Ookawa, and J.Y. Wong, *Evaluation of polydimethylsiloxane scaffolds with physiologically-relevant elastic moduli: interplay of substrate mechanics and surface chemistry effects on vascular smooth muscle cell response.* Biomaterials, 2005. **26**(16): p. 3123-3129.

2.   Nemir, S. and J.L. West, *Synthetic Materials in the Study of Cell Response to Substrate Rigidity.* Annals of Biomedical Engineering, 2010. **38**(1): p. 2-20.

3.   Quinlan, A.M.T. and K.L. Billiar, *Investigating the role of substrate stiffness in the persistence of valvular interstitial cell activation.* Journal of Biomedical Materials Research Part A, 2012. **100A**(9): p. 2474-2482.

4.   Nikkhah, M., et al., *Engineering microscale topographies to control the cell-substrate interface.* Biomaterials, 2012. **33**(21): p. 5230-5246.

5.   Rush, M.N., K.E. Coombs, and E.L. Hedberg-Dirk, *Surface chemistry regulates valvular interstitial cell differentiation in vitro.* Acta biomaterialia, 2015. **28**: p. 76-85.

6.   Balgude, A.P., et al., *Agarose gel stiffness determines rate of DRG neurite extension in 3D cultures.* Biomaterials, 2001. **22**(10): p. 1077-1084.

7.   Dewez, J.L., et al., *Competitive adsorption of proteins: Key of the relationship between substratum surface properties and adhesion of epithelial cells.* Biomaterials, 1999. **20**(6): p. 547-559.

91

8.   Ghanian, M.H., et al., *Nanotopographical control of human embryonic stem cell differentiation into definitive endoderm.* Journal of Biomedical Materials Research Part A, 2015. **103**(11): p. 3539-3553.

9.   Janson, I.A. and A.J. Putnam, *Extracellular matrix elasticity and topography: Material-based cues that affect cell function via conserved mechanisms.* Journal of Biomedical Materials Research Part A, 2015. **103**(3): p. 1246-1258.

10.   Hannigan, G.E., et al., *Regulation of cell adhesion and anchorage-dependent growth by a new beta(1)-integrin-linked protein kinase.* Nature, 1996. **379**(6560): p. 91-96.

11.   Danen, E.H.J., et al., *The fibronectin-binding integrins alpha 5 beta 1 and alpha v beta 3 differentially modulate RhoA-GTP loading, organization of cell matrix adhesions, and fibronectin fibrillogenesis.* Journal of Cell Biology, 2002. **159**(6): p. 1071-1086.

12.   Maleki, H., et al., *A metric for the stiffness of calcified aortic valves using a combined computational and experimental approach.* Medical & Biological Engineering & Computing, 2014. **52**(1): p. 1-8.

13.   Desmouliere, A., et al., *Apoptosis during wound healing, fibrocontractive diseases and vascular wall injury.* International Journal of Biochemistry & Cell Biology, 1997. **29**(1): p. 19-30.

14.   Gu, X.X. and K.S. Masters, *Role of the Rho pathway in regulating valvular interstitial cell phenotype and nodule formation.* American Journal of

Physiology-Heart and Circulatory Physiology, 2011. **300**(2): p. H448-H458.

15. Gu, X.X. and K.S. Masters, *Regulation of valvular interstitial cell calcification by adhesive peptide sequences.* Journal of Biomedical Materials Research Part A, 2010. **93A**(4): p. 1620-1630.

16. Schroer, A.K. and W.D. Merryman, *Mechanobiology of myofibroblast adhesion in fibrotic cardiac disease.* Journal of Cell Science, 2015. **128**(10): p. 1865-1875.

17. Liu, A.C., V.R. Joag, and A.I. Gotlieb, *The emerging role of valve interstitial cell phenotypes in regulating heart valve pathobiology.* American Journal of Pathology, 2007. **171**(5): p. 1407-1418.

18. Kheradvar, A., et al., *Emerging trends in heart valve engineering: part I. solutions for future.* Annals of Biomedical Engineering, 2015. **43**(4): p. 833-843.

19. Zacks, S., et al., *Characterization of Cobblestone Mitral-Valve Interstitial-Cells.* Archives of Pathology & Laboratory Medicine, 1991. **115**(8): p. 774-779.

20. Durbin, A.D. and A.I. Gotlieb, *Advances towards understanding heart valve response to in injury.* Cardiovascular Pathology, 2002. **11**(2): p. 69-77.

21. Gu, X.X. and K.S. Masters, *Role of the MAPK/ERK pathway in valvular interstitial cell calcification.* American Journal of Physiology-Heart and Circulatory Physiology, 2009. **296**(6): p. H1748-H1757.

93

22.   Benton, J.A., H.B. Kern, and K.S. Anseth, *Substrate Properties Influence Calcification in Valvular Interstitial Cell Culture.* Journal of Heart Valve Disease, 2008. **17**(6): p. 689-699.

23.   Merryman, W.D., et al., *Correlation between heart valve interstitial cell stiffness and transvalvular pressure: implications for collagen biosynthesis.* American Journal of Physiology-Heart and Circulatory Physiology, 2006. **290**(1): p. H224-H231.

24.   Yip, C.Y.Y., et al., *Calcification by valve interstitial cells is regulated by the stiffness of the extracellular matrix.* Arteriosclerosis Thrombosis and Vascular Biology, 2009. **29**(6): p. 936-U417.

25.   Rodriguez, K.J. and K.S. Masters, *Regulation of valvular interstitial cell calcification by components of the extracellular matrix.* Journal of Biomedical Materials Research Part A, 2009. **90A**(4): p. 1043-1053.

26.   Davis, J. and J.D. Molkentin, *Myofibroblasts: Trust your heart and let fate decide.* Journal of Molecular and Cellular Cardiology, 2014. **70**: p. 9-18.

27.   Hutcheson, J.D., et al., *Cadherin-11 Regulates Cell-Cell Tension Necessary for Calcific Nodule Formation by Valvular Myofibroblasts.* Arteriosclerosis Thrombosis and Vascular Biology, 2013. **33**(1): p. 114-+.

28.   Rodriguez, K.J., et al., *Manipulation of valve composition to elucidate the role of collagen in aortic valve calcification.* Bmc Cardiovascular Disorders, 2014. **14**: p. 10.

29.   Wang, H., et al., *Redirecting Valvular Myofibroblasts into Dormant Fibroblasts through Light-mediated Reduction in Substrate Modulus.* Plos One, 2012. **7**(7): p. 12.

30.   Johnson, C.M., M.N. Hanson, and S.C. Helgeson, *Porcine cardiac valvular subendothelial cells in culture: Cell isolation and growth characteristics.* Journal of Molecular and Cellular Cardiology, 1987. **19**(12): p. 1185-1193.

31.   Young, J.S., A.R. Kannurpatti, and C.N. Bowman, *Effect of comonomer concentration and functionality on photopolymerization rates, mechanical properties and heterogeneity of the polymer.* Macromolecular Chemistry and Physics, 1998. **199**(6): p. 1043-1049.

32.   Watts, J.F., *High resolution XPS of organic polymers: The Scienta ESCA 300 database. G. Beamson and D. Briggs. 280pp., £65. John Wiley & Sons, Chichester, ISBN 0471 935921, (1992).* Surface and Interface Analysis, 1993. **20**(3): p. 267-267.

33.   Beamson, G. and D. Briggs, *High-Resolution Monochromated X-ray Photoelectron-Spectroscopy of Organic Polymers - A Comparision Between Solid-State Data for Organic Polymers and Gas-Phase Data for Small Molecules.* Molecular Physics, 1992. **76**(4): p. 919-936.

34.   Kannurpatti, A.R. and C.N. Bowman, *Structural evolution of dimethacrylate networks studied by dielectric spectroscopy.* Macromolecules, 1998. **31**(10): p. 3311-3316.

35.   Kannurpatti, A.R., J.W. Anseth, and C.N. Bowman, *A study of the evolution of mechanical properties and structural heterogeneity of polymer*

networks formed by photopolymerizations of multifunctional *(meth)acrylates.* Polymer, 1998. **39**(12): p. 2507-2513.

36. Arima, Y. and H. Iwata, *Effect of wettability and surface functional groups on protein adsorption and cell adhesion using well-defined mixed self-assembled monolayers.* Biomaterials, 2007. **28**(20): p. 3074-3082.

37. Chen, J.H., et al., *Identification and characterization of aortic valve mesenchymal progenitor cells with robust osteogenic calcification potential.* American Journal of Pathology, 2009. **174**(3): p. 1109-1119.

38. Duan, B., et al., *Three-dimensional printed trileaflet valve conduits using biological hydrogels and human valve interstitial cells.* Acta Biomaterialia, 2014. **10**(5): p. 1836-1846.

39. Mol, A., et al., *Tissue engineering of heart valves: advances and current challenges.* Expert Review of Medical Devices, 2009. **6**(3): p. 259-275.

40. Khatiwala, C.B., S.R. Peyton, and A.J. Putnam, *Intrinsic mechanical properties of the extracellular matrix affect the behavior of pre-osteoblastic MC3T3-E1 cells.* American Journal of Physiology-Cell Physiology, 2006. **290**(6): p. C1640-C1650.

41. Walker, G.A., et al., *Valvular myofibroblast activation by transforming growth factor-beta - Implications for pathological extracellular matrix remodeling in heart valve disease.* Circulation Research, 2004. **95**(3): p. 253-260.

42.   Prager-Khoutorsky, M., et al., *Fibroblast polarization is a matrix-rigidity-dependent process controlled by focal adhesion mechanosensing.* Nature Cell Biology, 2011. **13**(12): p. 1457-U178.

43.   Pelham, R.J. and Y.L. Wang, *Cell locomotion and focal adhesions are regulated by substrate flexibility.* Proceedings of the National Academy of Sciences of the United States of America, 1997. **94**(25): p. 13661-13665.

44.   Rehfeldt, F., et al., *Cell responses to the mechanochemical microenvironment - Implications for regenerative medicine and drug delivery.* Advanced Drug Delivery Reviews, 2007. **59**(13): p. 1329-1339.

45.   Rehmann, M.S., et al., *Tuning microenvironment modulus and biochemical composition promotes human mesenchymal stem cell tenogenic differentiation.* Journal of Biomedical Materials Research Part A, 2016. **104**(5): p. 1162-1174.

Figures and Tables
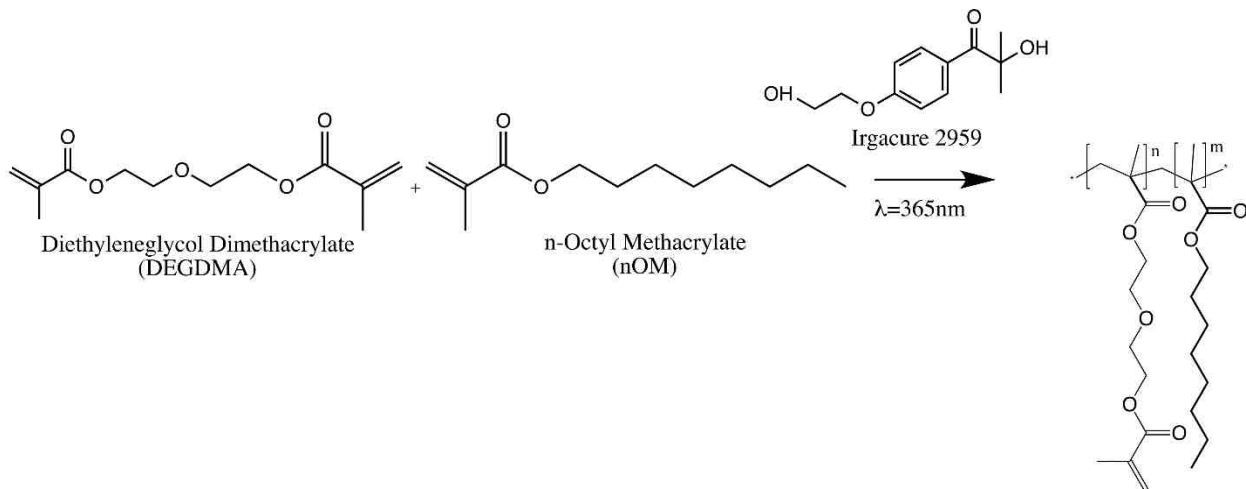
Figure 1. Network crosslinking scheme of DEGDMA/nOM.

Figure 2. Compressive modulus of 3% (25 kPa inset), 19% (925 kPA) and 33% (4750 kPa) DEGDMA/nOM are significantly different (p< 0.05*).

Table 1. X-ray Photoelectron Spectroscopy
Percentages

	C 1s	O 1s	C / O Ratio
3%DEGDMA Experimental	79.2	16.4	4.7
3% DEGDMA Stoichiometric	85.0	15.0	5.7
33% DEGDMA Experimental	80.7	17.4	4.6
33% DEGDMA Stoichiometric	81.0	19.0	4.3

Table 1. Elemental composition of the maximum and minimum DEGDMA content substrates made determined by XPS analysis. Values represent the relative atomic percentage of each species present on the surface averaged from two locations. Trace amounts of (<1%) nitrogen and silicon (<4%) was also detected.
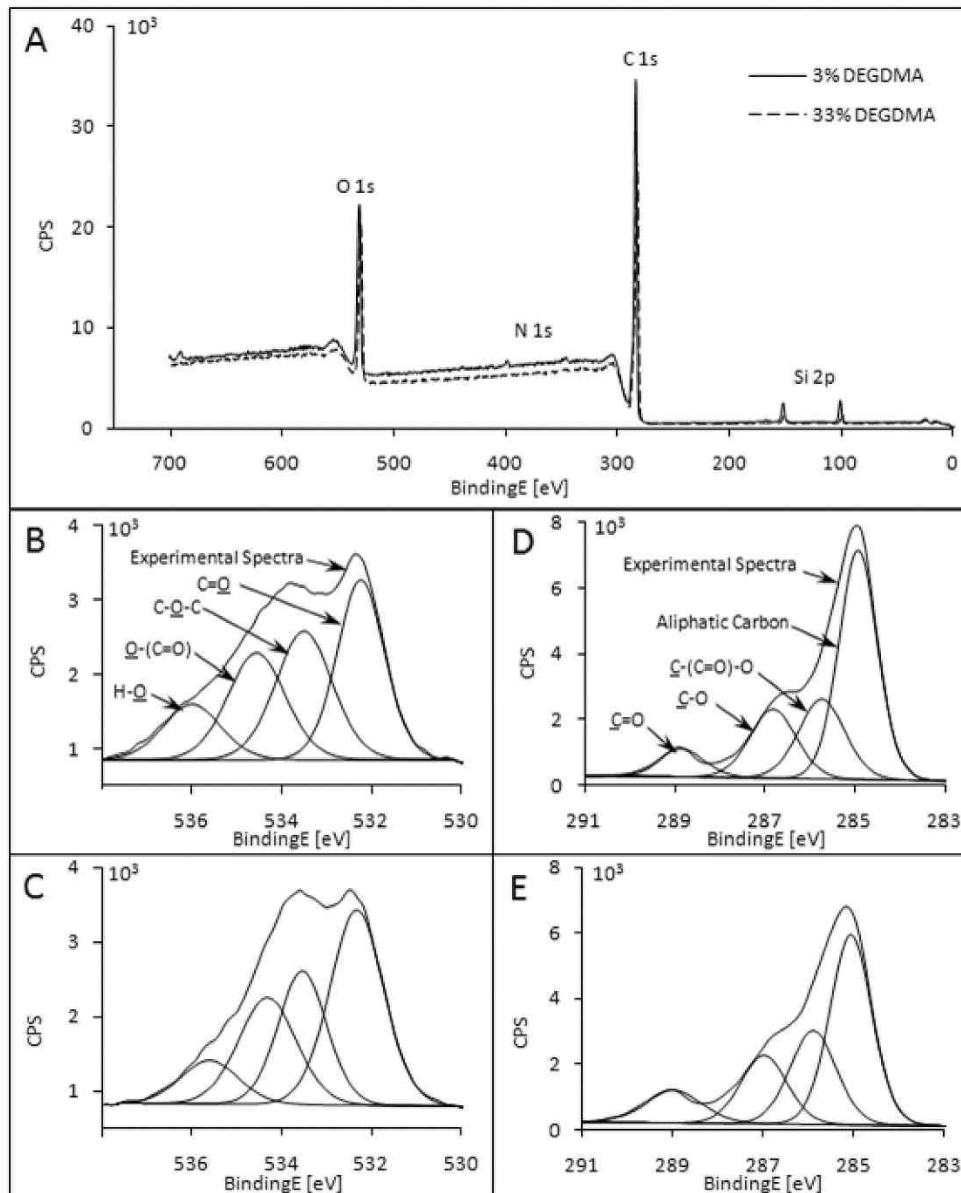
Figure 3. Representative survey and high-resolution scans from 3 and 33 wt% DEGDMA/nOM. A) Survey scans, show surface elemental composition of primarily oxygen and carbon with trace amounts of nitrogen and silicon. B) The O1s hi-resolution spectra for 3% and C) 33 % DEGDMA/nOM demonstrate similar peak shapes between the two formulations. The surface reproducibility is confirmed by the C1s high-resolution scans of the D) 3% and E) 33% DEGDMA/nOM substrates.
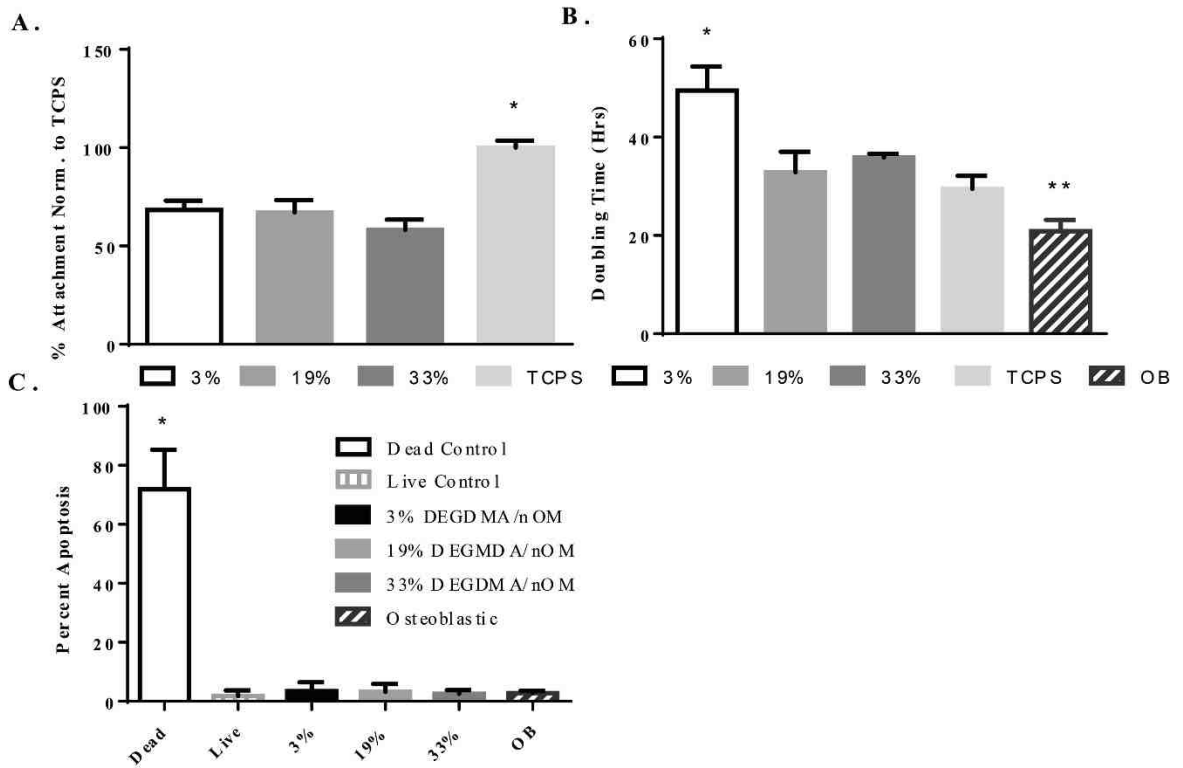
Figure 4. A) Attachment at 24 hrs shows a significant difference in VIC attachment of DEGDMA/nOM surfaces normalized to TCPS. B) Doubling times of VICs, with 3% growing significantly slower than 19 and 33% DEGDMA/nOM (* p ≤ 0.05) and OB growing significantly faster than TCPS (** p ≤ 0.05). C) Apoptosis at 7 days in culture is significantly increased in the dead control (*p ≤ 0.01).
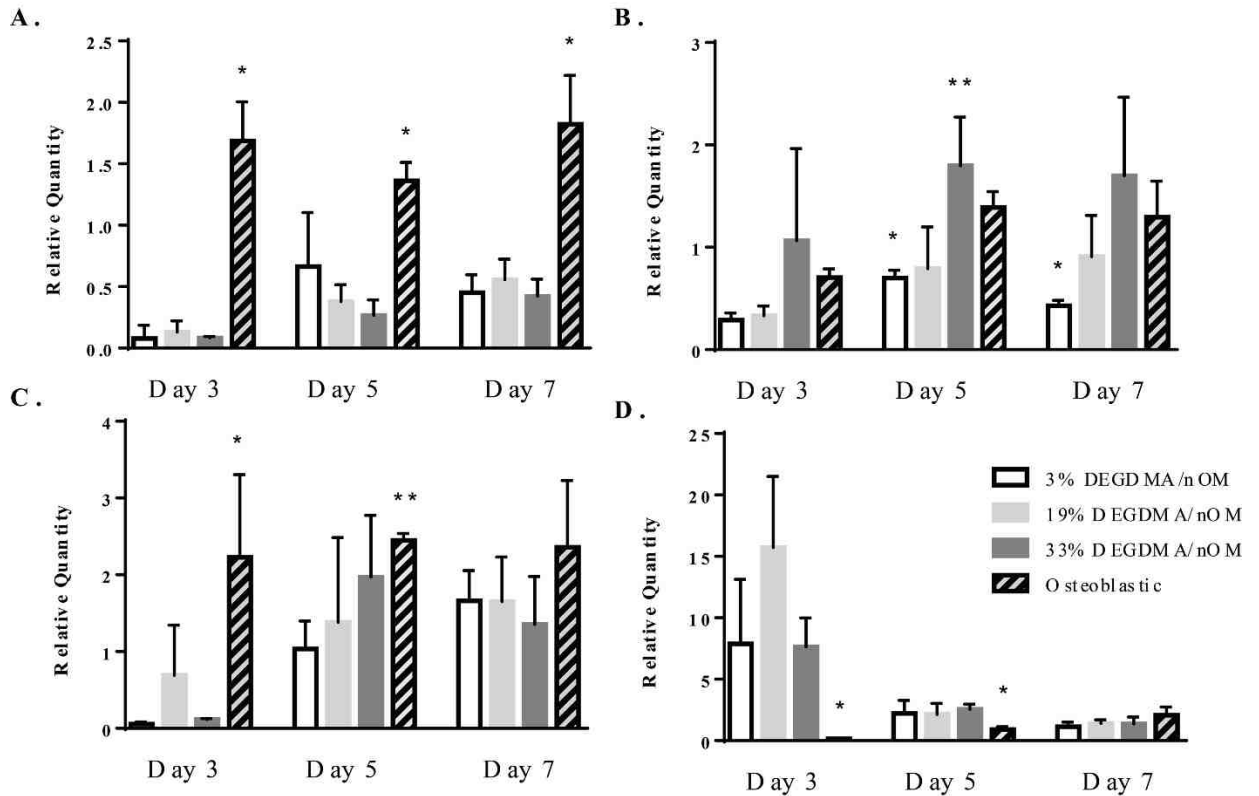
Figure 5. Gene expression of A) alpha smooth muscle actin (αSMA), B) osteocalcin (OCN), C) Collagen 1 alpha 2 (Collagen), and D) Elastin. A) Osteoblastic VICs express significantly higher αSMA at all time points compared to all DEGDMA/nOM substrates. B) 3% DEGDMA/nOM VICs express significantly less OCN than OB and 33% DEGDMA/nOM at 5 and 7 days (*p ≤ 0.05). 33% DEGDMA/nOM expresses significantly more OCN than 19% DEGDMA/nOM at day 5 (**p ≤ 0.05). C) OB VICs express significantly higher elastin than 3 or 33% DEGDMA/nOM at day 3 (*p ≤ 0.05), but remain significantly higher than 3% DEGDMA/nOM by day 5 (**p ≤ 0.05). D) DEGDMA/nOM surfaces have increase collagen 1α2 expression at day 3 and day 5 compared to OB VICs (*p ≤ 0.05).
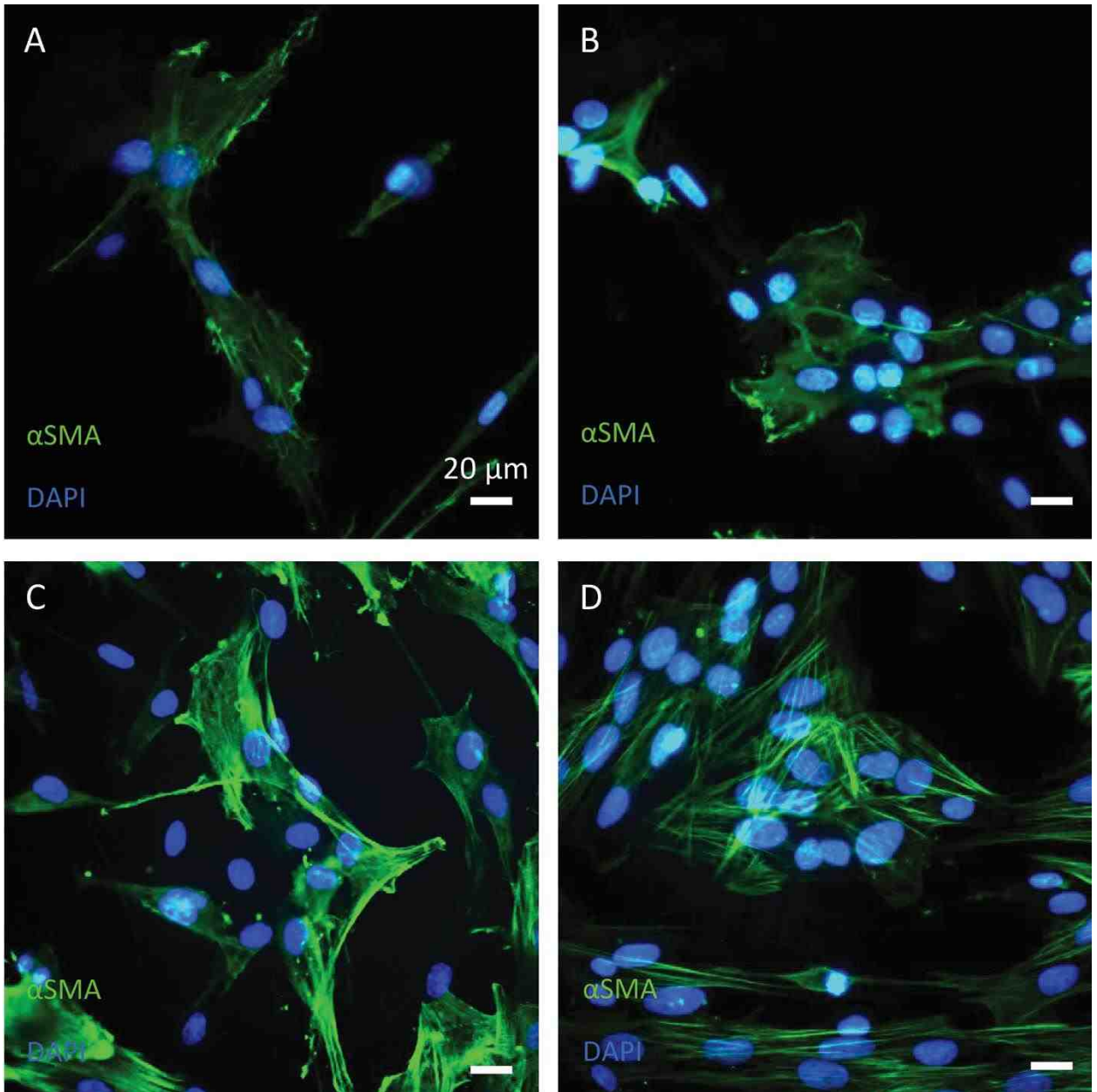
Figure 6. αSMA staining (green) on A) 3% B) 19%, C) 33% and D) OB VICs at day 3 counterstained nuclei with DAPI (blue). Notice the development of αSMA stress fibers (white arrows) on 33% DEGDMA/nOM and OB VICs compared to 3% and 19% DEGDMA/nOM.
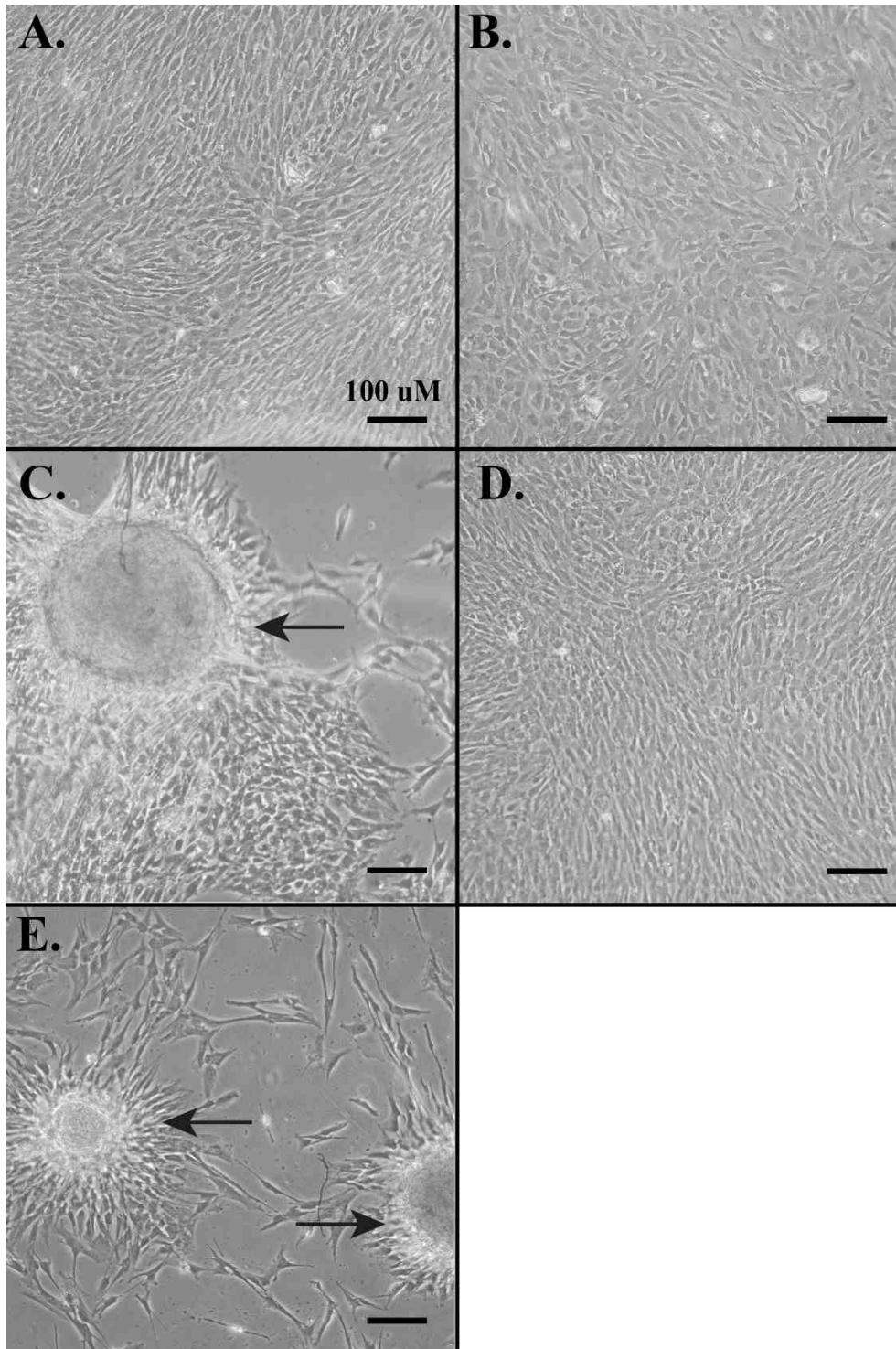
Figure 7. Optical images of all treatment at day 7. A) 3% B) 19% C) 33% D) TCPS and E) OB VICs. Arrows indicate nodules.

Chapter 5

Surface Chemistry Regulates Valvular Interstitial Cell Differentiation In Vitro

Matthew N. Rush[1,2], Kent E. Coombs[1,3], and Elizabeth L. Hedberg-Dirk[1,2,4*].

*[1]Center for Biomedical Engineering, [2]Nanoscience and Microsystems Engineering,
[3]Biomedical Science Graduate Program, [4]Chemical and Biological Engineering,
University of New Mexico, Albuquerque, NM, USA.*

Corresponding Author: Elizabeth L. Hedberg-Dirk
Address: Center for Biomedical Engineering
          MSC01 1141
          1 University of New Mexico
          Albuquerque, NM 87131
Email: edirk@unm.edu
Fax: 505-277-6209
Phone: 505-277-5906

Alternate Author Email:
Matthew N. Rush, mrush@unm.edu
Kent E. Coombs, kcoombs@salud.unm.edu

Abstract

The primary driver for valvular calcification is the differentiation of valvular interstitial cells (VICs) into a diseased phenotype. However, the factors leading to the onset of osteoblastic-like VICs (obVICs) and resulting calcification are not fully understood. This study isolates the effect of substrate surface chemistry on *in vitro* VIC differentiation and calcified tissue formation. Using ω-functionalized alkanethiol self-assembled monolayers (SAMs) on gold [CH_3 (hydrophobic), OH (hydrophilic), COOH (COO^-, negative at physiological pH), and NH_2 (NH_3^+, positive at physiological pH)], we demonstrate that surface chemistry modulates VIC phenotype and calcified tissue deposition independent of osteoblastic-inducing media additives. Over seven days VICs exhibited surface-dependent differences in cell proliferation ($COO^- = NH_3^+ > OH > CH_3$), morphology, and osteoblastic potential. Both NH_3^+ and CH_3-terminated SAMs promoted calcified tissue formation while COO^--terminated SAMs showed no calcification. VICs on NH_3^+-SAMs exhibited the most osteoblastic phenotypic markers through robust nodule formation, up-regulated osteocalcin and α-smooth muscle actin expression, and adoption of a round/rhomboid morphology indicative of osteoblastic differentiation. With the slowest proliferation, VICs on CH_3-SAMs promoted calcified aggregate formation through cell detachment and increased cell death indicative of dystrophic calcification. Furthermore, induction of calcified tissue deposition on NH_3^+ and CH_3-SAMs was distinctly different than that of media-induced osteoblastic VICs. These results demonstrate that substrate surface chemistry alters VIC behavior and plays an important role in calcified

107

tissue formation. In addition, we identified two novel methods of inducing VIC calcification *in vitro*. Further study of these environments may yield new models for *in vitro* testing of therapeutics for calcified valve stenosis and although additional studies need to be conducted to correlate results to *in vivo* models.

Introduction

Valvular heart disease (VHD) is estimated to affect 2.5% of the US population with a disproportionate impact on an increasing elderly community.[1, 2] Derived from infections, valve degeneration, or genetic disorders, VHD can manifest as regurgitation or stenosis of the valve. As a result of obstructed blood flow, valve stenosis generates transvalvular gradients that trigger compensatory ventricular hypertension, leading to increased risk for other cardiovascular disorders.[1-3] As such, VHD represents a significant health risk worldwide. Furthermore, rises in the prevalence of VHD will continue to increase as the elderly population grows due to advances in medical technology.[1-5]

The leading cause of VHD is valve stenosis, characterized by valve thickening, increased protein deposition, and eventual calcification.[3, 4, 6] The primary driver for valvular calcification is the differentiation of valvular interstitial cells (VICs) into a disease inducing phenotype.[6, 7] However, the factors leading to the onset of VIC differentiation and resulting calcification are not fully understood and a more complete characterization of VIC differentiation and phenotypic change is required before treatment of valve disease can be realized.

As the predominant cell type within the valve, VICs are responsible for valve formation, remodeling, and tissue homeostasis. VICs are a heterogeneous population that undergo phenotypic changes regulated by environmental factors. VICs have been shown to alter phenotype in response to soluble factors,[8-11] substrate stiffness,[6, 8, 12-15] and surrounding extracellular matrix proteins.[8, 10, 11, 16-21] Although phenotypic change is a dynamic event, VIC function is

frequently compartmentalized in order to clarify and separate the underlying causes.[22]

VICs are commonly characterized as quiescent (qVIC), activated (aVIC), and disease phenotypes. In a normal adult valve, qVICs are thought to preserve physiological structure and function while maintaining a low level of matrix synthesis and degradation inhibiting angiogenesis.[22] Following injury or abnormal hemodynamic/mechanical stress, VICs become activated (aVICs, myofibroblastic) and are associated with increased extracellular matrix secretion and expression of various biological markers including α-smooth muscle actin (α-SMA), matrix metalloproteinases, and transforming growth factor-β.[22, 23] Activated VICs exhibit increased contraction, prominent stress fiber formation, increased proliferation, and migration.[22] *In vitro,* aVICs display an elongated morphology and form orthogonal patterns of overgrowth resembling hills and valleys.[6] Upon completion of remodeling or wound healing, most aVICs are eliminated by apoptosis or reversion to qVICs.[24]

When VIC dysregulation or abnormal extracellular matrix production occurs, conversion to diseased phenotypes results in pathological fibrosis and calcification of the valve.[10, 24] The mechanisms of VICs tissue calcification have been intensely studied and currently two processes have been proposed. [5, 25-27] Dystrophic calcification is a passive degenerative process characterized by early cell injury and deposition of calcium associated with tissue damage and necrotic cells. [10, 25, 26] Alternatively, osteogenic calcification (ossification) is an active process involving bone and cartilage development,

marked by the expression of various osteogenic markers. [7, 25, 26, 28] *In vitro,* VICs undergoing osteogenesis and osteoblastic-like VICs (obVICs, are characterized by a round/rhomboid morphology followed by the formation of three-dimensional calcified nodules. It is important to note that these two processes are not mutually exclusive as a common activator of tissue calcification, TGF-β, has been shown to lead to cellular apoptosis as well as nodule formation.[10] However, different processes may arise due to variations in signaling in the cellular microenvironment. Forced obVIC differentiation *in vitro* is commonly achieved by adding soluble signaling factors (β-glycerophosphate, ascorbic acid, and dexamethasone) to media. However, spontaneous *in vitro* nodule formation in media lacking osteoblastic inducing additives,[8] as well as calcification of decellularized biological valves *in vivo,* suggests calcification may be mediated by additional physical cues.[29]

To understand how surface chemistry correlates to VIC behavior and initiation of valvular disease, we used alkanethiol self-assembled monolayers (SAMs) of ω-functionalized alkanethiolates on gold as model substrates with uniform chemistry. The chemisorption of thiols to gold and the hydrophobic interactions of alkane chains results in stable, ordered, and well-packed monolayers (Figure 1).[30] As such, SAMs offer well-defined models for systematically investigating phenotypic change directed by surface chemistry. Four physiologically relevant functional groups were used to assess the effects of substrate hydrophobicity and charge on VIC phenotypic behavior. Due to the negatively charged environment present during valvulogenesis through increased

hyaluronic acid expression, it was hypothesized that anionic functional groups would result in VIC activation and tissue production.[31, 32]

Materials and Methods

Reagents and Chemicals

All chemicals were purchased from Sigma-Aldrich chemicals unless otherwise noted. All cell culture media and reagents were purchased from Thermo Fisher Scientific, unless otherwise noted.

Fabrication of Self Assembled Monolayers

Gold-coated round 15 mm glass cover slips (26021, Ted Pella Inc.) were used as substrates for self-assembled monolayer (SAMs) formation. Coverslips were etched for 30 minutes prior to gold deposition in Piranha solution [70% (v/v) concentrated H_2SO_4, 30% industrial grade H_2O_2 (KMG Chemicals)] rinsed with diH_2O, and blown dry with N_2. Gold coating was conducted by sequential electro-evaporation of optically transparent films of chromium, adhesion layer (2 nm; High Vacuum Evaporator Systems), followed by gold (30 nm, 99.99% purity; Plasmaterials). Metal deposition was accomplished at 2 nm/s using a Thermionics VE-90 vacuum Evaporation System (TLI Enterprises) with chamber pressures at or below 1×10^{-5} Torr. Freshly prepared gold substrates were immersed in 1mM ethanolic alkanethiol solutions [1-dodecanthiol (47-136-4); 11-mercapto-1-undecanol (447528-16); 11-mercaptoundecanioc acid (450561-5G); 11-amino-1-undecanethiol, hydrochloride 1N NaOH (A423, Dojindo

Laboratories)] and SAMs were allowed to assemble for 12 hours.[30, 33] Etched cover glass and gold-coated controls were incubated alongside SAMs in absolute ethanol. Before use or characterization, samples were cleaned of unbound thiols in absolute ethanol and dried with N_2. In order to obtain desired charge on COOH (COO$^-$) and NH$_2$ (NH$_3^+$) surfaces, samples were rinsed in 1N basic (NaOH; EMD) and acidic (HCl; EMD) ethanol solutions, respective of charge group, blown dry with N_2 and then cleaned.[34]

Contact Angle Measurements

Static contact angles and images were evaluated using the sessile drop technique on a Model 100-00-115 Advanced goniometer (ramé-hart Inc.). Briefly, 5 µL of ultrapure water was pipetted onto sample surface and the contact angles were measured immediately after drop formation to minimize the effect of dynamic surface wetting and evaporation. Contact angle measurements between the water droplet and the sample surface were determined using DROPimage Standard software (ramé-hart).

X-Ray Photoelectron Spectroscopy (XPS)

XPS survey and high resolution spectra were obtained using Axis Ultra spectrometer (Kratos Analytical Ltd.) with a monochromatic Al K(α) (1486.6 eV) source at 225W. High-resolution spectra of carbon and oxygen were obtained for three areas for each sample at 30˚ and 90˚ take-off angles. Electron pass energy of 20 eV was used to analyze the regions of interest and curve fitting was

performed on each spectral region to calculate atomic percentages. Base pressure was less than 5×10^{-9} Torr. Charge compensation was accomplished using low energy electrons. Linear background was used for elemental quantification of C1s and O1s spectra. Quantification utilized sensitivity factors provided by the manufacturer. All the spectra were charge referenced to Au at 84 eV. Curve fitting was carried out using individual peaks of constrained width, position, and 70% Gaussian/ 30% Lorentzian line shape.

Atomic Force Microscopy

Scanning was performed at 2.50 µm/s (0.25 Hz) using a super sharp silicon probe (SSS-NCH, r > 5nm, Nanoworld) on an MFP3D-BIO (Asylum Research).

Ellipsometry

Freshly prepared samples were analyzed for film thickness using a Nanofilms EP3 optical ellipsometer @ 532nm (Accurion). Samples were collected at an incident angle of 70˚ for three areas on three different samples. The layer thickness was calculated using an index of refraction n = 1.52.[35, 36]

Primary Cell Extraction & Characterization

VICs were obtained through primary cell extraction from recently excised pig hearts (Hormel Foods Corp.) shipped overnight on ice. Aortic heart valves leaflets were removed and washed in 25 mL Dulbecco's phosphate buffered

solution (DPBS) containing 2% (v/v) penicillin/streptomycin (P/S, Life Technologies). Three hearts (9 leaflets) were combined in 25 mL collagenase solution [12,500 units collagenase (LS004174, Worthington Biochemical Grp.) in 50 mL Media 199 (Hyclone, SH30253.01)] filtered through 22 µm Steriflip unit (Millipore) and incubated at 37°C for 15 min with gentle agitation. Both sides of leaflets were scraped and rinsed in DPBS to remove endothelial cells. Leaflets were then incubated with 25 mL fresh collagenase solution at 37°c for 60 min with gentle agitation. Leaflets were vortexed for 2 min to loosen attached cells. Supernatant was collected and filtered through 100 µm cell strainer (BD Falcon). To remove valvular endothelial cells (VECs), cell solutions were incubated with 50 µL of magnetic beads labeled with CD31 antibody (Dynabead CD31, Life Technologies) at 4°C for 30 minutes with occasional mixing. Dynabeads were removed by magnetic separation. VICs were then placed in a new conical tube and centrifuged. Supernatant was removed and cells were re-suspended in VIC media [Media 199 (Hyclone), 10% FBS, 1% P/S, & 1% Fungizone]. Cells were seeded in T75 flasks (collagenase sample), and remaining leaflet material was diced and plated into 6-well plates (Corning), 1 leaflet/well, to allow remaining VICs to migrate from leaflet (explant sample).

VICs were incubated (37°C, 5% CO_2, ~90% RH) and grown for 7-10 days, with media changes every other day. Cell supernatant was removed from T75 flasks after 2 days of attachment. Heart valve leaflets were removed from well plates after 3 days. Cells were grown to 70% confluence and enzymatically detached from surface with 2 mL of .25% (w/v) trypsin (Life Technologies).

115

Collagenase and explant samples were combined in M199 media with 10% FBS (v/v) and 10% DMSO (EMD), and cryogenically frozen until use. VICs were seeded on SAMs between passages 3-4.

Cell Growth & Viability

Before seeding on substrates, VICs were thawed and grown to 80% confluence to ensure cell viability. For all experiments, substrates were equilibrated with complete growth media [Medium 199, 10% fetal bovine serum, 1% penicillin/streptomycin, 1% fungizone] prior to cell seeding at 21,500 cells/cm^2. Media was replaced after 12 hours to remove unbound cells (attachment) and changed every two days. Osteoblastic controls were grown in OB media [Media 199, 10% fetal bovine serum, 10mM β-glycerophosphate, 2 mM ascorbic acid, & 10^{-7}M dexamethasone] [6] after initial 12-hour attachment. Substrates were rinsed prior to testing. Cell attachment and proliferation was assessed after 12 hours, and at 3, 5, & 7 days using MTT calorimetric assay (30-1010K, ATCC) according to manufacturer's instructions.

VIC viability was further investigated using AlexaFluor 488 Annexin V/Dead cell apoptosis kit (V13241, Life Technologies) according to manufacturer's instructions. Briefly, at 12 hrs and 5 and 7 days, culture media was removed and retained for apoptotic/dead cell concentrations while attached cells were enzymatically removed from surfaces. Cells were centrifuged, supernatant removed, and cell pellet re-suspended in 1x annexin binding buffer. Necrotic controls were achieved by incubating with 70% (v/v) ethanol. Apoptotic

116

controls were achieved by leaving cultures at room temperature overnight. All

samples were incubated with 100 µL staining solution [5 µL Annexin V and 1 µL

propidium iodide @ 100µg/mL in 1x annexin binding buffer] for 15 minutes.

Samples were read on Accuri C6 flow cytometer (BD Bio.).

Calcium Content

After 5 and 7 days, calcium deposition was visualized by incubating cells

with the anthriquinone dye alizarin red S (ARS), forming a complex via chelation.

Briefly, culture medium was aspirated and cells were rinsed 3x with DPBS

followed by fixation using 10% formalin for 1 hour. After fixation, 100 µl of 40 mM

ARS staining solution (pH 4.1) was added to each well and incubated for a

minimum of 30 minutes in the dark at room temperature. [6] Upon completion the

ARS solution was aspirated and the wells were rinsed 3x with diH20 then PBS in

order to ensure removal of non-specific ARS stain. Samples were imaged under

brightfield with phase contrast 10x magnification objectives (Eclipse TS1000).

Calcified tissue and nodule diameter was determined using Image J (NIH).

Gene Expression

All reagents for gene expression were purchased from Life Technologies

unless otherwise noted. mRNA was extracted from cell samples using RNAeasy

plus micro kit (Qiagen 74034) with gDNA removal, according to manufacturer's

instructions. Total mRNA content was analyzed using Nanodrop UV/Vis

Spectrometer (Model 2000c, Thermo Fisher Sci.) and reverse transcription

carried out using GoScript reverse transcriptase system (Promega). Gene

expression of αSMA/ACTA (Ss04245588_m1), osteocalcin/BGLAP

(Ss03373655_s1), collagen I-α2 (Ss03375690_U1), and elastin (EMLIN: Custom

Primer#AJLJIR9) were analyzed using TaqMan Gene Expression master mix,

according to manufacturers specifications, and measured on a StepOne Real

Time-PCR (Applied Bio). Data was collected and analyzed using StepOne

software v2.2.2. All samples were compared to GAPDH (Ss03374854_g1)

endogenous controls.

Immunocytochemical (ICC) Staining

Cells were fixed with 10% formalin for one hour and washed twice with

DPBS. Cells were then permeabilized with 0.01% (v/v) Tween20 in DPBS

(PBST) for 15 min followed by reactive ion removal using 10% (m/v) sodium

azide and 10μM H_2O_2 in PBST. Samples were incubated with primary antibodies

(αSMA, ab7817) diluted 1:75 in a 3% (w/v) BSA solution for 90 minutes. Primary

antibodies were removed and samples washed twice with PBST followed by

secondary antibodies goat anti-mouse AlexaFluor 488 (A11001, Invitrogen)

1:400 in DPBS incubation for 90 minutes. Cells were counter stained with DAPI

in DPBS (1:1000, Invitrogen) for 5 minutes. Samples were mounted

(Fluoromount, F4680-25ML) on glass slides and sealed with clear nail polish.

Samples were imaged on a Zeiss LSM 510 META microscope with 40x oil 1.3

NA objective.

Statistical Analysis

All results were analyzed using one-way analysis of variance followed by Tukey-Kramer post hoc analysis with Sidak correction for multiple comparisons and a 95% confidence interval ($p < 0.05$). All analyses were done using Prism 6 software (GraphPad).

Results

Surface Characterization of Self-Assembled Monolayers

Self-assembled monolayers expressing four different functional groups (CH_3, OH, COO^-, NH_3^+) were used as model surfaces to assess the effect of substrate chemistry on VIC phenotype. These four chemistries exhibit different degrees of wettability and charge. CH_3-SAMs are non-polar and relatively hydrophobic, whereas, OH, COO^-, and NH_3^+ are relatively hydrophilic. At physiological pH (7.4) partially ionized COOH and NH_2 SAMs present negative or positive charges, respectively (COO^- and NH_3^+).[34, 35] Gold-coated and uncoated glass were run as negative control substrates. Results from all experiments performed showed no statistical difference between the gold (Au) and glass controls. Therefore, only Au data are included. As current methods of osteoblastic differentiation utilize supplemented media, obVIC-media induced positive control samples on glass were used. All surface treatments and controls were characterized prior to VIC studies.

Static water contact angles of SAMs measured by goniometry are summarized in Figure 1. Measured values are in agreement with those reported

in literature.[33, 37] X-ray photoelectron spectroscopy analysis of surface

chemistry agrees with theoretical percentages (Supplemental Figure I).

Ellipsometric measurements of SAMs indicate monolayer formation, with

confirmation by atomic force microscopy (Supplemental Figure II and Table

1).[34, 35]

Proliferation and Cellular Density of VICs

Initial differences in the number of attached cells were observed within the

first 12 hours (Supplemental Figure III). CH_3-SAMs resulted in significantly lower

attachment (53% of attachment average) as compared to all other treatments

when seeded at 21,500 cells/cm^2. Results reflect literature showing decreased

cell adhesion to hydrophobic surfaces.[37-39] In order to provide uniform seeding

density all subsequent experiments were seeded at 43,000 cells/cm^2 on CH_3-

SAMs and 21,500 cells/cm^2 on all other surfaces ensuring no significant

difference in initial cell density between treatments (Figure 2).

Proliferation of VICs was assessed over seven days, demonstrating

variations in growth rate due to substrate chemistry. A lack of initial proliferation

on CH_3 and OH-SAMs resulted in a significantly lower cell concentration at day 3.

Over the same time, VICs on glass induced with OB media demonstrated the

greatest proliferation rate and significantly higher cell concentration. All other

treatments (Au, COO^-, and NH_3^+) resulted in a moderate initial proliferation rate.

120

Morphological Variation Between Surfaces

By day 3 VICs on all surfaces exhibited an elongated morphology (Figure 3). However, between days 3 and 5, significant morphological differences amongst treatments emerged. Individual VICs in OB media developed a round/rhomboid morphology and spread to fill the entire growth area. Similar round/rhomboid VIC morphology was exhibited by NH_3^+, CH_3, and OH-SAMs to varying degrees (Figure 3, Supplemental Figure IV-V). VICs on COO^--SAMs and Au maintained elongated morphology through 5 days.

By day 7 VICs on Au, OH, and COO^--SAMs developed highly aligned confluent cultures, similar to aVICs,[6, 22] while VICs in OB media and on NH_3^+-SAMs tended to adopt a round/rhomboid morphology with non-linear/spread confluent cultures (Figure 3). As the only surface not to reach confluence, VICs on CH_3-SAMs had a round morphology in lower density regions, and formed clustered aggregates in higher density areas. The tendency for cellular aggregates on CH_3-SAMs to partially detach from the surface led to the formation of sheeted aggregates semi-suspended in culture media (cell sheets). Cell sheets were typically bound by a single edge resulting in the cell sheet folding back upon itself (Supplemental Figure VI).

Development of Calcified Nodules

At confluence (day 7), cells on all treatments except COO^--SAMs and osteoblastic culture exhibited some degree of calcification (Figures 3 and 4). On CH_3-SAMs early cellular clustering resulted in the formation of large cellular

121

aggregates (221 ± 123 µm). On Au and OH-SAMs, small spherical nodules were observed infrequently and the nodules were typically small (30-60 µm), indicative of recent formation. Distinct from all other treatments, VICs grown on NH_3^+-SAMs exhibited nodule formation by day 5, which increased in size (115 ± 40 µm) and frequency by day 7 (Figure 3 and Table 1). VICs grown in OB media exhibited no nodule formation through 7 days, consistent with the observation that nodules typically appear between 14 and 21 days under supplemental media conditions (without TGF-β).[6, 8, 40] Small nodules were observed in OB cultures when cultured at 14 days (Supplemental Figure VII).

Nodule formation is typically accompanied by apoptosis and deposition of Ca^{2+}. In order to determine calcium deposition and apoptosis/necrosis, samples were stained with alizarin red S and imaged using bright field microscopy, or evaluated by flow cytometry using annexin V and propidium iodide. After 7 days, VICs grown on COO^--SAMs were the only cells to lack nodule formation or calcium staining (Figure 4). On Au and OH-SAMs VICs exhibited few small alizarin red S stained nodules, while VICs on CH_3-SAMs exhibited calcium within cellular aggregates with no distinct boundary. OB media induced VICs exhibit some cellular alizarin red S staining, but no aggregate nodular structures were observed. NH_3^+-SAMs, however, developed tightly bound, spherical calcium nodules with significant alizarin red S staining (Figure 4, arrows). When apoptosis was assessed at day 7, VICs exhibited equivalent levels of apoptosis on all treatments (Figure 5a). Overall cell death, staining positive for annexin V and propidium iodide, was statistically elevated on CH_3-SAMs (Figure 5b).

Genetic Analysis of Phenotypic Markers

In order to determine phenotype of VICs, samples were tested for common genetic markers. The development of contractile α-SMA cytoskeletal filaments is an accepted indicator of activation.[22, 41] At 3 and 5 days VICs grown on NH_3^+-SAMs and OB media had a significant up-regulation of α-SMA mRNA expression compared to other treatments (Figure 6A). Similar up-regulation was observed in VICs stained for α-SMA using immunocytochemistry (Supplemental Figure V). Osteocalcin (OCN), a late-stage marker of OB differentiation[6, 22] that typically accompanies the onset of nodule formation was evaluated at 5 and 7 days of culture. By day 7, VICs grown on NH_3^+-SAMs had a significant increase in OCN mRNA expression compared to all other treatments including media-induced obVICs (Figure 6B). To assess ECM production, collagen I and elastin mRNA expression were quantified at 3 and 5 days (Figure 7). After 3 days, collagen was upregulated on NH_3^+-SAMs hand media induced osteoblastic controls. Collagen expression appeared to be elevated in CH_3-SAMs, but results were not statistically different from Au controls. By day 5, all SAMs treatments are significantly lower than Au controls. Elastin expression was elevated on NH_3^+ surfaces at day 5, accompanying nodule formation.

Discussion

Many factors influencing VIC phenotype have been studied to better understand calcified nodule formation and to manipulate *in vitro* culture for healthy tissue production.[6, 8-11, 17-21] Previous research investigating the effect of distinct protein layers on VIC phenotype has attempted to control the cellular binding environment through adsorption and presentation of specific proteins onto tissue culture polystyrene. [6, 8-11, 17-21] However, the non-homogeneous surface of tissue culture substrates causes disorganized deposition of proteins with uncontrolled orientations,[8, 42] resulting in conflicting results in the literature.[18, 20]

Alkanetiolate Self-Assembled Monolayers

The uniform SAMs surface chemistry appears to facillitate for controlled protein deposition and orientation, with distinct and reproducible culture surfaces to study cell behavior in different microenvironments.[37, 38, 42, 43] In previous work, it has been observed that proteins in culture adsorb at a faster rate than cell attachment, and dictate cell-surface interactions.[38, 44] Specifically the adsorption of serum proteins and specific extracellular matrix proteins varies with hydrophobic/hydrophilic and charged surfaces. Variability in their tertiary structure changes with surface chemistry, resulting in variation in available cellular attachment domains.[37-39, 43, 45]

Media-Induced Osteoblastic VICs

As a positive control VICs were grown in OB media on glass. Proliferation rate and cell spreading was similar to results reported in the literature.[6] While calcification did not occur in cell cultured in OB media within the seven days of this study, cultures extended for 14 days developed the expected nodule formation. This is in agreement with previous studies showing nodule formation occurs between 14-21 days in low-density (<25,000 cells/cm^2) cultures, typically after the development of αSMA stress fibers, cellular detachment, and contraction.[6, 9, 40] For this reason, αSMA is considered necessary for osteoblastic differentiation, suggesting that qVICs must go through activation to transform to in obVICs and develop tissue calcification.[9, 23] However, cells grown on CH$_3$-SAMs suggest a direct transition through well-defined stress fiber formation (quiescent → activated → osteoblastic) is not always necessary for the development of calcification, similar to previous observations of dystrophic calcification caused by cell death.[10]

Non-activated VIC Calcium Deposition on CH3-SAMs

As hydrophobic CH$_3$-SAMs have been shown to irreversibly adsorb and denature proteins resulting in loss of cellular binding domains, CH$_3$-SAMs provide examples of into changes in VIC phenotype that result from low cell adhesion.[38, 39, 44] The slow proliferation, cellular aggregation, and formation of loosely adhered cell sheets suggest minimal interaction between the VICs and

CH$_3$-SAMs. As such, the early aggregate behavior of VICs maybe the result of cell-cell adhesion to compensate for a lack of cell-surface adhesion.

Previous experiments have shown the release of mechanical tension on VICs also leads to increased apoptosis and *in vitro* calcification.[6, 7, 46, 47] Increased αSMA expression typically accompanies nodule formation, thus, calcification on hydrophobic surfaces without elevated αSMA expression suggests that VIC detachment may result in calcification without the need for αSMA-mediated contraction.[9, 23] Higher Ca^{2+} deposition under hydrophobic conditions are therefore likely related to the high cell necrosis levels observed through classical dystrophic mechanisms of cell death resulting in release of intracellular calcium and aggregation under this condition. Previous results by Jain B. *et al.* have shown that tissue calcification *in vitro* does not require cellular contraction and spherical nodule formation to induce apoptosis and calcium deposition.[6, 10] As such, less cell adhesion and possibly altered integrin and cell-cell signaling may be the triggering events for increased cell death and Ca^{2+} deposition under these experimental conditions.[6, 48] Further studies are needed to determine if this observed behavior is similar to that *in vivo* disease.

Osteoblastic VIC Differentiation on NH$_3^+$-SAMs

With increased proliferation, elongated morphology, and increased αSMA expression over other functionalized SAMs, VICs grown on NH$_3^+$ surfaces exhibit early myofibroblastic behavior. With the onset of a round/rhomboid morphology,

robust nodule formation, and OCN expression, NH_3^+-SAMs undergo a clear transition from an aVIC to obVIC between days 3 and 5. The expression of OCN, a late stage osteoblastic marker, and the early appearance of calcified nodules suggests an accelerated transition between activated and osteoblastic phenotypes on cationic surfaces. Such behavior correlates with the observed osteoblastic differentiation of pre-osteoblastic cells on NH_3^+ surfaces.[39] Compared to the soluble factors used in OB media induction, the rapid obVICs differentiation on NH_3^+-SAMs is controlled by cell-surface interactions, as no media additives were present. As no calcium deposition and gene expression in osteoblastic culture were observed during this same timepoint, the accelerated obVIC behavior is likely the result of signaling induced by cell-material interactions specific to protein adsorption on NH_3^+ surfaces.

NH_3^+-SAMs have been shown to preferentially adsorb greater amounts collagen and fibronectin than other hydrophilic groups (COO^- and OH).[43] However, the influence of collagen and fibronectin on VIC nodule formation is unclear.[10, 18-20] Such behavior may result from different extracellular matrix proteins in these cultures. Interestingly, NH_3^+-surfaces also resulted in a significant up-regulation of elastin expression over all other surfaces, which seems to correspond with development of nodules in culture at day 5. As fibronectin is required for microfibril formation onto which elastin is deposited, the early availability of fibronectin on NH_3^+-SAMs may be at least partially responsible for the increased rate of nodule formation by VICs.[49, 50]

Delayed Growth on OH-SAMs

Previous research has demonstrated decreased protein adhesion on OH-SAMs, and thus, lower levels of binding domains available for cell attachment and proliferation.[36, 37, 45, 51] In this study VICs have shown limited attachment and proliferation over the first 3 days, but do not undergo significant apoptosis (Figure 5). No significant increase in collagen or elastin mRNA expression was observed up to 3 days in culture. However, collagen expression increased by 5 days. The increased cell spreading and proliferation of VICs on OH-SAMs suggests secretion of ECM proteins by VICs on these surfaces is sufficient to maintain viability and recover cellular functions. Lack of OCN expression and adoption of an elongated morphology with highly aligned cultures suggests OH-SAMs maintain the aVIC phenotype. However, as VICs on OH-SAMs eventually develop to nodule formation at high cell densities, OH substrates may not be ideal for VIC expansion *in vitro*.

Non-Osteoblastic Activation of VICs on COO⁻-SAMs

The activation of VICs on COO^--SAMs characterized by rapid proliferation and maintenance of an elongated, myofibroblastic morphology at confluence indicates COO^--SAMs are a favorable substrate for cell amplification. While confluent VIC cultures tend to undergo rapid conversion to obVICs,[8, 10, 40] COO^--SAMs do not exhibit such behavior, suggesting the negative charged environment inhibits osteoblastic differentiation of VICs.[18, 39, 43] Proliferation without confluent nodule formation with confluence supports the hypothesis that

activation of VICs on negatively charged substrates is similar to hyaluronic-acid rich valvulogenesis.[31] However, the lack of increased αSMA expression and protein (collagen or elastin), suggests secondary signaling may be required for healthy tissue production.

Cell-Material Phenotypic Signaling

It has been suggested that VICs in osteoblastic media do not become true osteoblasts due to a lack of osteoblastic expressed gene markers. This has led to the theory of dystrophic calcification mechanisms in VICs.[52] In this study, osteocalcin expression and an osteoblastic morphology suggest VIC phenotype on NH_3^+ SAMs may mimic osteogenic differentiation rather than dystrophic mechanisms. This may be due to changes in integrin expression and focal adhesion formation resulting in up an osteoblastic phenotype. Previous research has shown NH_3^+-SAMs expose more α5β1integrin binding domains, causing differentiation of pre-osteoblastic cell (MC3T3-E1) to osteoblasts.[39] Similar responses using VICs and primary osteoblasts also indicate the necessity of α5β1 integrin binding is necessary for calcified nodule formation and osteoblastic gene expression.[18, 53]

Conversely, it has been observed that COO^- surfaces provide for greater binding availability of αvβ3, and reduce mineralization by MC3T3s, which was reversed when β3 binding was inhibited.[39] Furthermore, increased αvβ3 integrin expression in MC3T3s increases proliferation but down-regulates expression of osteocalcin and other osteoblastic markers, similar to VICs on

COO⁻-SAMs.[54] Although some correlations between integrins are suggested in the current data, a more complete examination of integrin expression and phenotype is needed to better understand the importance and influence of specific cell-material interactions on VIC phenotype. Once these are better understood a correlation between *in vitro* and *in vivo* conditions can be sought.

Experimental Limitations

It is well understood that self-assembled monolayers allow control of surface chemistry to investigate the effects of charge on cell behavior. However, the use of gold-bound alkanethiolate SAMs on glass do present some experimental difficulties for comparison with *in vivo* tissue development, primarily though the use of stiff substrates [55] and two-dimensional environments. It has previously been observed that VIC growth on stiffer matrixes results in greater differentiation towards myofibroblastic and calcifying phenotypes.[6] However, this is also a limitation of standard methods of *in vitro* expansion of VICs on TCPS.

It is also well understood that variations in fetal bovine serum (FBS) alters cell-behavior.[56] As batch-to-batch variations in FBS result in differences in protein constituents, this work conducted with a single lot of FBS. To accommodate for such changes, surfaces can be pre-incubated with specific proteins to create of a more-homogeneous environment. However, even surfaces treated for single protein interactions can become attenuated upon addition of FBS proteins layer can dissociate and be replaced by new protein with higher

affinities to the surface before cell attachment.[38, 43, 57] As such, when attempting to control cell-surface interactions, it is important to characterize protein adlayers or utilize well-defined surfaces such as SAMs to guide protein adsorption.[43, 58]

Furthermore, species-specific differences exist between VICs in culture. These differences lead to greater susceptibility of porcine VICs to develop calcified nodules in vitro. However, the limited availability of human VICs and the similarities between human and porcine heart tissue, make porcine VICs the predominant cell type used to investigate the development of valve stenosis.[59, 60]

Conclusions

Although VIC activation and proliferation can result in calcified nodule formation in confluent cultures, tissue mineralization is likely the result of several distinct mechanisms *in vitro*. Through variations in surface chemistry we have identified an osteoblastic-inhibiting environment (COO$^-$), and surfaces which possess characteristics of dystrophic calcification (CH$_3$) and osteogenic differentiation/calcification (NH$_3^+$). The rapid nodule formation by VICs on NH$_3^+$-SAMs may provide an accelerated *in vitro* model of heart valve disease, although additional studies remain to verify that our results resemble VIC differentiation in aortic valve disease *in vivo*. While cell-signaling cascades will be the subject of future investigations, these results clearly establish surface-dependent effects on VIC phenotypic behavior. Using SAMs to study VIC behavior should also provide

131

a clinically relevant guide the selection of biomaterials for heart valve implants and tissue engineering scaffolds. Overall, these results establish the importance of surface chemistry on VIC phenotypic behavior and establish SAMs as excellent model surfaces for studying *in vitro* VIC differentiation.
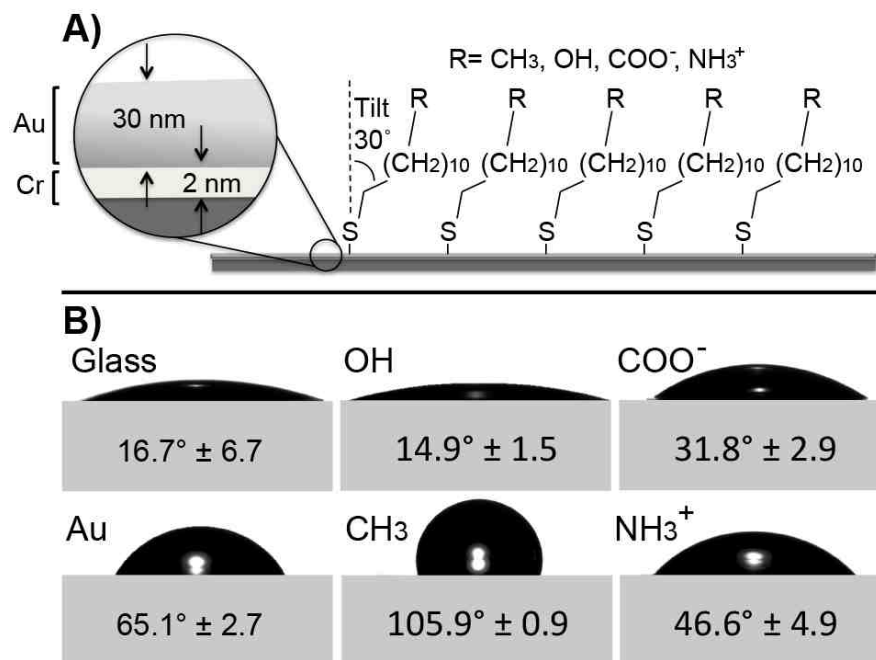
Figures

Figure 1. A) Schematic of alkanethiol self-assembled monolayer (SAM) on gold (Au, 30nm) coated glass with chromium (Cr, 2nm) adhesion layer. B) Air-water-surface contact angles determined using the sessile drop goniometry (ultrapure H_2O in air).
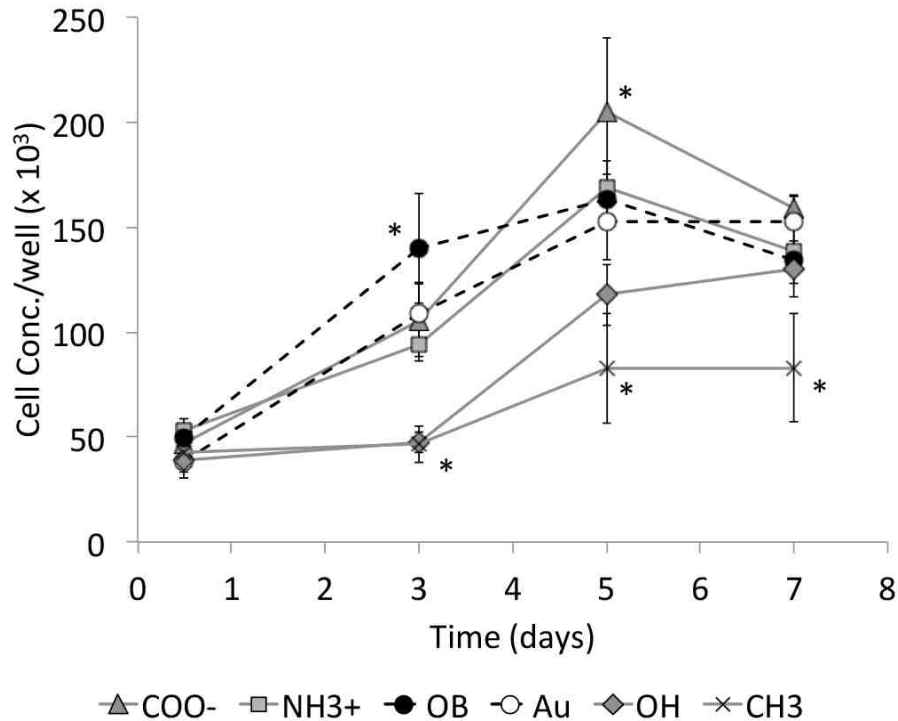
Figure 2. Valvular interstitial cell (VIC) proliferation on monolayer surfaces as compared to bare glass/osteoblastic (OB) and gold controls (dashed lines). Initial inhibition of VIC growth (1-3 days) is exhibited by OH and CH_3-SAMs with significant lower cell concentration, while osteoblastic (OB) controls are significantly greater than other treatments. Between 3 and 5 days, VICs on OH-SAMs begin proliferating while CH_3-SAMs yields significantly lower cell concentration throughout the experiment. By day 5, COO⁻-SAMs have significantly higher cell concentrations than any other treatment. Between five and seven days in culture all samples, except CH_3-SAMs, reach confluence. *$p < 0.05$, n = 6.
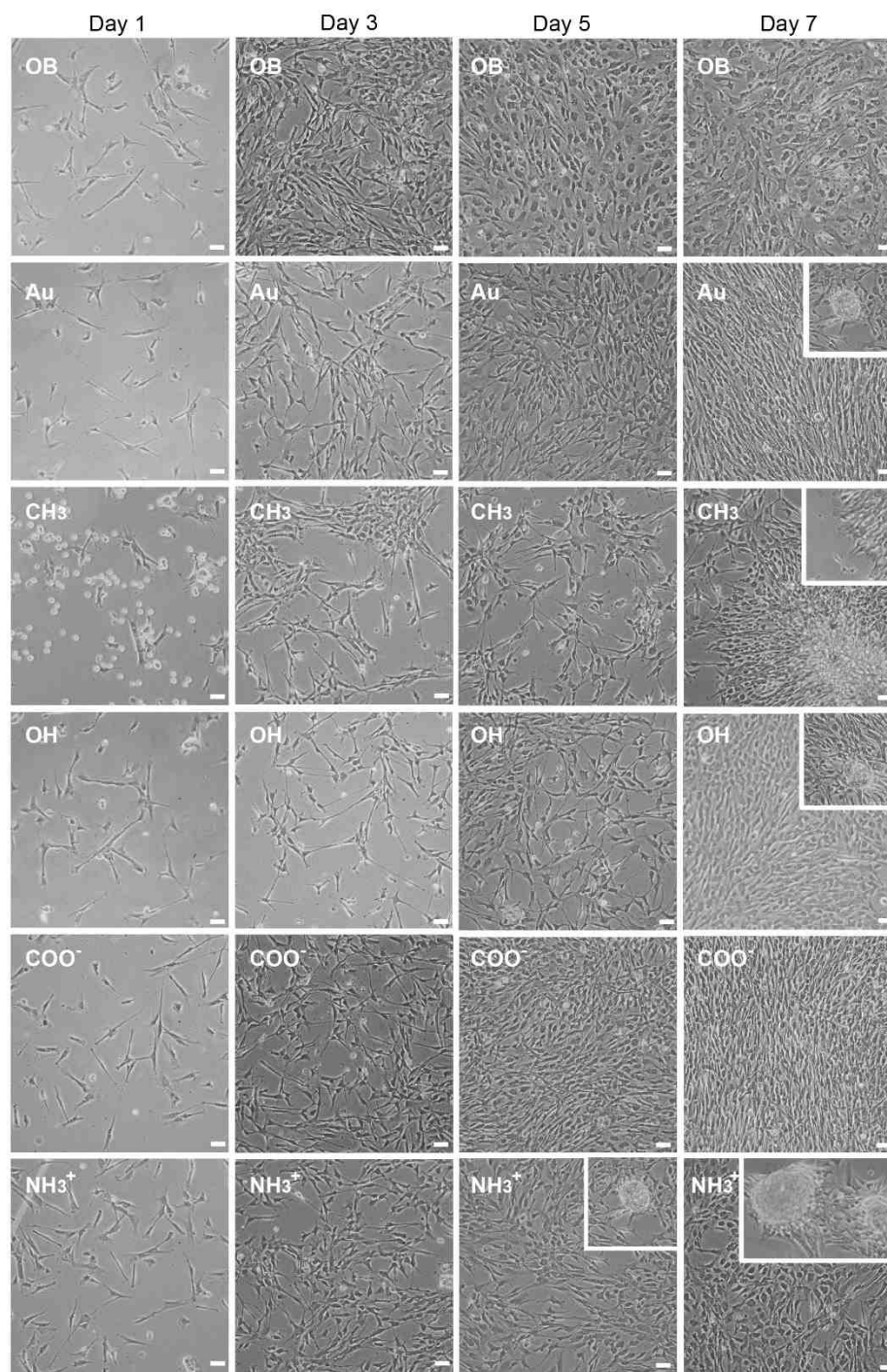
Figure 3. Bright field (phase contrast) representative images of cell morphology on varying surfaces chemistry compared to gold (Au) and osteoblastic controls over seven days of growth. Day 5 and 7, insets show morphology and relative size of nodules formed in culture, COO⁻ surfaces did not show any nodule formation over the course of this study. Further images can be found in online data supplement. Scale = 50 µm, inset images same scale.
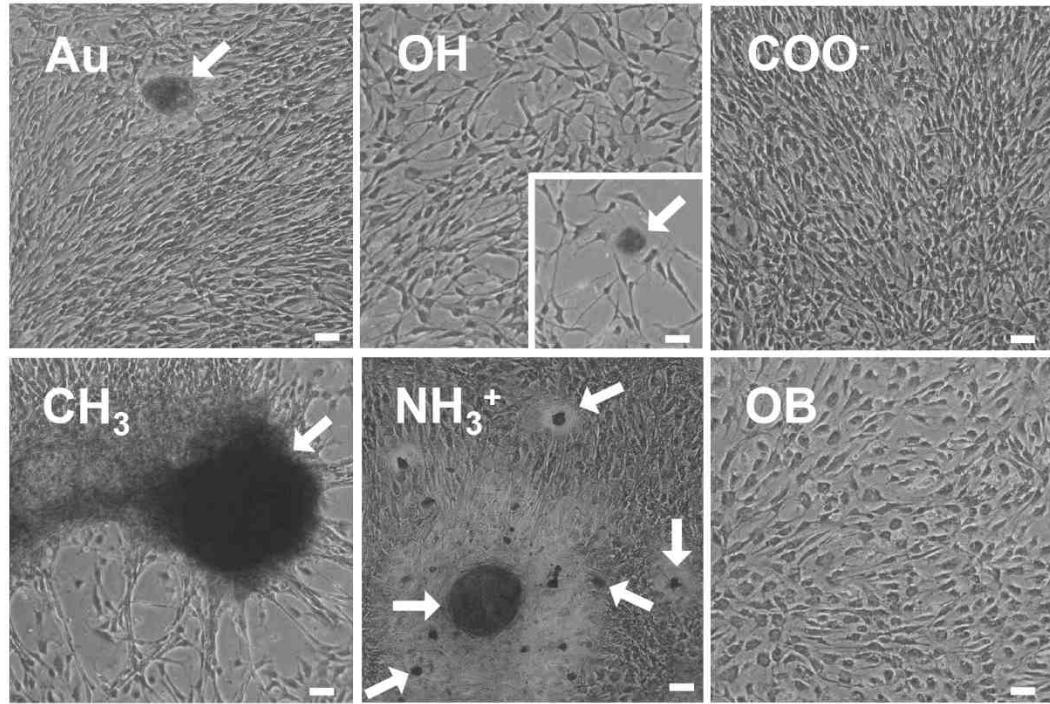
Figure 4. Representative images of alizarin red S calcium staining after seven days of growth. Arrows indicate distinct calcium-stained nodules. Scale = 50μm
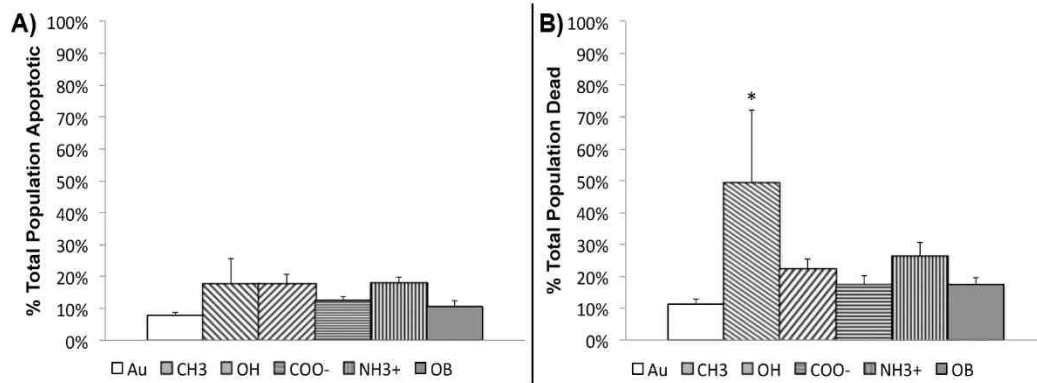
Figure 5. Measurement of valvular interstitial cell A) apoptosis and B) overall cell death after seven days. CH$_3$-SAMs result in significant increase of dead cells over all other treatments. Cell death assessed through measurement of annexin V activity (apoptosis) and propidium iodide infiltration (dead). *$p < 0.05$, n = 6.
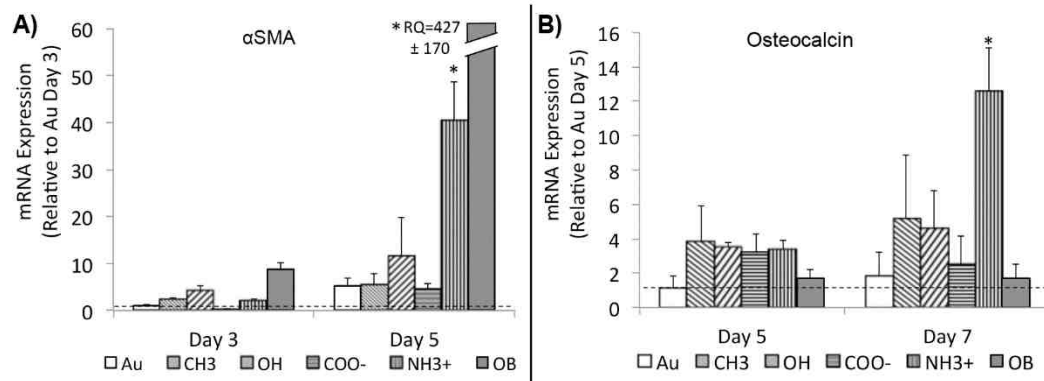
Figure 6. A) α-smooth muscle actin (αSMA) and B) osteocalcin (OCN) gene expression (mRNA) by valvular interstitial cells (VICs) at later stages of growth on functionalized surfaces. Initial expression of αSMA visualized through immunocytochemical staining (data not shown) is reduced by day 5 on most surfaces except NH_3^+-SAMs and osteoblastic controls, which have a significantly higher in αSMA expression. NH_3^+-SAMs also express significant increases in OCN expression (a late stage osteoblastic marker observed in between days 14 & 21 in osteoblast-like VICs) as early as day 7. *p < 0.05, n = 6.
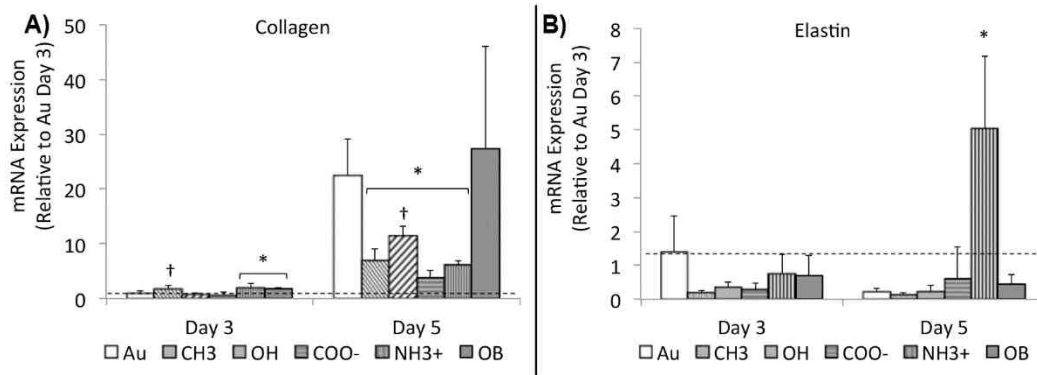
Figure 7. A) Collagen-I and B) Elastin genetic expression (mRNA) by valvular interstitial cells (VICs) at three and five days of growth on functionalized surfaces. After 3 days, collagen is up regulated on NH_3^+-SAMs and media induced osteoblastic controls. Elevated collagen expression was also observed on CH_3-SAMs, but results were not statistically different from Au controls. Collagen expression is significantly greater in all treatments between days 3 and 5. By day 5, all SAMs treatments are significantly lower than Au controls. * Indicates a statistically significant difference ($p < 0.05$) between treatments and Au controls and † indicates significant differences among SAMs treatments, n = 4.

Table 1. Calcified tissue/nodule diameter after 7 days

Treatment	Average Nodule Diameter (μm)
Au	60.5 ± 27.0
CH_3 [†]	221 ± 123*
OH	29.8 ± 10.9
COO^-	-
NH_3^+ [‡]	115 ± 39.8*
OB	-

(-) No nodules observed during culture

[†] Highly irregular cellular aggregates, no distinct boundary

[‡] Tightly bound, spherical calcium nodules

References

[1] Go AS, Mozaffarian D, Roger VL, Benjamin EJ, Berry JD, Blaha MJ, Dai S, Ford ES, Fox CS, Franco S, Fullerton HJ, Gillespie C, Hailpern SM, Heit JA, Howard VJ, Huffman MD, Judd SE, Kissela BM, Kittner SJ, Lackland DT, Lichtman JH, Lisabeth LD, Mackey RH, Magid DJ, Marcus GM, Marelli A, Matchar DB, McGuire DK, Mohler ER, 3rd, Moy CS, Mussolino ME, Neumar RW, Nichol G, Pandey DK, Paynter NP, Reeves MJ, Sorlie PD, Stein J, Towfighi A, Turan TN, Virani SS, Wong ND, Woo D, Turner MB, American Heart Association Statistics C, Stroke Statistics S. Heart disease and stroke statistics--2014 update: a report from the American Heart Association. Circulation 2014;129:e28-e292.

[2] Nkomo VT, Gardin JM, Skelton TN, Gottdiener JS, Scott CG, Enriquez-Sarano M. Burden of valvular heart diseases: a population-based study. Lancet 2006;368:1005-11.

[3] Carabello BA, Crawford FA. Valvular heart disease. New Eng J Med 1997;337:32-41.

[4] Novaro GM, Griffin BP. Calcific aortic stenosis: Another face of atherosclerosis? Clev Clin J Med 2003;70:471-7.

[5] Li C, Xu SY, Gotlieb AI. The progression of calcific aortic valve disease through injury, cell dysfunction, and disruptive biologic and physical force feedback loops. Cardiovasc Pathol 2013;22:1-8.

141

[6] Yip CYY, Chen JH, Zhao RG, Simmons CA. Calcification by valve interstitial cells Is regulated by the stiffness of the extracellular matrix. Arterioscler Thromb Vasc Bio 2009;29:936-U417.

[7] Rajamannan NM, Evans FJ, Aikawa E, Grande-Allen KJ, Demer LL, Heistad DD, Simmons CA, Masters KS, Mathieu P, O'Brien KD, Schoen FJ, Towler DA, Yoganathan AP, Otto CM. Calcific aortic valve disease: not simply a degenerative process: A review and agenda for research from the National Heart and Lung and Blood Institute Aortic Stenosis Working Group. Executive summary: Calcific aortic valve disease-2011 update. Circulation 2011;124:1783-91.

[8] Benton JA, Kern HB, Anseth KS. Substrate Properties Influence Calcification in Valvular Interstitial Cell Culture. J Heart Valve Dis 2008;17:689-99.

[9] Benton JA, Kern HB, Leinwand LA, Mariner PD, Anseth KS. Statins block calcific nodule formation of valvular interstitial cells by inhibiting alpha-smooth muscle actin expression. Arterioscler Thromb Vasc Biol 2009;29:1950-7.

[10] Jian B, Narula N, Li QY, Mohler ER, Levy RJ. Progression of aortic valve stenosis: TGF-beta 1 is present in calcified aortic valve cusps and promotes aortic valve interstitial cell calcification via apoptosis. Ann Thorac Surg 2003;75:457-65.

[11] Clark-Greuel JN, Connolly JM, Sorichillo E, Narula NR, Rapoport HS, Mohler ER, Gorman JH, Gorman RC, Levy RJ. Transforming growth factor-beta 1 mechanisms in aortic valve calcification: Increased alkaline phosphatase and related events. Ann Thorac Surg 2007;83:946-53.

[12] Gould ST, Darling NJ, Anseth KS. Small peptide functionalized thiol-ene hydrogels as culture substrates for understanding valvular interstitial cell activation and de novo tissue deposition. Acta Biomater 2012;8:3201-9.

[13] Duan B, Hockaday LA, Kapetanovic E, Kang KH, Butcher JT. Stiffness and adhesivity control aortic valve interstitial cell behavior within hyaluronic acid based hydrogels. Acta Biomater 2013;9:7640-50.

[14] Mabry KM, Lawrence RL, Anseth KS. Dynamic stiffening of poly(ethylene glycol)-based hydrogels to direct valvular interstitial cell phenotype in a three-dimensional environment. Biomaterials 2015;49:47-56.

[15] Wang H, Haeger SM, Kloxin AM, Leinwand LA, Anseth KS. Redirecting Valvular Myofibroblasts into Dormant Fibroblasts through Light-mediated Reduction in Substrate Modulus. PLoS One 2012;7:12.

[16] Duan B, Kapetanovic E, Hockaday LA, Butcher JT. Three-dimensional printed trileaflet valve conduits using biological hydrogels and human valve interstitial cells. Acta Biomater 2014;10:1836-46.

[17] Gu XX, Masters KS. Role of the MAPK/ERK pathway in valvular interstitial cell calcification. Am J Physiol-Heart Circul Physiol 2009;296:H1748-H57.

[18] Gu XX, Masters KS. Regulation of valvular interstitial cell calcification by adhesive peptide sequences. J Biomed Mater Res Part A 2010;93A:1620-30.

[19] Rodriguez KJ, Masters KS. Regulation of valvular interstitial cell calcification by components of the extracellular matrix. J Biomed Mater Res Part A 2009;90A:1043-53.

[20] Gwanmesia P, Ziegler H, Eurich R, Barth M, Kamiya H, Karck M, Lichtenberg A, Akhyari P. Opposite Effects of Transforming Growth Factor-beta 1 and Vascular Endothelial Growth Factor on the Degeneration of Aortic Valvular Interstitial Cell Are Modified by the Extracellular Matrix Protein Fibronectin: Implications for Heart Valve Engineering. Tissue Eng Part A 2010;16:3737-46.

[21] Rodriguez KJ, Piechura LM, Porras AM, Masters KS. Manipulation of valve composition to elucidate the role of collagen in aortic valve calcification. BMC Cardiovasc Disord 2014;14:10.

[22] Liu AC, Joag VR, Gotlieb AI. The emerging role of valve interstitial cell phenotypes in regulating heart valve pathobiology. Am J Pathol 2007;171:1407-18.

144

[23] Hutcheson J, Chen J, Sewell-Loftin M, Ryzhova L, Fisher C, Su Y, Merryman W. Cadherin-11 Regulates Cell-Cell Tension Necessary for Calcific Nodule Formation by Valvular Myofibroblasts. Arterioscler Thromb Vasc Biol 2013;33:114-21.

[24] Desmouliere A, Badid C, BochatonPiallat ML, Gabbiani G. Apoptosis during wound healing, fibrocontractive diseases and vascular wall injury. Int J Biochem Cell Biol 1997;29:19-30.

[25] Mohler ER, Gannon F, Reynolds C, Zimmerman R, Keane MG, Kaplan FS. Bone formation and inflammation in cardiac valves. Circulation 2001;103:1522-8.

[26] Wirrig EE, Hinton RB, Yutzey KE. Differential expression of cartilage and bone-related proteins in pediatric and adult diseased aortic valves. J Mol Cell Cardiol 2011;50:561-9.

[27] Merryman WD, Schoen FJ. Mechanisms of Calcification in Aortic Valve Disease: Role of Mechanokinetics and Mechanodynamics. Curr Cardiol Rep 2013;15:7.

[28] Rajamannan NM, Subramaniam M, Rickard D, Stock SR, Donovan J, Springett M, Orszulak T, Fullerton DA, Tajik AJ, Bonow RO, Spelsberg T. Human aortic valve calcification is associated with an osteoblast phenotype. Circulation 2003;107:2181-4.

145

[29] Schoen FJ, Levy RJ. Calcification of tissue heart valve substitutes: Progress toward understanding and prevention. Ann Thorac Surg 2005;79:1072-80.

[30] Bain CD, Troughton EB, Tao YT, Evall J, Whitesides GM, Nuzzo RG. Formation of monolayer films by the spontaneous assembly of organic thiols from solution onto gold. J Am Chem Soc 1989;111:321-35.

[31] Butcher JT, Markwald RR. Valvulogenesis: the moving target. Philos Trans R Soc Lond B Biol Sci 2007;362:1489-503.

[32] Schroeder JA, Jackson LF, Lee DC, Camenisch TD. Form and function of developing heart valves: coordination by extracellular matrix and growth factor signaling. J Mol Med 2003;81:392-403.

[33] Khan MMT, Ista LK, Lopez GP, Schuler AJ. Experimental and theoretical examination of surface energy and adhesion of nitrifying and heterotrophic bacteria using self-assembled monolayers. Environ Sci Technol 2011;45:1055-60.

[34] Creager SE, Clarke J. Contact-angle titrations of mixed omega-mercaptoalkaonic acid alkanethio monolayers on gold-reactive vs nonreactive spreading, and chain length effects of surface pKa values. Langmuir 1994;10:3675-83.

[35] Fears KP, Creager SE, Latour RA. Determination of the surface pK of carboxylic- and amine-terminated alkanethiols using surface plasmon resonance spectroscopy. Langmuir 2008;24:837-43.

[36] Faucheux N, Schweiss R, Lutzow K, Werner C, Groth T. Self-assembled monolayers with different terminating groups as model substrates for cell adhesion studies. Biomaterials 2004;25:2721-30.

[37] Keselowsky BG, Collard DM, Garcia AJ. Surface chemistry modulates fibronectin conformation and directs integrin binding and specificity to control cell adhesion. J Biomed Mater Res A 2003;66:247-59.

[38] Arima Y, Iwata H. Effect of wettability and surface functional groups on protein adsorption and cell adhesion using well-defined mixed self-assembled monolayers. Biomaterials 2007;28:3074-82.

[39] Keselowsky BG, Collard DM, Garcia AJ. Integrin binding specificity regulates biomaterial surface chemistry effects on cell differentiation. Proc Natl Acad Sci USA 2005;102:5953-7.

[40] Mohler ER, Chawla MK, Chang AW, Vyavahare N, Levy RJ, Graham L, Gannon FH. Identification and characterization of calcifying valve cells from human and canine aortic valves. J Heart Valve Dis 1999;8:254-60.

[41] Blevins TL, Carroll JL, Raza AM, Grande-Allen KJ. Phenotypic Characterization of Isolated Valvular Intersitial Cell Subpopulations. J Heart Valve Dis 2006;15:815-22.

[42] Mrksich M. Using self-assembled monolayers to model the extracellular matrix. Acta Biomater 2009;5:832-41.

[43] Lin JH, Chang HY, Kao WL, Lin KY, Liao HY, You YW, Kuo YT, Kuo DY, Chu KJ, Chu YH, Shyue JJ. Effect of Surface Potential on Extracellular Matrix Protein Adsorption. Langmuir 2014;30:10328-35.

[44] Mrksich M, Whitesides GM. Using self-assembled monolayers to understand the interactions of man-made surfaces with proteins and cells. Annu Rev Biophys Biomolec Struct 1996;25:55-78.

[45] Lan MA, Gersbach CA, Michael KE, Keselowsky BG, Garcia AJ. Myoblast proliferation and differentiation on fibronectin-coated self assembled monolayers presenting different surface chemistries. Biomaterials 2005;26:4523-31.

[46] Latif N, Sarathchandra P, Taylor PM, Antoniw J, Brand N, Yacoub MH. Characterization of molecules mediating cell-cell communication in human cardiac valve interstitial cells. Cell Biochem Biophys 2006;45:255-64.

[47] Xia H, Nho RS, Kahm J, Kleidon J, Henke CA. Focal adhesion kinase is upstream of phosphatidylinositol 3-kinase/Akt in regulating fibroblast survival in

response to contraction of type I collagen matrices via a beta(1) integrin viability signaling pathway. J Biol Chem 2004;279:33024-34.

[48] Chen J, Peacock JR, Branch J, Merryman WD. Biophysical Analysis of Dystrophic and Osteogenic Models of Valvular Calcification. J Biomech Eng-Trans ASME 2015;137:6.

[49] Kielty CM, Sherratt MJ, Shuttleworth CA. Elastic fibres. J Cell Sci 2002;115:2817-28.

[50] Sabatier L, Chen DL, Fagotto-Kaufmann C, Hubmacher D, McKee MD, Annis DS, Mosher DF, Reinhardt DP. Fibrillin Assembly Requires Fibronectin. Mol Biol Cell 2009;20:846-58.

[51] Silin V, Weetall H, Vanderah DJ. SPR studies of the nonspecific adsorption kinetics of human IgG and BSA on gold surfaces modified by self-assembled monolayers (SAMs). J Colloid Interface Sci 1997;185:94-103.

[52] Monzack EL, Masters KS. Can Valvular Interstitial Cells Become True Osteoblasts? A Side-by-Side Comparison. J Heart Valve Dis 2011;20:449-61.

[53] Moursi AM, Globus RK, Damsky CH. Interactions between integrin receptors and fibronectin are required for calvarial osteoblast differentiation in vitro. J Cell Sci 1997;110:2187-96.

[54] Cheng SL, Lai CF, Blystone SD, Avioli LV. Bone mineralization and osteoblast differentiation are negatively modulated by integrin alpha v beta 3. J Bone Miner Res 2001;16:277-88.

[55] DelRio FW, Jaye C, Fischer DA, Cook RF. Elastic and adhesive properties of alkanethiol self-assembled monolayers on gold. Appl Phys Lett 2009;94:3.

[56] Zheng XY, Baker H, Hancock WS, Fawaz F, McCaman M, Pungor E. Proteomic analysis for the assessment of different lots of fetal bovine serum as a raw material for cell culture. Part IV. Application of proteomics to the manufacture of biological drugs. Biotechnol Prog 2006;22:1294-300.

[57] Thomas CH, McFarland CD, Jenkins ML, Rezania A, Steele JG, Healy KE. The role of vitronectin in the attachment and spatial distribution of bone-derived cells on materials with patterned surface chemistry. J Biomed Mater Res 1997;37:81-93.

[58] Liu LY, Chen SF, Giachelli CM, Ratner BD, Jiang SY. Controlling osteopontin orientation on surfaces to modulate endothelial cell adhesion. J Biomed Mater Res Part A 2005;74A:23-31.

[59] Bowler MA, Merryman WD. In vitro models of aortic valve calcification: solidifying a system. Cardiovasc Pathol 2015;24:1-10.

[60] Cloyd KL, El-Hamamsy I, Boonrungsiman S, Hedegaard M, Gentleman E, Sarathchandra P, Colazzo F, Gentleman MM, Yacoub MH, Chester AH, Stevens MM. Characterization of Porcine Aortic Valvular Interstitial Cell 'Calcified' Nodules. PLoS One 2012;7:9.

Chapter 6

Nitrogen Sparge Synthesis and Characterization of Oligo(Poly(Ethylene Glycol) Fumarate) Macromer

Matthew N. Rush[1,2,3], Kent E. Coombs[1,4], Kirsten N. Cicotte[1,5], David Santistevan[1], Quan M. Huynh[1,5], Chester K. Simocko[3], and Elizabeth L. Hedberg-Dirk[1,2,5,6].*

[1]Center for Biomedical Engineering, University of New Mexico, Albuquerque, NM. [2]Nanoscience and Microsystems Engineering Graduate Program, University of New Mexico, Albuquerque, NM. [3]Center for Integrated Nanotechnologies, Sandia National Laboratories/Los Alamos National Laboratory, Albuquerque, NM, USA. [4]Biomedical Sciences Graduate Program, University of New Mexico, Albuquerque, NM, USA. [5]Biomedical Engineering Graduate Program, University of New Mexico, Albuquerque, NM, USA. [6]Department of Chemical and Biological Engineering, University of New Mexico, Albuquerque, NM, USA.

Corresponding Author: Elizabeth L. Hedberg-Dirk
Address: Center for Biomedical Engineering
     MSC01 1141
     1 University of New Mexico
     Albuquerque, NM 87131
Email: edirk@unm.edu
Fax: 505-277-6209
Phone: 505-277-5906

Abstract

The macromolecule oligo(poly(ethylene glycol) fumarate) (OPF) exhibits promising attributes for creating 3D hydrogel environments to study cell behavior, deliver therapeutics, and serve as a degradable, non-fouling scaffold. However, previous synthesis techniques were time consuming, contained salt contaminants, and generated a large amount of solvent waste. These issues have been overcome with an alternative, one-pot approach utilizing inert gas sparging methods. Departing from previous synthetic schemes requiring acid scavengers, sparging removes HCl byproducts *in situ*; eliminating significant filtration and post processing steps while allowing for increased molecular weight, and producing a more uniform product. Furthermore, nitrogen-sparged OPF (N_2-OPF) readily cross-links using either UV initiator or thermal initiator methods with or without the addition of short chain diacrylate units which allows for greater tunability in the material properties of the resulting hydrogels. Overall, sparge synthesis provides a better polymer product for hydrogel material studies, while maintaining degradable hydrogel characteristics.

153

1.1.1. FIGURE FOR ToC_ABSTRACT
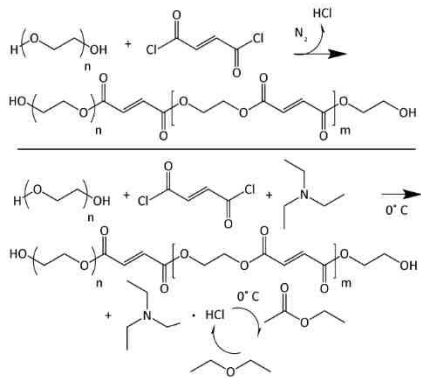
Introduction

Oligo(poly(ethylene glycol) fumarate) (OPF) has been extensively investigated as a biodegradable hydrogel for use in tissue engineered scaffolds and drug delivery [1-13]. The step-growth polymerization of polyethylene glycol (PEG) and fumaryl chloride produces a linear polyester and hydrochloric acid byproducts. The resulting oligomer consists of a repeating scheme of PEG and fumarate which chemically crosslink through unsaturated double bonds into a non-fouling hydrogel (Figure 1). The ability of OPF to undergo hydrolytic degradation through ester hydrolysis gives OPF greater utility over previous PEG diacrylate hydrogels [14-17]. Additionally, the physical properties of OPF can be easily tailored by changing the PEG molecular length [1, 18]. Due to the presence of unsaturated double bonds, modification of the oligomer backbone can also be achieved prior to or during cross-linking with the incorporation of short chain polymers [4, 10]. Overall, these factors make OPF a desirable synthetic polymer for multiple applications.

Originally developed by Jo, *et al.*, the OPF synthesis procedure has not been significantly modified since its inception [1, 2, 19]. However, several groups have reported issues with removal of secondary reaction byproducts affecting crosslinking efficiency and cell viability [20-22]. In order to trap hydrochloric acid, groups have used acid scavengers such as triethylamine, potassium carbonate, and sodium hydroxide [16, 23-28]. However, batch-to-batch inconsistencies in

155

polymer product are common due to inefficient removal of insoluble hydrochloric acid-acid scavenger salts [22].

Common in waste treatment and manufacturing procedures, sparging is a fast and efficient method which can be easily introduced into the process environment [29-33]. By bubbling a chemically inert gas such as nitrogen, argon, or helium through a liquid, sparging allows for the removal of low boiling-point solutes in real time, without post-processing steps [32, 33]. Furthermore, the introduction of compressed gas into the system serves as a heat sync, through adiabatic expansion, maintaining the low temperatures required for efficient step-growth polycondensation [34]. Through the introduction of gas sparging, we have developed a one-pot, straight-forward, and improved method for the production of OPF while simultaneously eliminating the complications of acid removal, cooling, filtration and post-processing, and working with peroxide forming chemicals.

Experimental Section/Materials and Methods

Reagents and Chemicals

Polyethylene glycol (PEG, Mn 4600, 1000, and 10000), fumaryl chloride (FuCl), ascorbic acid (AA), IRGACURE 2959, trimethylamine (TEA), polyethylene glycol diacrylate (PEGDA, Mn 575), deuterated chloroform ($CDCl_3$), and tetrahydrofuran (THF) were purchased from Sigma-Aldrich. Ammonium persulfate (APS, ACS

grade) and ethanol were purchased from Fisher Scientific. Dichloromethane (DCM), ethyl ether, ethyl acetate, anhydrous toluene (99.8%), and sodium hydroxide were purchased from EMD. Whatman qualitative 413 filter paper was purchased from VWR. The fine-fritted sparge/gas dispersion tube (CG-203-01) was purchased from Chemglass.

Synthesis of Oligo(Poly(Ethylene Glycol) Fumarate) (OPF)

Polyethylene Glycol (PEG) Drying

PEG was dried by azeotropic distillation prior to use as previously described [2]. Briefly, 100g of PEG was added to 200 mL of toluene. At least 150 mL of toluene and residual water were distilled off at 200°C. Toluene was removed on a rotary evaporator followed by drying in a vacuum oven overnight. Dried PEG was stored in a desiccator until use.

OPF Oligomer Synthesis – Triethylamine (TEA-OPF)

TEA-OPF was prepared according to previously described methods [1, 2]. Briefly, dried PEG (100g) was dissolved in 700 mL of dichloromethane (DCM) in a 1 L 3-neck round bottom flask set in an ice bath. Air was removed and replaced with a nitrogen (N_2) environment. Using molar ratios of 1: 0.9 PEG to fumaryl chloride (FuCl) and 1:2 FuCl to triethylamine (TEA), FuCl and TEA were dissolved in 60 mL DCM in separate addition funnels and simultaneously added,

dropwise, to PEG over 4 hrs. The reaction was stirred vigorously using a stir bar.

Upon complete addition of FuCl and TEA to the PEG solution, the reaction was

allowed to progress in an ice bath overnight, followed by solvent removal *in*

vaccuo. The product was subsequently dissolved in warm ethyl acetate, chilled

to recrystallize OPF, and filtered to remove trimethylamine hydrochloride salts.

This process was repeated three times. After the final collection, the OPF was

washed with ethyl ether, and fully dried under reduced pressure overnight.

OPF Oligomer Synthesis - Nitrogen Sparging (N2-OPF)

Similar to the TEA-OPF, dried PEG (100 g) was dissolved in 700 mL DCM in a

three-neck round bottom flask with stir bar and nitrogen environment. Sparging,

using nitrogen (N_2), was introduced through central arm with a 24/40 adaptor

fitted with a fine-fritted gas dispersion tip and forced out through 90° flow control

adapter into a secondary vessel containing of 10 wt% sodium hydroxide in

ethanol (Figure 1B). Fumaryl chloride was dissolved in 60 mL DCM at a molar

ratio of 1:0.9 PEG to FuCl and added dropwise to PEG over 4 hours while stirred

vigorously. Upon complete addition of FuCl to PEG solution, DCM was added to

the reaction mixture to bring the volume back up to 700 mL. The reaction was

allowed to progress overnight with sparging, followed by solvent removal *in*

vaccuo.

Characterization of OPF

Degree of Oligomerization

OPF products were characterized by 300M Hz ¹H NMR (Bruker Avance III 300) in CDCl₃. Peaks were assigned to confirm the hydrogen binding environment. The degree of polymerization was assessed through comparison of using peak integration of olefin (6.87 ppm) and PEG (3.38-3.85 ppm) functional groups.

Molecular Weight

Molecular weight of OPF was determined through gel permeation chromatography (GPC). Styragel HR 4 + 4E, 7.8x300mm (WAT044225, WAT044240) columns were used to elute the samples at a 1mL/min flow rate on an Agilent 1100 Series HPLC (Hewlett Packard, RID G1362A). Samples (3 mg) were run in tetrahydrofuran (1 mL). Sample weight-average (M_w) and number-average molecular weights (M_n) were calculated as compared to polyethylene glycol (PEG) standards (PL2070- 194, 440, 600, 1080, 1470, 4100, 7100, 12600, 23600, Polymer Laboratories/Agilent Technologies). The degree of oligomerization (X_n) was determined using Equation 1:

$$\overline{X_n} = \frac{M_{n,OPF}}{M_{n,PEG}} \tag{1}$$

$$\overline{X_n} = \frac{1+r}{1+r-2rp} \tag{2}$$

Here, $M_{n,OPF}$ and $M_{n,PEG}$ represent the number average molecular weight (M_n) of OPF and monomeric PEG, as determined by GPC. Carother's equation

159

(Equation 2) was used to determine monomer conversion percentage, where r represents the ratio of [fumaryl chloride]/[PEG] and p the monomer conversion percentage [35].

Changes in molecular weight over time were measured by removing a small volume (1 mL) of OPF product from both TEA-OPF and N_2-OPF synthesis reaction vessels over the initial 14 hours of synthesis in parallel reactions. Solvent was removed *in vacuuo* and 3 mg of product were suspended in 1 mL tetrahydrofuran. Refractive index intensity was normalized to the highest peak of the eluted product.

Fluorescent Byproduct

Fluorescence of the polymer product was detected during GPC through the use of a fluorescence detector (Hewlett Packard, FLD G1321A, Ex 250 nm, Em 410 nm) upstream of the refractive index detector; retention time difference approx. 1 min.

Melting Temperature and Crystallinity

Differential scanning calorimetry (DSC, TA instruments model 2920) was carried out to determine the properties of OPF. The samples were analyzed at a heating rate of 10 °C/min from 0 to 70 °C. Melting temperature (Tm) and the heat of

fusion, ¢Hm (cal/g), were obtained from the thermograms. The percent

crystallinity (X) of OPF was determined from the following equation:

$$X = \frac{\Delta H_m}{\Delta H_m^*} \; x \; 100 \tag{3}$$

Here, $H_{m,}^*$ is the theoretical heat of fusion of 100% crystalline PEG (49 cal/g) [36].

Yield

Percent yield was calculated by weighing the product recovered from the reaction

and dividing it by the weight of reagents originally added.

$$1.1.2. \quad \% \, Yield = \frac{weight \; OPF \; final \; product}{weight \; PEG + weight \; Fumaryl \; chloride}$$

$$\tag{4}$$

1.1.3.

Characterization of Crosslinked OPF Hydrogels

Crosslinking of OPF

OPF hydrogel products were crosslinked with and without polyethylene glycol

dimethacrylate (PEGDA) (Sigma Aldrich). The UV crosslinked formulations were

as follows; 25% (wt%) OPF, 0.5% Irgacure 2959 initiator, 74.5% DI water or

16.5% OPF, 8.5% PEGDA, 0.5% Irgacure 2959 initiator, 74.9% DI water. UV

formulations were exposed to 365 nm UV light in a UVP light box (CL-1000) for

15 min. The thermally crosslinked hydrogels had the same formulations stated

above, except 17.6×10^{-6} wt% (0.1 mM) ascorbic acid (AA) with 22.8×10^{-6} wt%

(0.1 mM) ammonium persulfate (APS) was added as a free-radical initiator

instead of Irgacure 2959. Polymer solutions (1 mL) were transferred to syringe molds before being crosslinked [21]. Thermally initiated formulations were placed in the incubator (37° C) for 15 min to form hydrogels. Final products were then dried overnight at room temp before being placed in the vacuum oven for 24 hours. TEA-OPF product only formed solid hydrogels when using thermal cross-linkers, 0.1 mM (AA/APS).

Water Ingress and Removal of Uncrosslinked Material

Hydrogels were weighed after drying in vacuum oven to measure the initial mass of polymer (W_i). Hydrogels were then soaked in 5 mL of deionized water and allowed to swell. Hydrogel weights were recorded each day, for 4 days, until mass loss was negligible. The maximum swollen weight (W_s) was recorded. Swollen gels were then removed from water and re-dried in the vacuum oven for 48 hrs before being weighed to measure the dry weight (W_d). The water ingress fraction was calculated by dividing the weight dry by the swollen weight (Equation 5). Sol fractions were calculated taking the weight initial minus the weight dry divided by the weight initial (W_i) (Equation 6).

$$Swelling\ ratio = \frac{W_s - W_d}{W_d} \tag{5}$$

$$Sol\ fraction = \frac{W_i - W_d}{W_i} \tag{6}$$

Hydrogel Elasticity

Twenty microliters (20 µL) of TEA-OPF and N_2-OPF samples, using thermal

cross-linking formulations described above, were deposited onto AFM metal

specimen discs (TedPella, 16218) and placed in the incubator (37° C) for 15 min

to form hydrogels. Samples were swollen for four days by immersion in deionized

water. Force maps, comprised of force distance curves, were gathered over 10

x10 µm area of each hydrogel sample using a TL-FM tip-less cantilever

(Nanoworld) affixed with 5 µm silica microsphere (Bangs Laboratory, SS05N)

using thermal-set epoxy (Epon 1004F), see supplement for more information.

Elastic modulus and virtual deflection of each cantilever was calibrated prior to

hydrogel indentation using thermal methods, followed by deflection on a rigid

substrate (glass) [37][38]. The hydrogel elastic modulus was calculated using

Oliver-Pharr model fitting [39].

Results and Discussion

Synthesis and Characterization of OPF

The polymerization of oligo(poly(ethylene glycol) fumarate) produces a linear

polyester through the reaction of PEG and fumaryl chloride to form dimers,

trimers, and eventually oligomers, in a step-growth process. The primary

limitation of this reaction is the production of hydrochloric acid byproducts which

must be isolated to prevent secondary reactions. Previously, removal of

hydrochloric acid was accomplished by acid scavengers such as trimethylamine, potassium carbonate, or sodium hydroxide [16, 23-28]. In the current work, previously published OPF synthesis using triethylamine was compared to a OPF synthesis using nitrogen sparging. The use of sparging for the *in situ* removal of hydrochloric acid eliminates the need for an acid scavenger, thereby avoiding the production of hard to remove TEA salts.

For both reaction methods, formation of PEG/fumarate oligomers were confirmed by ^{1}H-NMR with the appearance of an ester bond peak at 4.33 ppm. The shift in the olefin peak from 7.87 (fumaryl chloride) to 6.87 ppm indicates attachment of fumaryl chloride to PEG (Figure 2).[40] Nitrogen-sparged OPF (N_2-OPF) shows a greater olefin (6.87 ppm) to PEG (3.38-3.85 ppm) ratio as well as a reduction in signal from PEG hydroxyl end-groups (3.01 ppm) resulting in a greater degree of oligomerization and larger molecular weight than triethylamine OPF synthesis methods (TEA-OPF).[1] Size exclusion chromatography confirms a significant increase in N_2-OPF molecular weight over TEA-OPF (Figures 3A-4A&B). Furthermore, the polydispersity index was lower for N_2-OPF, indicating a more homogeneous product (Figure 3A and Table 1). In side-by-side TEA-OPF and N_2-OPF reactions, temporal analysis of the product demonstrates a limited maximum achievable molecular weight using TEA-OPF methods. After 4 hours, the maximum molecular weight was obtained by TEA-OPF with no additional oligomerization at subsequent time points. In contrast, the oligomerization of the

N$_2$-OPF method continues through 12 hours (Figure 4). In step-growth processes, the final conversion, and hence the average molecular weight, is affected by the concentration of condensation byproducts [41]. *In situ* removal of acid byproducts during nitrogen sparging eliminates TEA salt formation allowing for the synthesis of a higher molecular weight OPF (Figure 4A) [1, 22].

In contrast to the nitrogen sparge method, TEA-OPF synthesis requires the additional steps of filtration, re-crystallization, and solvent washing in order to remove acidic by-products [1, 2]. The incomplete removal of TEA salts during work-up is apparent in ^{1}H-NMR (1.4 ppm). The TEA-OPF also retains a brown coloration even after repeated filtrations steps. Alternatively, the pure N$_2$-OPF appears white immediately after synthesis and does not require additional purification steps (supplemental Figures 7 & 8). Fluorescent analysis of eluted product through size-exclusion chromatography reveals the presence of a fluorescent molecule within TEA-OPF that is absent from N$_2$-OPF (Figure 3B). The fluorescent signal corresponds with the elution time of TEA-OPF oligomers, indicating that the TEA salts are complexed to the OPF backbone. Cai and Wang, 2010 have previously reported the formation of a cell-cytotoxic TEA complexes during polymerization of fumaryl chloride in the presence of TEA that cannot be completely removed during purification [22]. The inability to completely remove the TEA salts limits the utility of the TEA-OPF.

165

Thermal characterization of OPF by DSC shows that there is little difference in crystallinity and melting temperature (Tm) among synthesis methods, see **Error! Reference source not found.**. This data implies the OPF products to be similar in composition. However, the slight decrease in crystallinity of N_2-OPF corresponds with the increased incorporation of rigid fumarate units which prevent close-packing of the flexible PEG chains [1].

Characterization of Crosslinked Hydrogel Properties

To examine the cross-linking capabilities of N_2-OPF and TEA-OPF, two different commonly used, free-radical initiators systems were applied; ascorbic acid/ammonium persulfate, a thermally activated initiator and IRGACURE 2959, a UV activated initiator [1, 2, 20, 21, 42]. In addition, hydrogels were fabricated with and without polyethylene glycol diacrylate (PEGDA), a copolymer commonly used in the cross-linking of PEG-based hydrogels. Hydrogels successfully crosslinked with ascorbic acid/ammonium persulfate and PEGDA for both TEA-OPF and N2-OPF. However, UV initiated TEA-OPF/PEGDA and TEA-OPF hydrogels did not cross-link adequately to maintain their 3D structure when placed in water, and subsequently fell apart. In comparison, N_2-OPF readily crosslinked using both initiator systems with and without PEGDA, highlighting the versatility of N_2-OPF product (Figure 5-6). The inefficient removal of triethylamine salts in the TEA-OPF synthesis method are likely a significant factor in the cross-

linking behavior of TEA-OPF. The brown color most likely limits UV intensity and penetration into the gels and the TEA salts may interfere with the initiator as well as the cross-linking reaction. In order to overcome the limitations of TEA-OPF, previous groups have increased reaction time to an hour to fully crosslink TEA-OPF [1, 18, 21]. As OPF is commonly used as a biomaterial for cell encapsulation, minimizing UV exposure time reduces cellular cytotoxicity [20, 21]. Cross-linking of hydrogels was therefore limited to a 15 minute exposure period, a time which has been shown to optimally balance the cross-linking reaction with cell viability [21].

Fully crosslinked OPF hydrogels exhibited swelling characteristics dependent on the synthesis method and the use of the cross-linking molecule. Using ascorbic acid/ammonium persulfate as the thermal initiator and PEGDA as the cross-linker, there was no difference in swelling between TEA-OPF and N_2-OPF hydrogels. However, TEA-OPF/PEGDA did not cross-link using the UV initiator, while N_2-OPF/PEGDA did using either initiator. The choice of initiator did not influence the swelling of the N_2-OPF/PEGDA hydrogels. Only N_2-OPF was able to form crosslinked hydrogels without the addition PEGDA. As expected, the absence of a cross-linking molecule resulted in a looser N_2-OPF hydrogel with greater swelling (Figure 5A) [17, 42]. Within the sol fraction data the only observable trend is an increase in sol fraction with the exclusion of PEGDA, indicating greater oligomer incorporation (Figure 5B&D).

167

Mechanical testing of OPF hydrogels with and without PEGDA was conducted utilizing colloidal nano-indentation methods (supplement). This method allows for the measurement of elastic modulus at the submicron level of molecular interactions, a factor important in characterizing OPF applicability for biomedical and microscale material applications [14, 39, 43]. Similar to swelling and sol fraction results, the mechanical properties of crosslinked OPF hydrogels were solely dependent on PEGDA, not OPF synthesis method (Figure 6). Since N_2-OPF is the only product that can be crosslinked with and without PEGDA, N_2-OPF can be fabricated into hydrogels of with a wider range of mechanical properties, increasing its utility beyond that of TEA-OPF [44].

Conclusions

Through the use of nitrogen sparging, we have shown that OPF can be produced with decreased post-processing, increased product purity, and greater oligomerization. These properties lead to greater tunability in mechanical properties and a more versatile hydrogel. Instead of using triethylamine as a proton scavenger, *in situ* nitrogen gas sparging eliminates the need for post-processing washes using ethyl acetate and ethyl ether, which have proven to be inefficient while also being acutely toxic and potentially explosive through peroxide formation. With greater oligomerization, N_2-OPF has more unsaturated double bonds per molecule that can be used for crosslinking and addition of

covalently bound side chains. This straightforward method of fabrication should allow for facile production that eliminates post-processing. The simplification of synthesis and elimination of impurities will expand the utility of N_2-OPF as a degradable hydrogel for cell culture, tissue engineering, regenerative medicine, and therapeutic delivery, among other applications.

Supporting Information

Supporting Information is available from the Wiley Online Library or from the author.

Appendix/Nomenclature/Abbreviations

Figures and Tables

Figure 1. Glassware set-up for the polycondensation of fumaryl chloride (FuCl) with polyethylene glycol (PEG) in dicholoromethane (DCM) using A) the acid scavenger triethylamine (TEA) or B) nitrogen sparging (N$_2$) to remove hydrochloric acid (HCl) byproducts. C) Reaction schemes for TEA-OPF and D) N$_2$-OPF. E) Crosslinking structure of OPF oligomers through consumption of unsaturated double bonds.
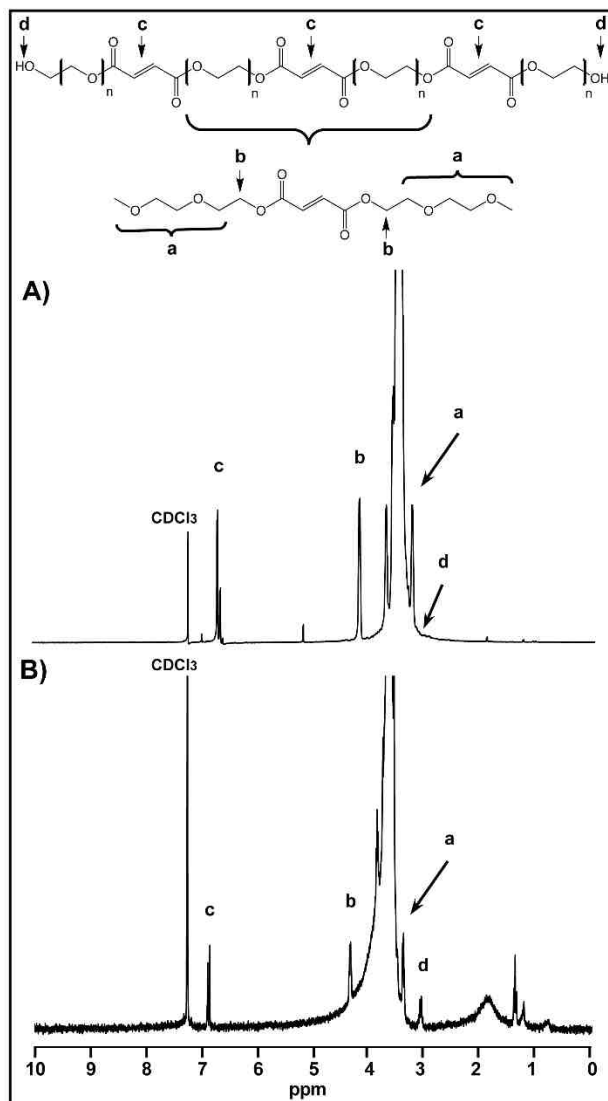
Figure 2. ^{1}H NMR spectra of 4.6K OPF from A) nitrogen sparging or B) triethylamine acid scavenging methods. The presence of ester groups (b, 4.33 ppm) and olefin groups (c, 6.87 ppm) indicate bond formation and oligomerization of OPF. NMR (300 MHz) measurements were carried out in CDCl$_3$ (7.24 ppm). Some residual dichloromethane can be observed at 5.26 ppm with triethylamine contaminates at 1.43 ppm.

Table 1. Properties of TEA-OPF and N_2-OPF[†]

Synthesis Method	% Yield	Tm [°C]	% Crystal. (x)	Mn [g/mol]	Mw [g/mol]	PDI	Xn
TEA OPF	86.8 ± 9.2	60.7 ± 0.4	64.1 ± 2.1	7,779 ± 847	10,891 ± 1,368	1.4 ± 0.04	1.8 ± 0.2
N₂ OPF	95.1 ± 3.0	60.3 ± 1.3	58.3 ± 3.4	13,097 ± 3,494	17,271 ± 3,632*	1.3 ± 0.1*	3.93 ± 0.8*

[†]All OPF synthesized with 4.6k PEG; * ($p < 0.05$) n = 3-4
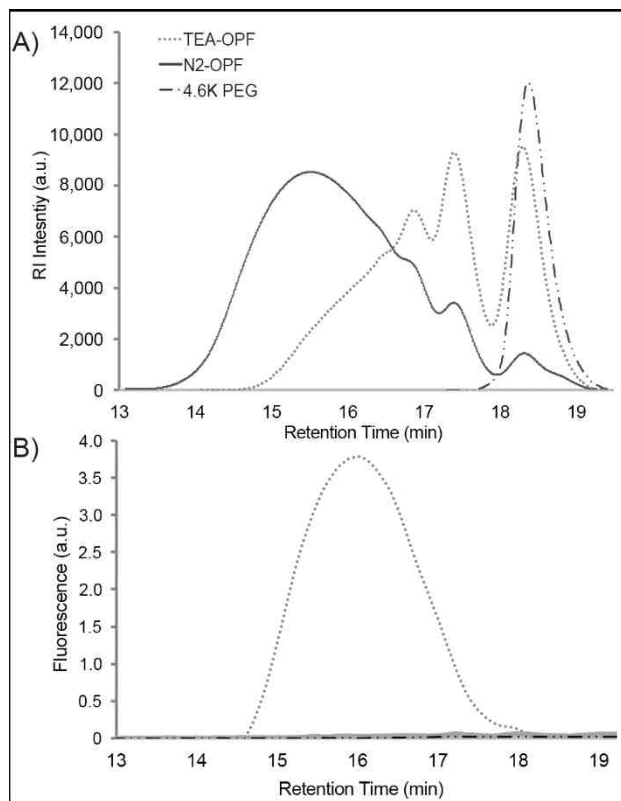
Figure 3. A) Representative elution profiles of OPF polymer products and
pure 4.6K PEG as determined by gel permeation chromatography. Decreased
retention time indicates higher molecular weight N_2-OPF oligomers. B)
Fluorescence profiles of OPF products and 4.6K PEG were collected in series
with GPC. A large fluorescence peak was detected only in TEA-OPF indicating
unremoved triethylamine hydrochloride, Ex 250 nm/Em 410 nm.
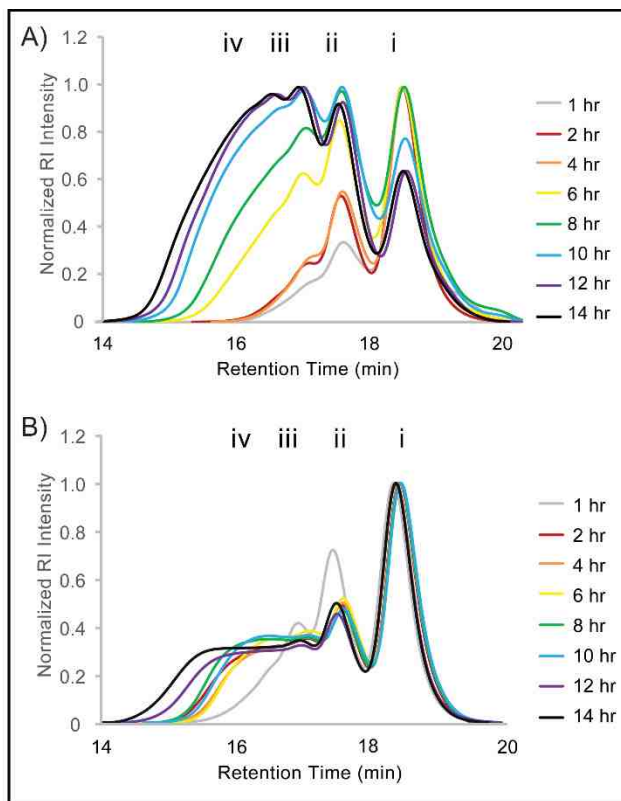
Figure 4. During synthesis small samples of A) N_2-OPF and B) TEA-OPF product were removed periodically over fourteen hours to and analyzed by GPC. Each labelled peak (i-iv) corresponds to an increasing oligomer length. TEA method limits molecular weight after addition of fumarate to reaction vessel (4 hours).
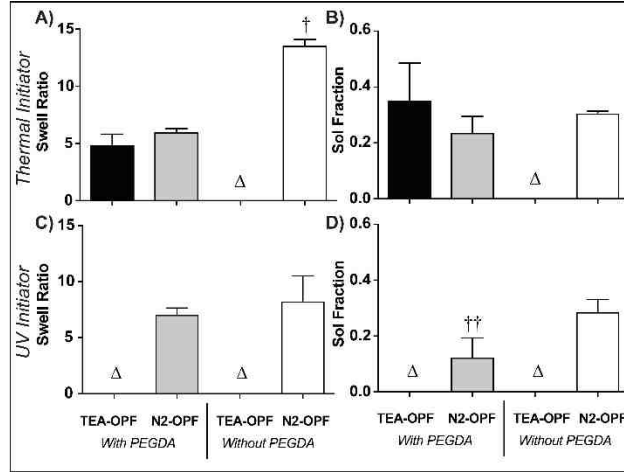
Figure 5. Swelling ratio of crosslinked OPF hydrogels using A) thermal and C) UV initiator methods. Sol Fraction of crosslinked OPF hydrogels using B) thermal and D) UV initiator methods. Swelling of N_2-OPF without PEGDA was significantly greater than all other gels, $\dagger p < 0.05$, $n = 6$. UV-initiated N_2-OPF with PEGDA had significantly lower sol fraction than N_2-OPF without PEGDA, $\dagger\dagger p < 0.05$, $n = 6$. Δ indicates gels did not cross-link sufficiently to be characterized. N_2-OPF is a more versatile polymer because it can be crosslinked with and without PEGDA.
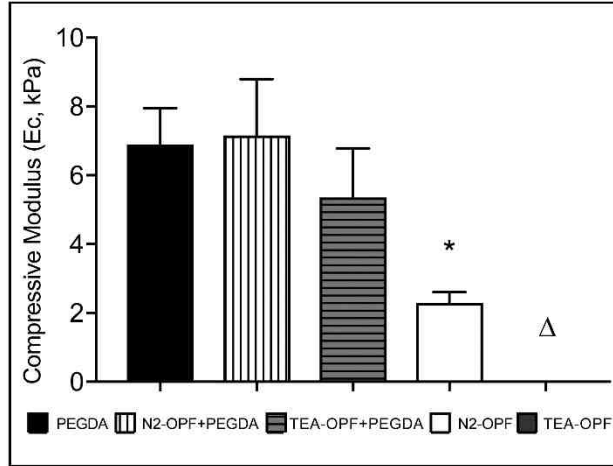
Figure 6. Compressive modulus of thermally crosslinked TEA-OPF and N_2-OPF with and without PEGDA as compared to crosslinked PEGDA alone. Compressive modulus was determined using atomic force cantilever nano-indentation with Oliver-Pharr fitting. N_2-OPF without PEGDA was significantly softer than hydrogels with PEGDA, * $p < 0.05$, $n = 3$. Δ indicates gels did not crosslink sufficiently to be characterized.

177

Table 2. Qualitative comparison between synthesis methods

Synthesis Method	TEA-OPF	N$_2$-OPF
Synthesis Time	2 Days	12-16 Hours
Molecular Weight	Variable-Low	High
Contaminates	Triethylamine Salts	N/A
Crosslinking	Requires Crosslinker	With and Without Crosslinker
Post Processing	Ethyl Acetate / Ethyl Ether	N/A
Waste Production	Rxn Solvents + Solvent Wash (x3)	Rxn Solvents

References

1. Jo, S., et al., *Synthesis and characterization of oligo(poly(ethylene glycol) fumarate) macromer.* Macromolecules, 2001. **34**(9): p. 2839-2844.

2. Kinard, L.A., F.K. Kasper, and A.G. Mikos, *Synthesis of Oligo(Poly(Ethylene Glycol) Fumarate).* Nature Protocols, 2012. **7**(6): p. 1219-1227.

3. Ewald, T.J., et al., *Safety of Intra-Articular Implantation of Oligo Poly(Ethylene Glycol) Fumarate Scaffolds into the Rabbit Knee.* Tissue Engineering Part C-Methods, 2016. **22**(10): p. 991-998.

4. Hakim, J.S., et al., *Positively Charged Oligo Poly(Ethylene Glycol) Fumarate Scaffold Implantation Results in a Permissive Lesion Environment after Spinal Cord Injury in Rat.* Tissue Engineering Part A, 2015. **21**(13-14): p. 2099-2114.

5. Lam, J., et al., *Strategies for Controlled Delivery of Biologics for Cartilage Repair.* Advanced Drug Delivery Reviews, 2015. **84**: p. 123-134.

6. Guo, X., et al., *Repair of Osteochondral Defects with Biodegradable Hydrogel Composites Encapsulating Marrow Mesenchymal Stem Cells in a Rabbit Model.* Acta Biomaterialia, 2010. **6**(1): p. 39-47.

7. Kim, K., et al., *Osteochondral Tissue Regeneration using a Bilayered Composite Hydrogel with Modulating Dual Growth Factor Release Kinetics in a Rabbit Model.* Journal of Controlled Release, 2013. **168**(2): p. 166-178.

179

8.   Park, H., et al., *Injectable Biodegradable Hydrogel Composites for Rabbit Marrow Mesenchymal Stem Cell and Growth Factor Delivery for Cartilage Tissue Engineering.* Biomaterials, 2007. **28**(21): p. 3217-3227.

9.   Park, H., et al., *Delivery of TGF-beta 1 and Chondrocytes via Injectable, Biodegradable Hydrogels for Cartilage Tissue Engineering Applications.* Biomaterials, 2005. **26**(34): p. 7095-7103.

10.   Jo, S., H. Shin, and A.G. Mikos, *Modification of Oligo(Poly(ethylene glycol) fumarate) Macromer with a GRGD Peptide for the Preparation of Functionalized Polymer Networks.* Biomacromolecules, 2001. **2**(1): p. 255-261.

11.   Park, H., et al., *Effect of Swelling Ratio of Injectable Hydrogel Composites on Chondrogenic Differentiation of Encapsulated Rabbit Marrow Mesenchymal Stem Cells In Vitro.* Biomacromolecules, 2009. **10**(3): p. 541-546.

12.   Kasper, F.K., et al., *In Vitro Release of Plasmid DNA from Oligo(Poly(Ethylene Glycol) Fumarate) Hydrogels.* Journal of Controlled Release, 2005. **104**(3): p. 521-539.

13.   Holland, T.A., Y. Tabata, and A.G. Mikos, *In vitro release of transforming growth factor-beta 1 from gelatin microparticles encapsulated in biodegradable, injectable oligo(poly(ethylene glycol) fumarate) hydrogels.* Journal of Controlled Release, 2003. **91**(3): p. 299-313.

14. Scott, R.A. and N.A. Peppas, *Compositional Effects on Network Structure of Highly Cross-linked Copolymers of PEG-containing Multiacrylates with Acrylic Acid.* Macromolecules, 1999. **32**(19): p. 6139-6148.

15. Scott, R.A. and N.A. Peppas, *Kinetics of Copolymerization of PEG-containing Multiacrylates with Acrylic Acid.* Macromolecules, 1999. **32**(19): p. 6149-6158.

16. Lu, S. and K.S. Anseth, *Release Behavior of High Molecular Weight Solutes from Poly(ethylene glycol)-based Degradable Networks.* Macromolecules, 2000. **33**(7): p. 2509-2515.

17. Keys, K.B., F.M. Andreopoulos, and N.A. Peppas, *Poly(ethylene glycol) Star Polymer Hydrogels.* Macromolecules, 1998. **31**(23): p. 8149-8156.

18. Temenoff, J.S., et al., *Effect of poly(ethylene glycol) molecular weight on tensile and swelling properties of oligo(poly(ethylene glycol) fumarate) hydrogels for cartilage tissue engineering.* Journal of Biomedical Materials Research, 2002. **59**(3): p. 429-437.

19. Jo, S., A.G. Mikos, and A. Mikos, *Biocompatible Macromer for Forming Polymeric Network Comprises Oligomer Containing Multiple Repeating Units, with Each Unit Containing Biocompatible Cross-linkable Moiety Bounded to Biocompatible Polymer*. UNIV RICE WILLIAM MARSH (RICV-C) UNIV RICE WILLIAM MARSH (RICV-C) JO S (JOSS-Individual) MIKOS A G (MIKO-Individual) UNIV RICE WILLIAM MARSH (RICV-C) UNIV RICE WILLIAM MARSH (RICV-C). p. 1282428-A1:.

20. Shin, H., J.S. Temenoff, and A.G. Mikos, *In Vitro Cytotoxicity of Unsaturated Oligo Poly(Ethylene Glycol) Fumarate Macromers and Their Cross-linked Hydrogels.* Biomacromolecules, 2003. **4**(3): p. 552-560.

21. Temenoff, J.S., et al., *In Vitro Cytotoxicity of Redox Radical Initiators for Cross-linking of Oligo(Poly(ethylene glycol) fumarate) Macromers.* Biomacromolecules, 2003. **4**(6): p. 1605-1613.

22. Cai, L. and S.F. Wang, *Elucidating Colorization in the Functionalization of Hydroxyl-Containing Polymers Using Unsaturated Anhydrides/Acyl Chlorides in the Presence of Triethylamine.* Biomacromolecules, 2010. **11**(1): p. 304-307.

23. Peter, S.J., et al., *Synthesis of Poly(propylene fumarate) by Scylation of Propylene Glycol in the Presence of a Proton Scavenger.* Journal of Biomaterials Science-Polymer Edition, 1999. **10**(3): p. 363-373.

24. Suggs, L.J., et al., *Synthesis and Characterization of a Block Copolymer Consisting of Poly(propylene fumarate) and Poly(ethylene glycol).* Macromolecules, 1997. **30**(15): p. 4318-4323.

25. Hedberg, E.L., et al., *Controlled release of an osteogenic peptide from injectable biodegradable polymeric composites.* Journal of Controlled Release, 2002. **84**(3): p. 137-150.

26. Hedberg, E.L., et al., *Effect of varied release kinetics of the osteogenic thrombin peptide TP508 from biodegradable, polymeric scaffolds on bone*

182

formation in vivo. Journal of Biomedical Materials Research Part A, 2005. **72A**(4): p. 343-353.

27.   Hedberg, E.L., et al., *In vitro degradation of porous poly(propylene fumarate)/poly(DL-lactic-co-glycolic acid) composite scaffolds.* Biomaterials, 2005. **26**(16): p. 3215-3225.

28.   Hedberg, E.L., et al., *In vivo degradation of porous poly(propylene fumarate)/poly(DL-lactic-co-glycolic acid) composite scaffolds.* Biomaterials, 2005. **26**(22): p. 4616-4623.

29.   Bredwell, M.D. and R.M. Worden, *Mass-transfer Properties of Microbubbles. 1. Experimental Studies.* Biotechnol. Progr., 1998. **14**(1): p. 31-38.

30.   Nosse, B., et al., *Optimization of Ring-Closing Metathesis: Inert Gas Sparging and Microwave Irradiation.* Advanced Synthesis & Catalysis, 2005. **347**(14): p. 1869-1874.

31.   Miller, W.D., et al., *Suppression of a Palladium-Mediated Homocoupling in a Suzuki Cross-Coupling Reaction. Development of an Impurity Control Strategy Supporting Synthesis of LY451395.* Organic Process Research & Development, 2007. **11**(3): p. 359-364.

32.   Tufvesson, P., C. Bach, and J.M. Woodley, *A Model to Assess the Feasibility of Shifting Reaction Equilibrium by Acetone Removal in the Transamination of Ketones Using 2-propylamine.* Biotechnology and Bioengineering, 2014. **111**(2): p. 309-319.

33. Pedersen, S.L. and K.J. Jensen, *Instruments for Automated Peptide Synthesis*, in *Peptide Synthesis and Applications, 2nd Edition*, K.J. Jensen, P.T. Shelton, and S.L. Pedersen, Editors. 2013, Humana Press Inc: Totowa. p. 215-224.

34. *Joule-Thomson Effect (1852) Physics*. 2002, Visible Ink Press. p. 289.

35. Carothers, W.H., *Polymers and Polyfunctionality.* Transactions of the Faraday Society, 1936. **32**(1): p. 0039-0053.

36. Chaikof EL, M.E., *Bulk Properties of Poly(ethylene Oxide)/Polysiloxane Networks.* New Polym. Mat., 1990. **2**: p. 23.

37. Hutter, J.L. and J. Bechhoefer, *Calibration of Atmoic-Force microscope Tips.* Rev. Sci. Instrum., 1993. **64**(7): p. 1868-1873.

38. Proksch R, C.J., *Quantifying Molecular Forces: Sensitivities and Spring Constants without Touching a Surface.* Asylum Research, 2005.

39. Drira, Z. and V.K. Yadavalli, *Nanomechanical Measurements of Polyethylene Glycol Hydrogels using Atomic Force Microscopy.* Journal of the Mechanical Behavior of Biomedical Materials, 2013. **18**: p. 20-28.

40. Gordon, A.J. and R.A. Ford, *The Chemist's Companion: A Handbook of Practical Data, Techniques, and References*. 1972, New York: John Wiley & Sons.

41. Choi, K.Y. and K.B. McAuley, *Step-Growth Polymerization.* Polym. React. Eng., 2007: p. 273-314.

42.   Dadsetan, M., et al., *Characterization of Photo-cross-linked Oligo Poly(Ethylene Glycol) Fumarate Hydrogels for Cartilage Tissue Engineering.* Biomacromolecules, 2007. **8**(5): p. 1702-1709.

43.   Timmer, M.D., et al., *Characterization of the Cross-linked Structure of Fumarate-Based Degradable Polymer Networks.* Macromolecules, 2002. **35**(11): p. 4373-4379.

44.   Lam, J., et al., *A Factorial Analysis of the Combined Effects of Hydrogel Fabrication Parameters on the in vitro Swelling and Degradation of Oligo(Poly(Ethylene Glycol) Fumarate) Hydrogels.* J Biomed. Mater. Res. A, 2014. **102**(10): p. 3477-3487.

Chapter 7

Modification of OPF for 3D Hydrogel Environments

Kent E. Coombs[1,2], Matthew N. Rush[2,3], Quan Huynh[2], Elizabeth L. Hedberg-Dirk[2,4]

[1]*Biomedical Science Graduate Program,* [2]*Center for Biomedical Engineering,*

[3]*Nanoscience and Microsystems Engineering Graduate Program,* [4]*Department of*

Chemical and Biological Engineering, University of New Mexico, Albuquerque,

NM.

Corresponding Author: Elizabeth L. Hedberg-Dirk
Address: Center for Biomedical Engineering
       MSC01 1141
       1 University of New Mexico
       Albuquerque, NM 87131
Email: edirk@unm.edu
Fax: 505-277-6209
Phone: 505-277-5906

Abstract

Studies have shown that surface chemistry can effect valvular interstitial cell behavior in two-dimensional cell culture systems, however the three-dimensionality of tissues is poorly emulated in monolayer environments. To create more relevant models for the study of valvular interstitial cell behavior we generated a hydrogel cell culture platform using polyethylene glycol and fumaryl chloride. The resulting polymer oligo(polyethylene glycol) fumarate was functionalized with specific alkanethiols along its backbone to control the charge of the resulting molecules and crosslinked in three dimensional (3D) hydrogels. This allowed for testing of valvular interstitial cell behavior in specific charged 3D environments to determine how they affect VIC growth and differentiation *in vitro*. In conclusion, charge alone was insufficient to induce VIC viability within the hydrogels. Therefore, further modification of OPF with adhesion molecules will be required for future research.

Introduction

With an increasing elderly population, health care expenditures for aortic valve disease (AVD) continue to rise. To address this increased burden better treatments for AVD need to be developed [1]. Left untreated the likelihood of death due to AVD is 50% within 2 years [2]. The current gold standard of treatment for AVD is surgical replacement of the diseased valve. Typically mechanical or decellularized biological valve replacements are used, but major limitations in their requirement for anticoagulation therapy or their 5-10 year limited lifespan before requiring replacement makes these valves undesirable for long term use [3]. Creating a replacement valve that could last a lifetime without deleterious effects, and could also be used as an accurate *in vitro* model for the study of AVD is essential to advance AVD care.

In order to address these issues research is being conducted to develop tissue engineered heart valve (TEHVs). TEHVs would overcome the current limitations of mechanical and decellularized biological valves replacing them as the gold standard of AVD treatment [3]. With the ability to integrate into the surrounding host tissue and utilize the body's natural repair functions, TEHV's would act just like native tissue [4]. Well-designed TEHVs could also be used as relevant *in vitro* testing platforms to study the cellular mechanisms involved in AVD progression and as models to develop and test therapeutic drugs. However, the technology to grow functional TEHV tissue is still in nascent stages. Different

strategies to create TEHVs utilizing natural polymers, deceullarized tissue, or synthetic polymers are popular in literature, but a gap in knowledge exists in how a cell's growth, behavior, and differentiation are effected by the scaffold environment they are grown on [5-10].

The main cells of the aortic valve, valvular interstitial cell (VICs), are commonly used to grow and study aortic valve tissue. However, biological and mechanical cues of the scaffold have been shown to alter valvular interstitial cell (VIC) phenotype and behavior, but the cellular signaling mechanisms behind these changes are not yet well defined [11-16]. Synthetic hydrogel platforms are used to study cell signaling mechanisms because they offer the benefit of isolating the effects of specific tailorable scaffold on cell behavior. This is due to their innate ability to be modified with specific chemical moieties that alter specific environmental conditions using simple chemistry. In addition, these synthetic scaffold can be further modified and shaped into 3 dimensional (3D) systems that better mimic the native tissue. Many synthetic materials also do not interact directly with cell, so cells placed on/in a synthetic scaffold are forced to interact with the engineered biologically active portions of these materials. As a result cell culture systems can be designed with individual bioactive molecules or with variations in a single mechanical property that can be reliably reproduced to control and study the effect of specific environmental cues on cell behavior.

189

A common synthetic polymer used to create hydrogels scaffolds for VICs is polyethylene glycol (PEG) [8, 12, 17, 18]. PEG hydrogels are desireable for their biocompatible hydrophilic properties, controllable pore size, mechanical properties, and their ability to be chemically modified. In addition, PEG can be polymerized and crosslinked through a number of chemistries to create 3D cell culture environments. Recent examples of VICs grown on top of PEG base hydrogels with an attached RGD, YGSIR, DEGA, or VAPG peptides have shown that VICs attach and grow differently dependent on the adhesion sequence [17]. When a similar PEG hydrogel system functionalized with RGD, VGVAPG, or P15 peptides were used to encapsulate and culture VICs over a 42 day period, differences in activation and extracellular matrix protein production were observed [5].

While peptide functionalization of 3D hydrogel has been utilized in the development of TEHVs, less research has been done to look at how the charge of the hydrogel environment effects VIC behavior. Charge is of interest because during embryogenesis the valves develop from the pericardial cushion, which is a soft gel-like substance that has high concentration of the negatively charged molecule hyaluronic acid and hyaluronan also makes up 60% of the glycosaminoglycans in valve tissue [19]. These data suggest VICs naturally exist within a negatively charge environment and recapitulating this environment in a 3D scaffold may help VICs to grow into healthy aortic valve tissue.

190

In a recent study VICs were grown on 2 dimensional (2D) surfaces where the chemistry of the underlying substrate was controlled [11]. It was found that VICs grown on negatively charged 2D surfaces grew rapidly, did not express VIC osteoblastic markers, and avoided confluence based nodule formation. However, positively charged 2D substrates caused VICs to rapidly undergo osteoblastic differentiation [11]. These results show that the surface chemistry of the underlying substrate can effect cellular behavior in monolayer culture.

In order to transition into a 3D systems we used a PEG based polymer, oligo(poly(ethylene glycol) fumarate) (OPF), to form functionalized hydrogels. Unlike the previously described PEG hydrogels, OPF has a repeating unsaturated double bond along the polymer's backbone which can be functionalized. OPF also has a repeating ester groups which can undergo hydrolytic degradation allowing the hydrogel to slowly degrade and be replaced by developing tissue over time. The repeating unsaturated double bond of OPF allows the alkanethiol chemicals used in chapter 5, 11-mercaptoundecanoic acid or 11-aminoundecanoic acid, to be attached to OPF to make a negatively charge OPF (OPF-COO$^-$) and positively charged OPF (OPF NH$_3^+$) functionalized molecules. The slow degradation of OPF via hydrolysis means that the scaffold can slowly degrade and allow new tissue growth to eventually take over the scaffold. These functionalized OPF molecules can also be used to generate 3 dimensional (3D) hydrogel environments with encapsulated VICs to test how a

negative or positively charged 3D environments effect VIC behavior. Based on the observation of VICs in 2D culture we hypothesized that OPF-COO⁻ 3D hydrogels will promote VIC proliferation and prevent osteoblastic differentiation *in vitro*.

Material and Methods

Synthesis of Oligo(Poly(Ethylene Glycol) Fumarate) (OPF)

OPF was synthesized as described in chapter 5. Briefly, 1K PEG (Sigma Aldrich) was dried and fumaryl chloride (Sigma Aldrich) purified using distillation. 100g of dried PEG was dissolved in 700 mL of methylene chloride and placed in a nitrogen environment. Nitrogen gas was continuously bubbled through the liquid using a sparge and forced out through tubing into a base bath. Distilled fumaryl chloride (1:0.9, PEG:FuCl) was dissolved in 60 mL methylene chloride and injected at 10 mL/hour into the reaction vessel using a syringe pump. As FuCl was added, DCM was added periodically added to maintain the reaction volume at 700 mL. After 10 hours of stirring and addition of DCM the vessel was left stirring overnight with nitrogen sparging. Upon completion, remaining solvent was removed by rotary evaporation at 30°C followed by drying at a reduced pressure in a vacuum oven overnight before being stored at -20 °C.

GPC of OPF

The molecular weight of OPF was determined using a Waters Breeze GPC system equipped with a 2707 autosampler, a 1515 isocratic HPLC pump, and a 2414 refractive index detector. For each sample 10-20 mg of OPF was dissolved in 2 mL of chloroform, run at 1 mL/min, and compared to a PEG A 16100, 3870, 1020, 410, 106; PEG B 21160, 8160, 1450, 615, 194 (Polymer Laboratories/Agilent Technologies) standard to calculate the molecular weight.

Dialysis and Functionalization of OPF

Dried OPF was dissolved in 190 proof EtOH (ACS) at a 1:1 g/ml ratio and sealed inside Spectra/Pore 7 Dialysis Membrane Pre-Treated RC tubing MWCO 1000 (Spectrum Labs). The membrane was transferred into a large covered beaker with 100 times the sample volume in 190 proof EtOH and left stirring overnight to remove any unreacted PEG. The next day dialyzed solution was collected and dried using a rotovap at 30°C to remove the majority of solvent before being transferred to a Pyrex dish and dried in a reduced pressure environment overnight . To attach alkanethiols to dialyzed OPF, it was dissolved in 0.1 M sodium bicarbonate (6:1 Buffer:OPF) with various amounts of 11-mercaptoundecanoic acid (COO^-) or 11-aminoundecanoic acid ($NH3^+$) overnight (Table 1).

The reacted solution was dried on the rotovap at 50° C for 30 min to remove most of the water. The left over solution was poured into a Pyrex dish and finished drying at a reduced pressure in the vacuum oven overnight. The final product was collected and stored at -20 °C in a sealed container.

Nuclear Magnetic Resonance (NMR) of OPF

6-10 mg of sample was dissolved in 2 mL of deuterated chloroform (Sigma-Aldrich) and filtered using a 0.45 um nylon Aerodisc syringe filter to remove salts (Fisher Scientific). 700 µL of filtered solution was transferred to 5 mm, 500 MHz NMR sample tubes (Wilmad LabGlass) and were read on a Bruker Avance III 300 at 300 Hz for ^{1}H NMR. The degree of functionalization was calculated by using ratio of olefin (6.78 ppm) to PEG (3.4-4.0 ppm) peak integration values between un-functionalized and functionalized OPF.

Crosslinking of Functionalized OPF Hydrogels

OPF, and OPF-COO[-] molecules were crosslinked using a UV initiator and polyethylene glycol dimethacrylate (PEGDA). The formulations were mixed as follows; 25 wt% OPF, 5% PEGDA, 0.05-1% Irgacure 2959 initiator, with remaining wt% as Dulbecco's Phosphate Buffered Saline without calcium or magnesium (DPBS). Hydrogel were poured into 3 mL syringes to create a 2:1

height to width sample before being exposed to 15 min of 365 nm UV light in a

UVP light box (CL-1000).

Primary Cell Extraction and Culture

VICs were isolated as previously described [20]. Porcine hearts were

shipped overnight from Hormel and aortic valve leaflets were excised. Leaflets

were incubated in collagenase type 2 (Worthington) in 199 medium (Hyclone)

before scraping to remove valvular endothelial cells (VECs). Residual VECs were

removed using CD31+ magnetic dynabeads (ThermoFisher Scientific). VICs

were cultured under normal conditions, 37 ºC with 5% CO_2 in 199 EBSS Hyclone

growth media [10% Fetal Bovine Serum (FBS) (Hyclone), 1%

Penicillin/Streptavidin (Hyclone), and 1% Fungizone (Hyclone)] and allowed to

reach ~80% confluence before being frozen down and stored in liquid nitrogen.

Encapsulation of Cells

OPF, and OPF-COO⁻

Functionalized OPF 1:0.27, 1: 1.1, 1: 1.7 (Alkanethiol:PEG molar ratio)

and unfunctionalized OPF hydrogels were crosslinked using the following

formulation; 25 wt% OPF/OPF-COO⁻, 2-5% PEGDA, 0.05-1% Irgacure 2959

initiator, and remaining wt% DPBS, with 1×10^6-5×10^6 cells/mL. 500 μL of

solution was moved to 10 mL syringe molds before being exposed to 15 min of 365 nm UV light in a UVP light box (CL-1000). The resulting gels had a diameter of 17.3 mm and were ~3 mm thick. After crosslinking gels were placed in 6 well plates with 3 mL of growth media 199 medium a (Hyclone) with 10% FBS (Gibco), 1% Penicillin Streptavidin (Gibco), 1% Fungizone (Gibco) and cultured under normal conditions.

Live/Dead assay

Immediately after crosslinking and after 24 hours of incubation VIC viability was analyzed using a Live/Dead Mammalian Cell Assay Kit (Life Technologies). Briefly, media was removed from the wells and replaced with live/dead solution (2 µM calcein AM and 4 µM EthD-1 in 199 medium). After 30 min of incubation hydrogels were washed with DPBS 2 time with a 5 min incubation, and imaged on a Nikon Eclipse TS100 fluorescent microscope.

Results

Characterization and Functionalization of OPF

Using nitrogen sparging method from chapter 5, 1K PEG and fumaryl chloride were used to synthesize OPF. The final product OPF had the chemical structure expected seen via NMR with an olefin peak at 6.8 ppm, and PEG at

3.2-4 ppm (Figure 1) [21]. GPC showed the average molecular weight (Mw) of OPF was 6063 ± 706 and a polydispersity index (PDI) of 1.5 (n=4).

Successful functionalization of OPF with 11-mercaptoundecanoic acid (COO^-) or 11-aminoundecanoic acid (NH_3^+) was demonstrated via H^1 NMR with the appearance of a peak at 4.2 ppm and reductions of the olefin signal at 6.8 ppm, indicating a successful reaction of the thiol group on COO^- or NH_3^+ to the unsaturated double bond of the OPF backbone (Figure 1). In addition the amount of functionalization of OPF with COO- was varied by adjusting the stoichiometry of COO^- to OPF in the reaction. Comparing the ratio of olefin (6.8 ppm) to PEG peak (3.2-4 ppm) integration values before and after functionalization indicated the percent of OPF double bonds consumed during functionalized could be varied from 11-42% (Table 1). Although a higher levels of functionalization were tested the resulting products did not crosslink under conditions acceptable for cell encapsulation (data not shown).

Viability of Encapsulated VICs

Initial Live/Dead assays were conducted on VICs encapsulated in 25 wt% OPF using 0.05-1% Irgacure 2959, 2.5% PEGDA, with the remaining wt% as DPBS. Immediately after encapsulation Live/Dead was conducted and showed greater viability (~80%) was observed when Irgacure 2959 concentrations were limited to 0.1 wt% and below (Figure 2). Therefore, all experiments of VICs

encapsulated in OPF-COO⁻ were run at 0.1 wt% Irgacure 2959 concentrations, 25 wt% OPF, and 5 wt% PEGDA, 70% DPBS. VICs were again encapsulated in OPF by itself with $1X10^6$ VICs and in OPF-COO⁻ (1:0.27) at a higher concentration of $5X10^6$ cells/ml. Optical images show cells were successfully encapsulated at both cell concentrations however live/dead indicates that the majority of VICs died after 24 hours of incubation in all conditions (Figure 3).

Discussion

Previously, it is was shown that VICs grown on 2D surfaces with either a positive and negative surface chemistry induced an osteoblastic or proliferative healthy phenotype, respectively. This work focused on developing a 3D hydrogel system with charged functional groups. OPF was synthesized using a 1K PEG and had a final molecular weight of 6046. Therefore, each OPF molecule had an average of ~5.2 olefin bonds per molecule. Traditional PEG hydrogels are modified with acrylates to so they can only functionalized on one end and crosslinked into a 3D structure on the other [22]. With OPF, however, the ~5 double bonds on available on the backbone of each OPF can functionalization with more than one molecule and still are able to be crosslinked. Therefore OPF has increased the utility and versatility as a molecule to create controlled hydrogel environments.

198

Crosslinking OPF into a hydrogel using Irgacure 2959 is initiated by the generation of free radicals using UV light. Free radicals are known to be cytotoxic, therefore optimization of Irgacure 2959 concentration for OPF hydrogel crosslinking while maintaining VIC viability was assessed. The greatest viability was observed at 0.05% Irgacure 2959 however the efficient hydrogel formation occurred with 1% Irgacure. With ~80% viability in 0.1% Irgacure hydrogels this concentration was chosen as the ideal condition to encapsulated VICs while forming solid hydrogels (Figure 2).

Next OPF was functionalized with the alkanethiols 11-mercaptoundecanoic acid or 11-aminoundecanoic acid using a thiol-ene click chemistry to create OPF molecules with negative (OPF-COO$^-$) and positive (OPF-NH$_3^+$) charges (Figure 1). These OPF molecules were tailored to have increase or decrease concentration alkanethiol moiety attachment by changing the stoichiometry of alkanethiol to OPF used in the functionalization reaction (Table 1). This simple method allows for the amount of charge within the final hydrogel to be tailored while allowing for the possibility of attaching other molecules, like peptides, to the same OPF molecule.

For VIC encapsulation studies OPF-COO- (1:1.7) 42% functionalization was used to maximize the negative charge in the final hydrogel. We hypothesized that this negative charge would be sufficient to help encapsulated VICs proliferate and remain in an activated phenotype over time. However, 12

199

hours after encapsulation under normal culture conditions all the VICs died. The inability of VICs to adhere to the modified OPF-COO and OPF hydrogels is likely the largest contributing factor to cell death. Due to the result seen with OPF-COO- hydrogels, OPF-NH3$^+$ hydrogels systems will not be tested until VIC viability is increased.

In the two dimensional system cell adhesion wasn't an issue because proteins from the serum added to media was able to quickly absorb to the modified surfaces when cells were seeded. The VICs could then attach to these absorbed serum proteins and survive [11, 23, 24]. In the hydrogel system the serum proteins would have a hard time moving into the hydrogel so cell are forced to attempt to interact with the OPF backbone or the functionalized alkanethiols. The OPF backbone is made of PEG, which has previously been shown to resist protein absorption and cellular interactions creating a blank slate material [25]. In many studies to help VIC attachment to PEG, bioactive molecules such as attachments peptides were covalently attach to the PEG molecules [5, 8, 17, 26]. The fact that VICs did not survive in OPF-COO$^-$ suggest that proteins from the media did not penetrate the hydrogel fast enough and were unable to absorb to the alkanethiol molecules in the hydrogel to support cell attachment. Therefore, the negative environment provided by the OPF-COO$^-$ hydrogels by itself was not sufficient to support VIC attachment.

Previous studies have added adhesion peptide RGD, P15, and YGSIR to special PEG hydrogels, showing VIC viability out to 48 days of culture [15]. In future studies with OPF it would be prudent to add some attachment peptides to OPF in addition to the alkanethiols. With the peptide being immediately available for VIC attachment they could survive the initial encapsulation and cell culture, but still allow for the long term study of VIC growing in a charged 3D scaffolds.

A second theory for why the VICs didn't survive is that there were not enough alkanethiols present within the gel for VICs to bind. Unfortunately, increasing the functionalization of OPF with alkanethiols above 42% inhibited crosslinking. A strategy to overcome this issue would be to make OPF with a smaller molecular weight PEG. The current length of OPF is limited by the steric hindrance caused by the large PEG molecules. By decreasing the PEG molecular weight more repeat units of PEG to FuCl could be oligimerized than our current system and therefore would have more unsaturated double bonds per OPF molecule that could be functionalized and crosslinking. The concentration of the alkanethiols could then be increased and still have enough remaining functional groups for crosslinking.

Conclusion

The understanding of how VICs react to scaffold cues is essential to the production of healthy heart valve tissue. In this study the negative environment of

the pericardial cushion created by the high concentrations of hyaluronic acid was mimicked in a unique PEG based hydrogel system [27]. The molecule OPF was functionalized with 11-mercaptoundecanoic acid to create a negatively charged hydrogel environment with a carboxyl group being presented to encapsulated cells. In contrast OPF was also functionalized with 11-aminoundecanoic acid to create positively charge environment, which has been shown previously to induce osteoblastic differentiation in 2D cultures [11].

Successful functionalization of OPF with COO^- and NH_3^+ was demonstrated as well as the ability to tailor the amount attached using stoichiometric controls. This control creates a versatile hydrogel system were the concentration of functionalized molecules can be easily altered for biological studies. As the concentration of peptides has been shown to effect VIC behavior in PEG hydrogels we hypothesized that changing the concentration of COO^- in OPF will similarly affect VICs in 3D hydrogels [17]. However, results showed that a negative charge by itself was not enough to allow for VIC survival after being encapsulated in this system.

In the previous 2D studies proteins could easily be absorb from the media onto the surface that was completely covered in COO^- or NH3+ surface chemistries. The absorbed proteins in turn allowed for VIC to attach and grow on the surface. In a 3D hydrogel system, however, the dominating the PEG environment, a molecule known for its non-fouling properties prevents cell or

protein attachments. Adding the alkanethiol 11-mercaptoundecanol to the backbone should have helped to increase protein absorption to the gel, however it was either not at a high enough concentration to effect the overall PEG dominate environment or the proteins were not able diffuse into the hydrogel quickly enough to help VICs adhere in the early stages of hydrogel swelling. Therefore, future work with OPF functionalized with attachment peptides and COO^- need to be synthesized to create a 3D hydrogel systems in which VICs can survive initial encapsulation.

Figures and Tables

Table 1. Formulation for alkanethiol Functionalization of OPF			
11-mercaptoundecanoic acid : OPF (mol)	0.27:1	1.1:1	1.7:1
Double Bonds Functionalized (%) NMR Calculation	11.1 ± 5.7*	28.2 ± 8.0*	42.2 ± 2.5*
Theoretical Functionalization (%)	5.4	21.0	35.0

* p=0.05, n=3

Oligo(poly(ethylene glycol) fumarate) (OPF)

11-mercapto-1-undecanol

H_2O

11-amino-1-undecanethiol HCL

OPF functionalized 11-mercapto-1-undecanol
OPF

OPF functionalized 11-amino-1-undecanol
OPF
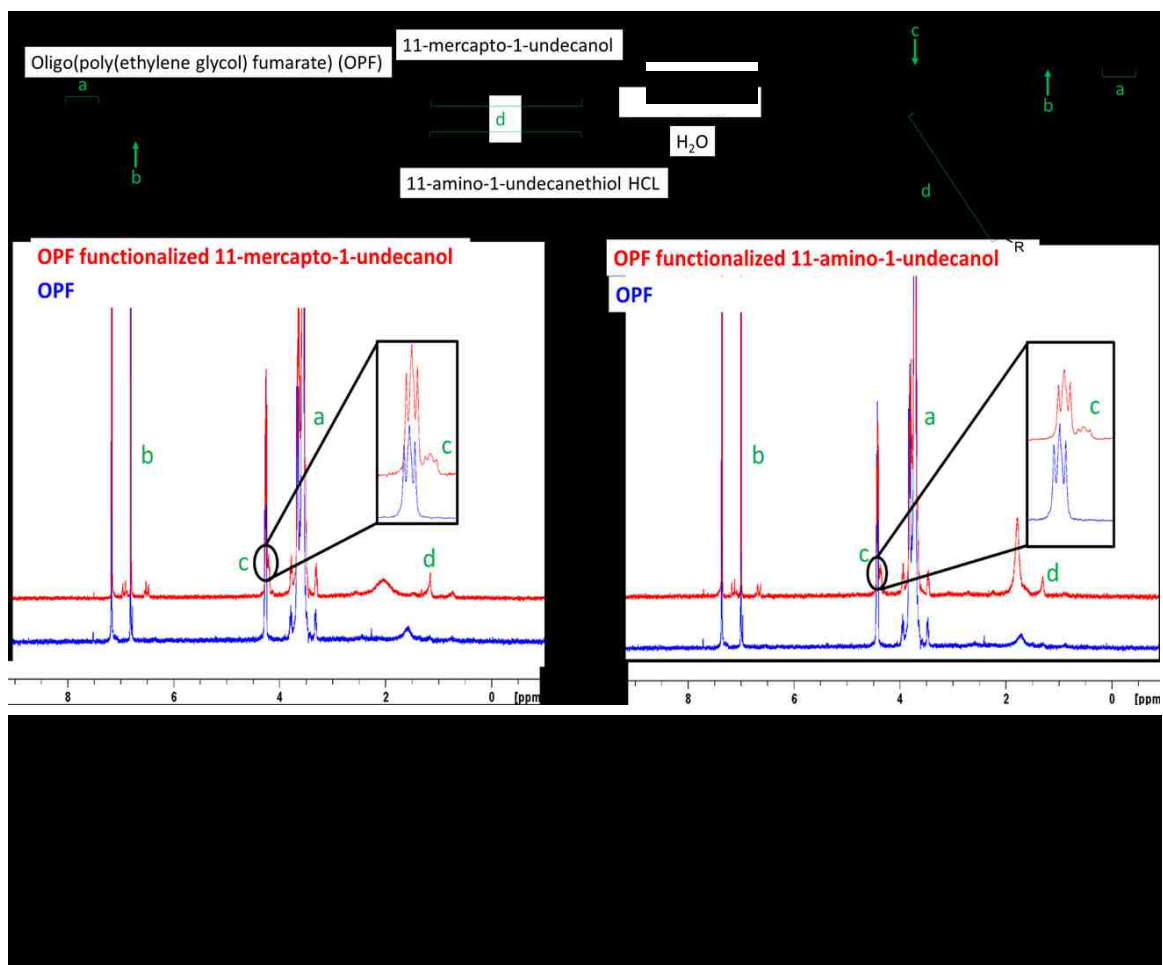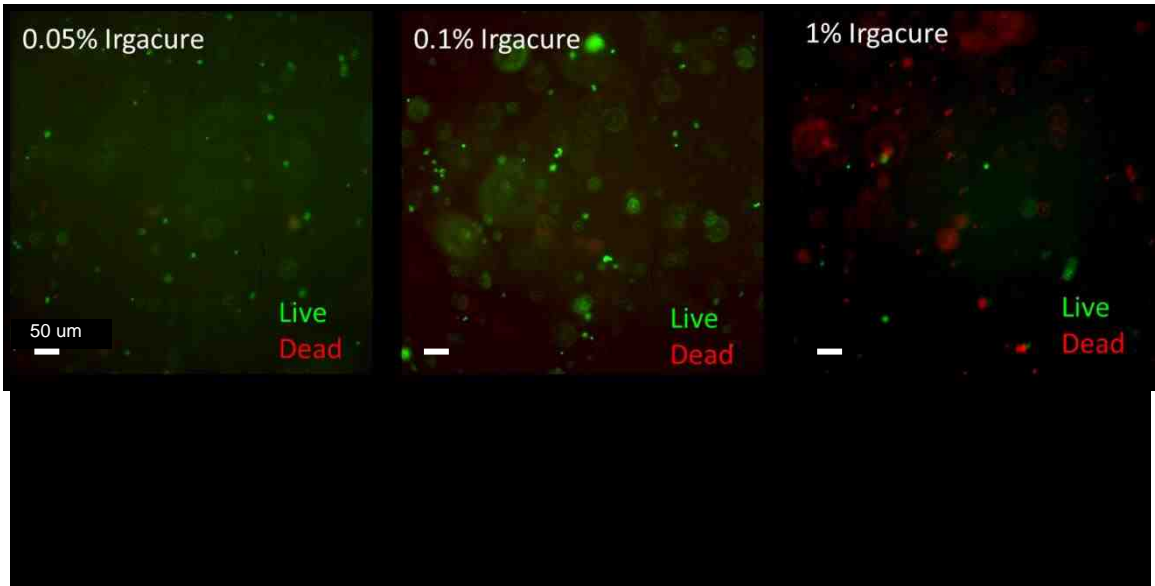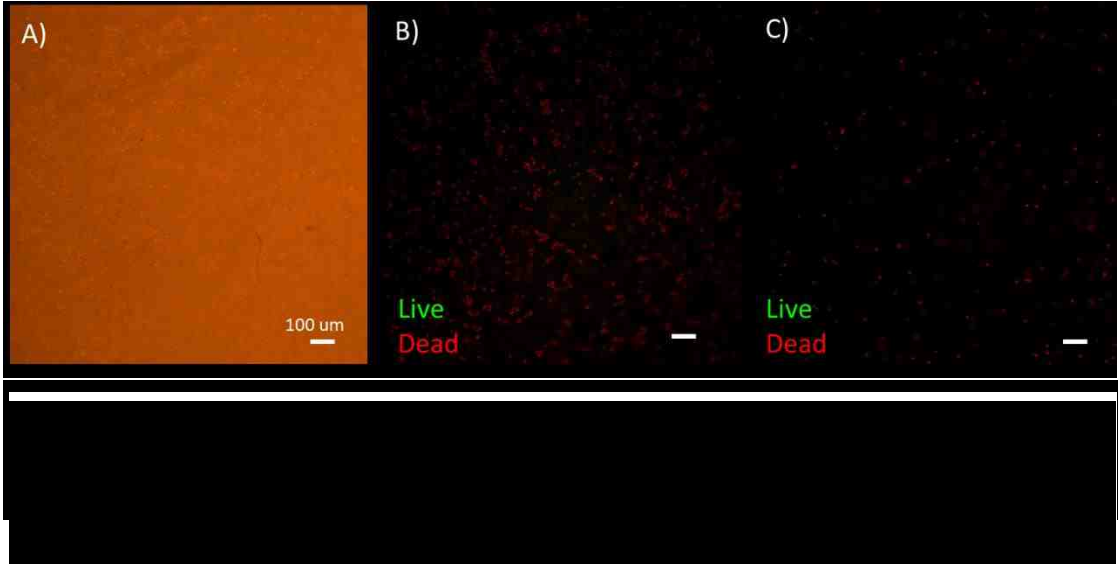
References

1.   Yacoub, M.H. and J.J.M. Takkenberg, *Will heart valve tissue engineering change the world?* Nature clinical practice. Cardiovascular medicine, 2005. **2**(2): p. 60-1.

2.   Otto, C.M., *Timing of aortic valve surgery.* Heart, 2000. **84**(2): p. 211-218.

3.   Tillquist, M.N. and T.M. Maddox, *Cardiac crossroads: deciding between mechanical or bioprosthetic heart valve replacement.* Patient preference and adherence, 2011. **5**: p. 91-99.

4.   Kheradvar, A., et al., *Emerging Trends in Heart Valve Engineering: Part I. Solutions for Future.* Annals of Biomedical Engineering, 2015. **43**(4): p. 833-843.

5.   Gould, S.T. and K.S. Anseth, *Role of cell–matrix interactions on VIC phenotype and tissue deposition in 3D PEG hydrogels.* Journal of Tissue Engineering and Regenerative Medicine, 2016. **10**(10): p. E443-E453.

6.   Schroer, A.K. and W.D. Merryman, *Mechanobiology of myofibroblast adhesion in fibrotic cardiac disease.* Journal of Cell Science, 2015. **128**(10): p. 1865-1875.

7.   Ruiz, J.L., J.D. Hutcheson, and E. Aikawa, *Cardiovascular calcification: current controversies and novel concepts.* Cardiovascular Pathology, 2015. **24**(4): p. 207-212.

8. Puperi, D.S., et al., *3-dimensional spatially organized PEG-based hydrogels for an aortic valve co-culture model.* Biomaterials, 2015. **67**: p. 354-364.

9. Janson, I.A. and A.J. Putnam, *Extracellular matrix elasticity and topography: Material-based cues that affect cell function via conserved mechanisms.* J Biomed Mater Res A, 2015. **103**(3): p. 1246-1258.

10. Rodriguez, K.J., et al., *Manipulation of valve composition to elucidate the role of collagen in aortic valve calcification.* BMC Cardiovasc Disord, 2014. **14**: p. 10.

11. Rush, M.N., K.E. Coombs, and E.L. Hedberg-Dirk, *Surface chemistry regulates valvular interstitial cell differentiation in vitro.* Acta Biomater, 2015. **28**: p. 76-85.

12. Coombs, K.E., et al., *Isolated effect of material stiffness on valvular interstitial cell differentiation.* Journal of Biomedical Materials Research Part A, 2017. **105**(1): p. 51-61.

13. Yip, C.Y.Y., et al., *Calcification by Valve Interstitial Cells Is Regulated by the Stiffness of the Extracellular Matrix.* Arteriosclerosis Thrombosis and Vascular Biology, 2009. **29**(6): p. 936-U417.

14. Benton, J.A., H.B. Kern, and K.S. Anseth, *Substrate Properties Influence Calcification in Valvular Interstitial Cell Culture.* Journal of Heart Valve Disease, 2008. **17**(6): p. 689-699.

15. Gould, S.T., N.J. Darling, and K.S. Anseth, *Small peptide functionalized thiol-ene hydrogels as culture substrates for understanding valvular interstitial cell activation and de novo tissue deposition.* Acta Biomaterialia, 2012. **8**(9): p. 3201-3209.

16. Wang, H., et al., *Redirecting Valvular Myofibroblasts into Dormant Fibroblasts through Light-mediated Reduction in Substrate Modulus.* Plos One, 2012. **7**(7): p. 12.

17. Wu, Y., K.J. Grande-Allen, and J.L. West, *Adhesive Peptide Sequences Regulate Valve Interstitial Cell Adhesion, Phenotype and Extracellular Matrix Deposition.* Cellular and Molecular Bioengineering, 2016. **9**(4): p. 479-495.

18. Rehmann, M.S., et al., *Tuning microenvironment modulus and biochemical composition promotes human mesenchymal stem cell tenogenic differentiation.* Journal of Biomedical Materials Research Part A, 2016. **104**(5): p. 1162-1174.

19. Grande-Allen, K.J., et al., *Glycosaminoglycan synthesis and structure as targets for the prevention of calcific aortic valve disease.* Cardiovascular Research, 2007. **76**(1): p. 19-28.

20. Johnson, C.M., M.N. Hanson, and S.C. Helgeson, *Porcine cardiac valvular subendothelial cells in culture: Cell isolation and growth characteristics.* J Mol Cell Cardiol, 1987. **19**(12): p. 1185-1193.

21. Jo, S., et al., *Synthesis and characterization of oligo(poly(ethylene glycol) fumarate) macromer.* Macromolecules, 2001. **34**(9): p. 2839-2844.

22. Peter, M. and P. Tayalia, *An alternative technique for patterning cells on poly(ethylene glycol) diacrylate hydrogels.* Rsc Advances, 2016. **6**(47): p. 40878-40885.

23. Arima, Y. and H. Iwata, *Preferential adsorption of cell adhesive proteins from complex media on self-assembled monolayers and its effect on subsequent cell adhesion.* Acta Biomaterialia, 2015. **26**: p. 72-81.

24. Lin, J.H., et al., *Effect of Surface Potential on Extracellular Matrix Protein Adsorption.* Langmuir, 2014. **30**(34): p. 10328-10335.

25. Sharma, S., R.W. Johnson, and T.A. Desai, *Evaluation of the Stability of Nonfouling Ultrathin Poly(ethylene glycol) Films for Silicon-Based Microdevices.* Langmuir, 2004. **20**(2): p. 348-356.

26. Gould, S.T., et al., *The role of valvular endothelial cell paracrine signaling and matrix elasticity on valvular interstitial.* Biomaterials, 2014. **35**(11): p. 3596-3606.

27. Schroeder, J.A., et al., *Form and function of developing heart valves: coordination by extracellular matrix and growth factor signaling.* Journal of Molecular Medicine, 2003. **81**(7): p. 392-403.

Chapter 8

Conclusion

Summary

In the realm of tissue engineered heart valves (TEHV) there are many concepts that need to be expounded to successfully grow tissue in the laboratory. In this work, we have examined some specific questions about *in vitro* aortic valve (AV) tissue growth including; which subpopulation of heart valve cells should be used to grow aortic valve tissue models and how specific mechanical and chemical properties of the scaffold influence cellular behavior and differentiation. To answer these questions specific tunable properties of tissue growth environments were identified. These properties were then systematically engineered into an *in vitro* model to create experimental systems used to study the effect of each property on valvular interstitial cells (VICs) growth and behavior.

Specific Aim 1: *Identify relevant VIC subpopulations for tissue engineering.*

The first question investigated in this work was whether unique cell subpopulations could be readily separated out from a heterogeneous VICs population. Use of a heterogeneous population of VIC is problematic due to

212

observed changes in propensity for disease arising from different locations within the valve [1, 2]. Each aortic valve leaflet is comprised of spatially and structurally defined layers; the fibrosa, spongiosa, and ventricularis [3]. These three layers are integral to the proper opening and closing of the AV, have distinct extracellular matrix (ECM) structures and composition, and also exhibit specific mechanical properties [4]. On the arterial side of the valve the fibrosa contains large collagen 1 fibrils, which provide mechanical stability and withstand the high pressures experienced on the valve when it is closed. Directly underneath the fibrosa is the spongiosa. This layer is primarily composed of sulfated glycosaminoglycans, which absorb mechanical stress by dampening the force exerted on the valve during valve cycling [4]. On the bottom side of the AV is the ventricularis. Comprised primarily of elastin, the ventricularis is highly elastic and returns the valve to a closed position after ejection of the blood from the heart. *In vitro* both ECM and mechanical properties have been shown to alter the behavior of many different cell types [5-7]. In the case of the AV it has also be observed that calcific nodule formation generally starts in the fibrosa layer of the AV [1, 2]. It has been observed that VICs induced to an osteoblastic phenotype (OB VICs) using osteoblastic induction media as well as a small population of VICs in normal culture take much longer to detach during passaging [8]. Taking advantage of this natural phenomenon, we separated the heterogeneous VIC population taken from the valve into less adherent or more adherent VIC subpopulations. We hypothesized that attachment and focal adhesion formation

cause different subpopulations to express different phenotypes in culture. However, without a rapid method to isolate each VIC subpopulation the study and identification of these specific subpopulations remains difficult.

In chapter three, differences in adhesion were utilized to separate VIC subpopulations *in vitro*, characterize each subpopulation, and identify unique protein surface markers. The more adherent subpopulation exhibited increased expression of osteoblastic gene markers, proliferated significantly slower, and had a rhomboidal morphology similar to osteoblastic media induced OB VICs. This more adherent subpopulation may be useful for developing diseased models to study the mechanisms behind AVD or as an *in vitro* platform for the development of therapeutic drugs. In contrast, the less adherent VIC subpopulation which proliferated rapidly and did not express OB gene markers are better suited for tissue engineering aimed at growing healthy valve tissue.

To further distinguish these subpopulations integrin proteins were investigated due to their involvement in cell substrate adhesion, ability to alter cell phenotype, and the natural difference in attachment strength seen between our subpopulations. We found that the integrin αvβ3 was upregulated in the more adherent VICs but was not present in the less adherent VIC subpopulation. In combination with data showing the osteoblastic nature of more adherent VIC subpopulation we can concluded that increased αvβ3 expression on the surface of the VICs correlates with the OB VIC phenotype.

214

Future work could take advantage of the differences in αvβ3 expression and use as a unique surface maker to sort OB VIC subpopulations. If VICs could be separate directly from freshly excised valves using methods such as fluorescence activated cell sorting, the environmental stresses caused by passaging in this study could be bypassed. Another positive aspect of sorting would be that extraction of purified VIC subpopulations with specific phenotypes, which could be used to develop more accurate models of AV health or disease. To our knowledge no other surface marker has been identified that could be used to distinguish between activated and OB VIC phenotypes, making this work impactful to the field of AV cell biology.

Specific Aim 2: *Define environmental factors that will create the ideal substrate to grow valvular interstitial cell models of health or disease.*

The next question addressed was whether the mechanical or chemical properties of the scaffold affect the growth and differentiation of VICs. During valve aging and disease valve thickening and tissue deposition result in increased stiffness of the valve [9]. Conversely, during embryogenesis as the AV develops from the endocardial cushion, large amounts of the negatively charged polysaccharide hyaluronic acid (HA) are expressed and serve as scaffold from which the healthy valve develops [10, 11]. With a terminal carboxylic acid group repeating along its backbone, HA is the dominant molecule in the endocardial

cushion and results in a negatively charged environment. From these two observations, we hypothesized that physical cues like mechanical stiffness and substrate charge affect VIC growth and phenotype *in vitro*. To investigate these behaviors, in chapters 3 and 4 we engineered two environmental properties into unique cell culture systems designed to isolated and mimic the cues of mechanical stiffness and environmental charge observed *in* vivo.

In chapter 3 the co-polymer system dietheylenegycol dimethacrylate and n-Octyl methacrylate (DEGDMA/nOM) was utilized to test the affect of increasing substrate mechanical stiffness on VICs behavior. Using this FDA approved dental material we generated cell culture platforms that could be mechanically tailored without altering surface chemistry [12, 13]. Three different stiffness ranges were created with the softest having a compressive modulus close to that of the native heart valve at 25 kPA [4]. This soft substrate allowed VICs to proliferate, but did not induced osteoblastic differentiation. In comparison, when VICs were grown on the surfaces with the greatest stiffness level (4700 kPa), they underwent osteoblastic differentiation upregulating osteoblastic gene markers and forming calcific nodules in culture. This study indicates that stiffness of the underlying substrate alone is able to cause VICs to undergo osteoblastic differentiation. Since the VIC OB phenotype is responsible for calcific nodule development in AVD, stiff biomaterials should be avoided for future TEHV studies.

216

A main limitation of this work was the reduced adhesion of VICs to DEGDMA/nOM in comparison to TCPS cell culture flasks. Future work could alleviate this issue by plasma treating the surface of DEGDMA/nOM. This method oxidizes the surface of the DEGDMA/nOM decreasing its hydrophobicity and thereby promoting cellular attachment [14]. This technique is commonly used on tissue culture polystyrene (TCPS) which is universally used in the growth of adherent cell lines.

In summary, using DEGDMA/nOM highlights the importance of material stiffness in VIC behavior. The softest material (25 kPa) showed sufficient VIC proliferation and avoided the expression of osteoblastic markers and calcified nodules. Previous research has shown that materials with compressive modulus lower than 2-8 kPa promote a quiescent VIC state that fail to proliferate [15, 16]. Therefore, we hypothesize that an ideal biomaterial for the growth of healthy aortic valve tissue from VICs should possess a compressive modulus between 2-25 kPa. This stiffness range should better allow VICs to be grown into healthy tissue and influence the next generation of biomaterials.

Using a well characterized cell culture system, alkanethiol self-assembled monolayers (SAM), in chapter five we investigated the growth and behavior of VICs on 2D surfaces with different charge and hydrophobicity [17]. While each surface resulted in distinct VIC behaviors, the surface most interesting for tissue engineering applications was alkanethiol 11-mercaptoundecanoic acid (COO$^-$).

When VICs were cultured on COO$^-$ SAM's they proliferated quickly, resisted nodule formation after reaching confluence, and did not express osteoblastic gene markers. In comparison positively charged 11-aminoundecanthiol (NH$_3^+$) functionalized SAMs resulted in rapid and robust osteoblastic differentiation with nodule formation, upregulation of osteoblastic diseased gene markers, and exhibited pronounced αSMA stress fiber formation and expression after 3-5 days in culture. This indicates that negatively charged surfaces can help prevent VIC differentiation to an OB phenotype. Therefore, future iterations of biomaterials should be engineered with negatively charged surfaces to help maintain a proliferative and healthy VIC phenotype for future TEHV studies.

To our knowledge this is the first time that the differentiation of VICs has been shown to be dictated solely through surface chemistry. In comparison to classic OB media induction, which activates cellular signaling cascades with soluble factors like transforming growth factor beta 1, dexamethasone, β-glycerolphosphate, or ascorbic acid, we hypothesize that VICs on COO$^-$ SAMs and NH$_3^+$ SAMs are interacting with the culture surfaces through adhesion based mechanical receptors that induce changes in VIC differentiation [18]. Therefore, we hypothesize that an ideal biomaterial for the growth of healthy aortic valve tissue from VICs should possess a negatively charged environment. Conversely, a positive charged biomaterial could be a very effective method to create a

218

diseased cell model to study AVD development, progression, and could be used as a platform to develop novel AVD therapeutics.

Future work also needs to be done to look more closely at how these cell-material interactions occur in both the DEGDMA/nOM and SAMs VIC systems. It is generally accepted that cells don't attach directly to synthetic materials. Instead the material absorbs proteins to the surface or is modified with biologically active molecules that allow cell attachment [19-21]. In the case of the 2D models discussed, the concentration and bioactivity of serum proteins absorbed onto the surface of our materials is being investigated for their responsibility in controlling cell attachment and behavior. It has been shown that surfaces do not only preferentially absorb certain proteins but that protein confirmation and availability of cellular adhesion domains can be affected by surface chemistry [21-25]. Therefore, investigating absorbed proteins as well as protein confirmation on the different SAMs surfaces and DEGDMA/nOM will be important in further studies defining the driving factors in VIC phenotype.

Another interesting concept that arises from the work of chapters 3 and 4 relates back to the current method to grow VICs *in vitro*. In almost every lab, TCPS flasks are routinely used to grow and expand every type of adherent cell *in vitro* . With a modulus of 20 GPa, 4 times greater than the osteoblastic-inducing DEGDMA/nOM substrates in chapter four, TCPS is unsuited for TEHV studies [26]. However, as TCPS undergoes plasma treatment to create a negatively

219

charged environment for cell attachment, confounding factors in cellular signaling are likely at work [14]. The combination of negative charge and high stiffness of TCPS may help to explain why VICs grow so well on this material, but form nodules at confluence. From these data, it is likely that the first cell culture environment VICs encounter in the laboratory induces them toward a diseased OB phenotype and we should reconsider using TCPS to expand VICs in the future [27, 28].

Through the use of these model surfaces, it has also become apparent that the use of alpha smooth muscle (α-SMA) as a marker of activated or myofibroblastic VICs (aVICs) can lead to misinterpretations in VIC phenotpye. Classically aVICs proliferate rapidly, produce ECM proteins, expresses α-SMA, and are thought to be the most useful phenotype for producing tissues in the lab [15, 29, 30]. However, in our studies α-SMA was expressed highest in more adherent, disease prone VICs. If this gene is highly upregulated in the osteoblastic phenotype as well as an activated phenotype it needs to be used in conjunction with additional markers of osteoblastic differentiation like runx-2, osteocalcin, and osteopontin to help identify which treatments are creating aVIC versus OB VICs [7, 31-33].

Specific Aim 3: *Develop a modifiable 3D hydrogel system to elucidate the effects of microenvironmental cues on VIC behavior in 3D.*

220

The final goal of this dissertation, chapters 5 and 6, was to synthesize a synthetic polymer to create tailorable three-dimensional hydrogels to test the effect of chemical and mechanical cues on VIC behavior. With previous studies conducted on 2D monolayer surfaces, we recognized the need to investigate cell behavior in a more biologically relevant 3D platform that mimics the structure and properties of the aortic valve. Creating a modifiable cell culture platform would help to bridge this understanding in cell behavior in more complex environments. To this end, the polymer oligo(polyethylene glycol) fumarate (OPF) was chosen to create a mechanically tunable, 3D culture system with unsaturated double bonds along its backbone which could be chemically modified to control the local environment. These modified OPFs can then be crosslinked together to create a 3D hydrogel cell culture scaffolds with well-defined environments.

The original synthesis method for producing OPF (TEA-OPF), published in 2001 by Jo S. *et al.*, had major limitations due to a long synthesis time and inability to completely remove triethylamine HCl salt byproducts [34]. Triethylamine HCl salts have been shown to be cytotoxic to cells as well as interfere with crosslinking, therefore we sought a new synthesis method that would eliminate this problem [35]. Chapter 5 discusses our strategy to address this issue with a new synthesis method utilizing nitrogen gas sparging to generate OPF (N_2-OPF). This technique removes hydrochloric acids *in situ*, precluding the need for triethylamine during synthesis and therefore the

generation of cytotoxic triethylamine HCl salt byproducts . As a result of fewer post-processing steps in the nitrogen sparging method, synthesis time is also decreased while yield was increased. These optimizations resulted in a cleaner, higher molecular weight N_2-OPF polymer product which is advantageous for downstream applications, such as modifying the OPF backbone. Overall, the advantages of using nitrogen sparging make OPF a far better product that standard TEA-OPF methods.

In chapter 6 we utilized our superior synthesis method to generate N2-OPF to develop tunable 3D hydrogel environments for VIC growth. As discussed previously, the surface chemistry of a scaffold effects VIC behavior and our focus was to show that OPF can be modified with the same alkanethiol molecules used in chapter five. Addition of alkanethiols to the backbone of OPF creates modified OPF molecules that have a negative or positive charge dependent on the alkanethiol attached. These charged OPF molecules were then crosslinked to form 3D cell culture environments. We have shown that both 11-mercaptoundecanoic acid and 11-aminoundecanol can be attached to OPF using a simple thiol-ene click chemistry. OPF functionalized with 11-mercaptoundecanoic acid (OPF-COO^-) was then tested for its crosslinking ability. As the OPF molecule is functionalized with more COO^- alkanethiol molecules it becomes more charged but has less double bonds available to be utilized for crosslinking. Therefore, a balance between functionalization and remaining

double bonds for crosslinking had to be found. To allow for a highest percentage of thiols functionalization to OPF the molecule PEDGA was added the help facilitate crosslinking of the modified molecule into solid hydrogels. This strategy allowed for OPF ranging from 11-42% of double bonds functionalized with alkanethiols to still for a solid hydrogel charged environments.

After showing OPF-COO$^-$ could be crosslinked successfully, VICs were added to OPF-COO$^-$ and crosslinked into a three-dimensional hydrogel. Live-dead studies show that while VICs survive the initial encapsulation and crosslinking of the hydrogel they do not survive past 24 hours. We hypothesize this is due to their inability to bind to the OPF hydrogel. One explanation for the die off of VICs after 24 hours is that the small alkanethiol molecule is too close to the OPF PEG backbone. This steric hindrance by the large PEG molecules make the thiol unavailable to absorb serum proteins which are need for VIC attachment. Future work could alleviate this issue by attaching the alkanethiol molecules to the end of a pendent group before attaching it to the OPF backbone. This will cause the alkanethiol to stick out more from the backbone and thereby increase its availability for interactions.

A second possibility is that VICs were unable to bind to the hydrogel because proteins were unable to penetrate and be absorbed to the inside of the hydrogel. In 2D systems serum proteins are easy absorbed to the flat surface and cells can attach to these absorbed proteins. In a hydrogel system however

proteins have a much harder time diffusing into the hydrogel and coating the surfaces to allow for cellular attachment. In addition, the main component of our hydrogel, PEG, has previously been shown to prevent protein absorption. We hypothesized that adding a charge to the hydrogel would increase the absorption of proteins but is seems this was not the case. As a result, the encapsulated VICs have nothing to attach to after encapsulation and as an adhesion dependent cell, they eventually die.

In future work, functionalizing the OPF backbone with the attachment peptide RGD will help to alleviate this issue of cellular attachment. VICs will be able to attach immediately onto the RGD peptides after encapsulation thereby allowing for the survival of the attachment dependent VICs. Further culture of VICs within these negatively charged OPF-COO$^-$ hydrogels can then be assessed to understand how 3D charged environments affect VICs growth and behavior. Additionally, OPF functionalization is not limited to RGD peptides and alkanethiols, any molecule that can dissolve in water and has a free thiol group can be attached to OPF using a thiol-ene click chemistry. This makes OPF a highly versatile material that could be functionalized with a large array of bioactive molecules.

Broader Impacts

Overall this dissertation impacts the future design of biomaterials and laboratory practices of aortic valve tissue engineering. It is important that any biomaterial used to grow aortic valves in the laboratory be near the same modulus as the aortic valve tissue since substrate stiffness alters the cellular behavior of valvular interstitial cells. The ideal material should lie between the somewhere between 2-25 kPa [15, 16]. Although the perfect stiffness is not yet defined this work helps to define the upper limit of this range significantly decreasing the range that should be used to engineered and developed future biomaterials.

Additionally, the use of TCPS as the standard material being used to expand valvular interstitial cells needs to be reconsidered. The high modulus near 20 GPa is four times higher than the stiffest DEGDMA/Nom substrate [26]. Current research practices isolate VICs from the valve and then expand them in TCPS flask and wells plates. This means VICs are immediately being exposed to stiff mechanical cues that were shown in this work to cause VIC osteoblastic differentiation.

This work also reflects the first experiments to examine how the surface chemistry of materials can alter VIC behavior. Our work using 2D model self-assembled monolayers shows that a substrate with positive charge induces OB VIC differentiation while a substrate with a negative charge allows for VIC proliferation and maintenance of the aVIC phenotype. This not only suggests

mechanically activated cell signaling pathways can control VIC behavior, but also indicates that designed future scaffolds with negatively charged surfaces will help VICs to form healthy valve tissue.

Finally we started translating this work into a 3D cell culture system using the polymer oligo(poly(ethylene glycol) fumarate) (OPF). With our new synthesis method this unique molecule can now be synthesized rapidly in a pure form that enables us attach alkanethiols and create OPF molecules with a charge. In addition these molecules can be tailored to have increased or decrease amounts of charge and can be generated with varying Mw PEG molecules to alter the final hydrogels stiffness.

References

1.   Chen, J.H., et al., *Identification and characterization of aortic valve mesenchymal progenitor cells with robust osteogenic calcification potential.* Am J Pathol, 2009. **174**(3): p. 1109-1119.

2.   Merryman, W.D. and F.J. Schoen, *Mechanisms of Calcification in Aortic Valve Disease: Role of Mechanokinetics and Mechanodynamics.* Current cardiology reports, 2013. **15**(5): p. 355-355.

3.   Schoen, F.J. and R.J. Levy, *Tissue heart valves: Current challenges and future research perspectives.* Journal of Biomedical Materials Research, 1999. **47**(4): p. 439-465.

4.   Buchanan, R.M. and M.S. Sacks, *Interlayer micromechanics of the aortic heart valve leaflet.* Biomechanics and Modeling in Mechanobiology, 2014. **13**(4): p. 813-826.

5.   Rehfeldt, F., et al., *Cell responses to the mechanochemical microenvironment - Implications for regenerative medicine and drug delivery.* Advanced Drug Delivery Reviews, 2007. **59**(13): p. 1329-1339.

6.   Nemir, S. and J.L. West, *Synthetic Materials in the Study of Cell Response to Substrate Rigidity.* Annals of Biomedical Engineering, 2010. **38**(1): p. 2-20.

7.   Rodriguez, K.J. and K.S. Masters, *Regulation of valvular interstitial cell calcification by components of the extracellular matrix.* Journal of Biomedical Materials Research Part A, 2009. **90A**(4): p. 1043-1053.

8.   Blevins, T.L., et al., *Phenotypic characterization of isolated valvular interstitial cell subpopulations.* J Heart Valve Dis, 2006. **15**(6): p. 815-822.

9.   Dweck, M.R., N.A. Boon, and D.E. Newby, *Calcific Aortic Stenosis: A Disease of the Valve and the Myocardium.* Journal of the American College of Cardiology, 2012. **60**(19): p. 1854-1863.

10.   Schroeder, J.A., et al., *Form and function of developing heart valves: coordination by extracellular matrix and growth factor signaling.* Journal of Molecular Medicine, 2003. **81**(7): p. 392-403.

11.   Camenisch, T.D., et al., *Disruption of hyaluronan synthase-2 abrogates normal cardiac morphogenesis and hyaluronan-mediated transformation of epithelium to mesenchyme.* Journal of Clinical Investigation, 2000. **106**(3): p. 349-360.

12.   Kannurpatti, A.R., J.W. Anseth, and C.N. Bowman, *A study of the evolution of mechanical properties and structural heterogeneity of polymer networks formed by photopolymerizations of multifunctional (meth)acrylates.* Polymer, 1998. **39**(12): p. 2507-2513.

13.   Kannurpatti, A.R., et al., *Use of "living" radical polymerizations to study the structural evolution and properties of highly crosslinked polymer networks.* Journal of Polymer Science Part B-Polymer Physics, 1997. **35**(14): p. 2297-2307.

14.   France, R.M. and R.D. Short, *Plasma treatment of polymers: The effects of energy transfer from an argon plasma on the surface chemistry of*

polystyrene, and polypropylene. A high-energy resolution X-ray photoelectron spectroscopy study. Langmuir, 1998. **14**(17): p. 4827-4835.

15.   Wang, H., et al., *Redirecting Valvular Myofibroblasts into Dormant Fibroblasts through Light-mediated Reduction in Substrate Modulus.* Plos One, 2012. **7**(7): p. 12.

16.   Duan, B., et al., *Three-dimensional printed trileaflet valve conduits using biological hydrogels and human valve interstitial cells.* Acta Biomaterialia, 2014. **10**(5): p. 1836-1846.

17.   Love, J.C., et al., *Self-assembled monolayers of thiolates on metals as a form of nanotechnology.* Chemical Reviews, 2005. **105**(4): p. 1103-1169.

18.   Schroer, A.K. and W.D. Merryman, *Mechanobiology of myofibroblast adhesion in fibrotic cardiac disease.* Journal of Cell Science, 2015. **128**(10): p. 1865-1875.

19.   Curtis, A.S.G., et al., Adhesion of cells to polystyrene srufaces. Journal of Cell Biology, 1983. **97**(5): p. 1500-1506.

20.   Dewez, J.L., et al., *Competitive adsorption of proteins: Key of the relationship between substratum surface properties and adhesion of epithelial cells.* Biomaterials, 1999. **20**(6): p. 547-559.

21.   Arima, Y. and H. Iwata, *Effects of surface functional groups on protein adsorption and subsequent cell adhesion using self-assembled monolayers.* Journal of Materials Chemistry, 2007. **17**(38): p. 4079-4087.

22. Roach, P., D. Farrar, and C.C. Perry, *Interpretation of protein adsorption: Surface-induced conformational changes.* Journal of the American Chemical Society, 2005. **127**(22): p. 8168-8173.

23. Nakanishi, K., T. Sakiyama, and K. Imamura, *On the adsorption of proteins on solid surfaces, a common but very complicated phenomenon.* Journal of Bioscience and Bioengineering, 2001. **91**(3): p. 233-244.

24. Lin, J.H., et al., *Effect of Surface Potential on Extracellular Matrix Protein Adsorption.* Langmuir, 2014. **30**(34): p. 10328-10335.

25. Arima, Y. and H. Iwata, *Preferential adsorption of cell adhesive proteins from complex media on self-assembled monolayers and its effect on subsequent cell adhesion.* Acta Biomaterialia, 2015. **26**: p. 72-81.

26. Leonard, A.T., *Fabrication and Characterization of Synthetic Substrates for Use in Rigididty Cell Culture Studies of Valvular Interstital Cells for Aortic Valve Tissue Engineering.* 2011.

27. Wang, H., et al., *Hydrogels preserve native phenotypes of valvular fibroblasts through an elasticity-regulated PI3K/AKT pathway.* Proceedings of the National Academy of Sciences of the United States of America, 2013. **110**(48): p. 19336-19341.

28. Hutmacher, D.W., *Scaffolds in tissue engineering bone and cartilage.* Biomaterials, 2000. **21**(24): p. 2529-2543.

29.   Liu, A.C., V.R. Joag, and A.I. Gotlieb, *The emerging role of valve interstitial cell phenotypes in regulating heart valve pathobiology.* American Journal of Pathology, 2007. **171**(5): p. 1407-1418.

30.   Walker, G.A., et al., *Valvular myofibroblast activation by transforming growth factor-beta - Implications for pathological extracellular matrix remodeling in heart valve disease.* Circulation Research, 2004. **95**(3): p. 253-260.

31.   Monzack, E.L. and K.S. Masters, *Can valvular interstitial cells become true osteoblasts? A side-by-side comparison.* J Heart Valve Dis, 2011. **20**(4): p. 449-461.

32.   Coombs, K.E., et al., *Isolated effect of material stiffness on valvular interstitial cell differentiation.* Journal of Biomedical Materials Research Part A, 2017. **105**(1): p. 51-61.

33.   Rush, M.N., K.E. Coombs, and E.L. Hedberg-Dirk, *Surface chemistry regulates valvular interstitial cell differentiation in vitro.* Acta Biomater, 2015. **28**: p. 76-85.

34.   Jo, S., et al., *Synthesis and characterization of oligo(poly(ethylene glycol) fumarate) macromer.* Macromolecules, 2001. **34**(9): p. 2839-2844.

35.   Cai, L. and S.F. Wang, *Elucidating Colorization in the Functionalization of Hydroxyl-Containing Polymers Using Unsaturated Anhydrides/Acyl Chlorides in the Presence of Triethylamine.* Biomacromolecules, 2010. **11**(1): p. 304-307.